Characterisation of natural radioactivity in Karoo Basin groundwater prior to shale gas exploration

Ryno Botha

Thesis presented in fulfilment of the requirements for the degree of Masters of Physics at the University of the Western Cape

Supervisors: Professor R. Lindsay

Department of Physics, University of Western Cape, Private Bag X17 Bellville 7535, South Africa

Professor R.T. Newman

Department of Physics, Stellenbosch University, Merensky Building, Merriman Ave, Private Bag X1, Matieland, 7601, South Africa

Dr. P.P. Maleka

Department of Subatomic Physics, NRF-iThemba LABS, PO Box 722, Somerset West 7129, South Africa

DECLARATION

I declare that "Characterisation of natural radioactivity in Karoo Basin groundwater prior to shale gas exploration" is my own work, that it has not been submitted for any degree for examination at any other university, and that all the sources I have used or quoted have been indicated and acknowledge by complete reference.

Full Name: Ryno Botha

Date: 31 May 2017

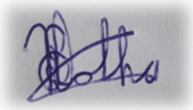

Signature:.....

Characterisation of natural radioactivity in Karoo Basin groundwater prior to shale gas exploration

Ryno Botha
Department of Physics, University of the Western Cape, Private Bag X17, Bellville, South Africa.
devalarish@yahoo.com

ABSTRACT

The prospect of unconventional shale-gas development in the Karoo Basin (South Africa) has created the need to obtain baseline data on natural radioactivity in Karoo groundwaters. The Karoo Basin groundwater radiological baseline developed through this study could serve as a reference to research potential future radiological contamination effects due to hydraulic fracturing. The major naturally occurring radioactive material (NORM) studied was radon (^{222}Rn), in particular in-water activity concentrations; however, supplementary radium (^{226}Ra and ^{228}Ra) in-water activity concentrations and uranium (^{238}U) in-water concentrations measurements were also made. A total of 53 aquifers across three provinces were sampled for groundwater and measured, with three measurement series from 2014 to 2016. The aquifers were categorized as shallow, mixed, or deep source. The radon-in-water baseline of the Karoo Basin can be characterised by a minimum of 0.6 ± 0.9 Bq/L, a maximum of 183 ± 18 Bq/L and mean of 41 ± 5 Bq/L. The radon-in-water levels from shallow sources (with water temperature < 20 °C) were systematically higher (40 Bq/L) than for deep sources (with water temperature > 20 °C). The natural fluctuations in radon-in-water levels were predominantly associated with shallow aquifers compared to almost none observed in the deep sources. The uranium in-water baseline can be characterised by a minimum of below detection level, a maximum of 41 µg/L, and the mean of 5.10 ± 0.80 µg/L. Similar to radon-in-water levels, uranium in-water levels for shallow sources were systematically higher than for deep sources. The limited (six aquifers) radium (^{228}Ra and ^{226}Ra) in-water activity-concentration measurement results were very low, with a maximum of 0.008 Bq/L (^{226}Ra) and 0.015 Bq/L (^{228}Ra). The ^{228}Ra/^{226}Ra ratio baseline were characterised by a minimum of 0.93, a mean of 3.3 ± 1.3, and a maximum of 6.5. The radium isotopes' activity concentration ratio is an isotopic tracer for hydraulic fracturing wastewater. Pollution and contamination (radiological), due to unconventional shale gas development, in water resources has been noticed in the Marcellus Basin (United States). Consequently, developing and improving continuous baseline monitoring are of importance to study the environmental radiological effect of hydraulic fracturing.

Keywords: Karoo Basin; hydraulic fracturing; baseline; radon; groundwater.

ACKNOWLEDGEMENTS

I would like to thank my supervisors – Prof. Richard Thomas Newman, Prof. Robert Lindsay, and Dr. Peane Maleka–for their commitment, support, and mentoring throughout my work on this thesis. Without the backing, scholarship, and financing from the University of the Western Cape (Department of Physics), Stellenbosch University (Department of Physics), iThemba LABS, the MANuS program, and the National Research Foundation (NRF), this thesis would not have been possible.

I would like to sincerely thank the individuals who collaborated on this study as an extension of their research and work: Kelley, Swana, Dr. J. Miller, Anja Eilers, Andrew Watson, Tyron Hartle, and Kay-Lee Kaywits from the Stellenbosch University (Department of Earth Science); Prof. Avner Vengosh from Duke University; Prof. Thomas Darrah and Billy Eymold of Ohio State University; and Siep Talma and Ricky Murray of Groundwater Africa. A special thank-you to the authors of the Water Research Commission (WRC) report, which included the radon data from this study. Without the collaboration of farm owners and other members of the public, such research projects would not be possible, and therefore we are grateful for your time and assistance.

Finally, I would like to thank my fiancée, parents, friends and family for their unprecedented support and inspiration throughout this journey to pursue a deeply embedded passion for learning and discovering.

CONTENTS

LIST OF FIGURES

LIST OF TABLES

CHAPTER 1 Introduction

The Karoo Basin (South Africa) groundwater radiological baseline developed within this research project could act as a reference to study potential groundwater contamination effects. The groundwater radiological baseline can assist to gain knowledge and understanding of probable health risks due to naturally occurring radioactive materials (NORM) exposure and hydrology radioisotope tracers and pioneering NORM (radon) in-groundwater characterisation in the semi-arid Karoo Basin. The central research focus was to create an initial natural radiological groundwater baseline to review potential environmental contamination due to future unconventional shale gas developments. Unconventional shale gas is petroleum produced or extracted utilizing techniques other than conventional methods (oil wells). Unconventional hydrocarbon reservoirs do not have an oil-water or gas-water contact per se. South Africa as a whole, specifically the Karoo area, is a water-scarce region (DWS, 2015). Hydraulic fracturing is a sensitive issue within water scarce regions since a considerable amount of water is required for hydraulic fracturing on an industrial scale, and there is also the risk of contamination to the existing limited water resources. Water contamination studies in water-scarce regions are vital to protecting this essential, limited natural resource. The main naturally occurring radioisotope studied was radon-in-water (^{222}Rn); however, supplementary (WRC, 2015) in-water radium (^{226}Ra and ^{228}Ra) and in-water uranium (^{238}U) measurement results were included.

1.1 Unconventional shale gas development and hydraulic fracturing

1.1.1 Hydraulic fracturing

Hydraulic fracturing involves the creation of vertical or horizontal wells by fracturing rocks with pressurised hydraulic fluids. Floyd Farris invented this method in 1947 while working at Stanolind Oil and Gas Corporation. Hydraulic fracturing was invented with the aim to extract shale gas (see figure 1-1), tight gas, tight oil, and coal-seam gas (Charlez, 1997). It requires a specialised setup to conduct the hydraulic fracturing operations (see figure 1-2). The main energy focus at South Africa's Karoo Basin (612 273 km^2) will be to extract hydrocarbons in the form of shale gas (see figure 1-4). The Karoo Basin is one of the main sedimentary basins

(see figure 1-4), which stretches across two-thirds of the country and contains organic-rich shales (EIA, 2013).

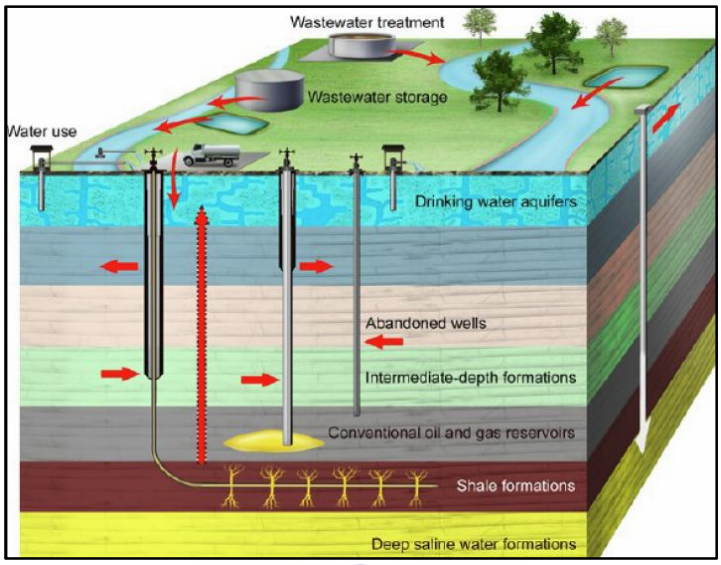

Figure 1-1: Diagram of a typical hydraulic fracturing production site and the associated risks to water resources (Vengosh et al., 2014).

The mechanism which makes hydraulic fracturing functional is based on the pumping of fracturing fluid into a wellbore with enough pressure to surpass the fracture gradient of the rock (GWPC, 2009). This process is implemented for both horizontal and vertical drilling. The fracturing fluid contains multiple chemicals (between 750 and 1000), water, sand, and more (see table.1-1). The hydraulic fluids can leak into materials surrounding the fracturing channel, known as fracturing fluid leak-off. The fluids utilized in the process of hydraulic fracturing are also known as fracturing fluids and production fluids. The recovered flow-back fluid contains chemical additives mixed into the fracturing fluid, dissolved solids from production, NORM and other natural components (EISGE, 2014; Vengosh et al., 2014). The estimated percentage of fracturing-fluid that can be returned to the surface (flow-back fluid) ranges from 15 to 80%. The flow-back wastewater in the United States is stored mostly in lined surface ponds (reserve pits) or tanks from where the treatment process will either occur onsite or at an offsite treatment facility (see figure 1-1, 4). The alternative method to manage the production fluid is referred to as deep-well disposal, also known as deep-injection disposal. The deep-well disposal of hydraulic-fracturing fluid occurs by injecting this waste fluid into permeable porous formations. The oil and gas industry considers the deep-well

disposal method to be the optimal practice for disposal of waste fluid (EISGE, 2014). Within the UK wastewater for instance may not be stored on the hydraulic fracturing site and is transported to treatment facilities immediately to avoid surface water contamination.

Table 1-1: Example of a typical hydraulic fracturing fluid composition and the associated volume of chemicals utilized, taken from EPA, 2011.

Chemical component, additive type	Example compound/s	Purpose	Percent composition (by volume)	Volume of chemical, [L]
Water		Deliver proppant	90	10 220 607
Proppant	Silica, quartz sand	Keep fractures open to allow gas flow out	9.51	1 079 977
Acid	Hydrochloric acid	Dissolve minerals, initiate cracks in the rock	0.123	13 968
Friction reducer	Polyacrylamide, mineral oil	Minimise friction between fluid and the pipe	0.088	9 993
Surfactant	Isopropanol	Increase the viscosity of the fluid	0.085	9 653
Potassium chloride		Create a brine carrier fluid	0.06	6 814
Gelling agent	Guar gum, hydroxyethyl cellulose	Thicken the fluid to suspend the proppant	0.056	6 359
Scale inhibitor	Ethylene glycol	Prevent scale deposits in the pipe	0.043	4 883
pH adjusting agent	Sodium or potassium carbonate	Maintain the effectiveness of other components	0.011	1 249
Breaker	Ammonium persulfate	Allow delayed breakdown of the gel	0.01	1 136
Cross-linker	Borate salts	Maintain fluid viscosity as temperature increases	0.007	795
Iron control	Citric acid	Prevent precipitation of metal oxides	0.004	454
Corrosion inhibitor	n-dimethyl formamide	Prevent pipe corrosion	0.002	227
Biocide	Glutaraldehyde	Eliminate bacteria	0.001	114

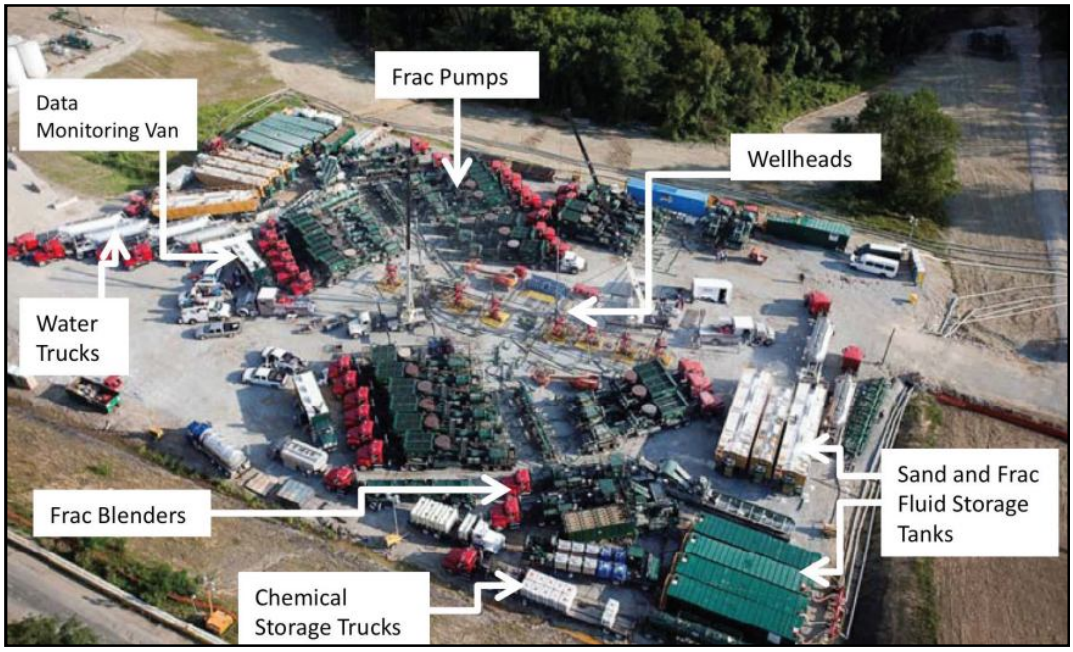

Figure 1-2: A hydraulic fracturing production site on the Marcellus shale multi-well pad in Pennsylvania (Suchy and Newell, 2012).

1.1.2 Shale gas development in South Africa

South Africa's technically recoverable shale-gas reserves were estimated at 390 trillion cubic feet (Tcf) in 2013 (see table 1-2) by the U.S. Energy Information Administration (EIA). South Africa has the eighth largest estimated technically recoverable shale-gas reserves in the world, allocated in a single basin with three different geological formation groups (EIA, 2013). The three shale formation groups are Prince Albert, Whitehill, and Collingham. A temporary hydraulic fracturing development and exploration moratorium was imposed by the South African Government in July 2011 stemming from public pressure, limited water resources, socio-economic implications, and environmental concerns. The moratorium was lifted on 7 September 2012 in the wake of a report released by a task force appointed by the Department of Mineral Resources (DOE, 2012); the report was not made public. The South African Government imposed a 28% income tax and 7% royalties tax on potential profit generated from shale-gas development (EIA, 2013), while exploration operating permits have been given to oil and gas companies (see figure 1-4). South Africa would potentially benefit from shale-gas development in the following ways:

i. Shale gas could serve as a "bridge fuel" resource between coal and alternative fuels. South Africa is facing considerable challenges in terms of national electricity supply. The state-owned company, Eskom, supplies and manages South Africa's electricity. Eskom had been implementing irregular load shedding from 2013 to 2015. Shale gas could be added as a potential energy resource to generate electricity.

ii. Creation of up to 700,000 potential jobs. The sustainability aspect of this potential job creation is questionable, but with unemployment levels at 25.2% according to Statistics South Africa in 2014, the country is in need of a sector that would increase sustainable jobs.

iii. As mentioned above, the government would benefit financially from the 28% income tax and 7% royalties from shale-gas sales.

iv. Growth of the economy and GDP: using the indicative average price of $4.00 per thousand cubic feet of gas and moderately optimistic recovery of between 30 Tcf to 100 Tcf shale gas and at an exchange rate of R14.10 per US Dollar (20-12-2016), a gross sales value of between R1.69 trillion to R5.64 trillion could be generated.

The aspects for concern regarding shale-gas development within the Karoo Basin of South Africa are as follows:

I. The largest part of South Africa is considered a water-scarce region. The World Resource Institute in 2014 indicated a water scarcity risk of medium to high for the largest parts of South Africa (DWS, 2015). It is thus imperative that freshwater reserves are protected comprehensively against contamination.

II. The estimated technically recoverable shale gas reported by the EIA/ARI in 2011 was 485 Tcf (EIA, 2011) and 390 Tcf (EIA, 2013, see table 1-2) in 2013. There is a large degree of uncertainty regarding how much shale gas is technically recoverable, and full-scale exploration will be needed to achieve a more accurate indication of the amount of technically recoverable shale gas.

III. The Karoo Basin has a considerable amount of igneous intrusions (see figure 1-3); these geological factors creates a significant risk for exploration and hydraulic fracturing.

IV. A legacy of potential large-scale environmental contamination, as has occurred in the mining sector stemming from environmental contamination due to acid mine drainage

(AMD) (Mine water management in the Witwatersrand Gold Fields with special emphasis on acid mine drainage, 2010).

V. Contamination of freshwater reserves in the Karoo Region would have devastating effects on the agricultural sector in that region and could result in added risk to South Africa's food security and job sustainability in the sector.

VI. South Africa received a bid on 25 May 2012 to host and construct the largest component of the ground-breaking Square Kilometre Array (SKA) radio telescope, which is one the most ambitious scientific projects of the twenty-first century. It has been reported that hydraulic fracturing can cause induced seismicity or earthquakes (Won-Young, 2013), which is a considerable risk for the delicate instrumentation to be used in this project.

Table 1-2: Estimated shale gas resource assessment in 2013 by the EIA/ARI, taken from EIA, 2013.

Country	Risked Gas In-Place, [Tcf]	Technically Recoverable, [Tcf]
Canada	2413	573
Mexico	2233	545
Australia	2046	55
Columbia	308	167
Venezuela	815	222
Argentina	3244	802
Brazil	1279	245
Bolivia	154	38
Chile	228	48
Paraguay	350	75
Uruguay	13	2
Poland	763	148
Lithuania	4	0
Kaliningrad	20	2
Bulgaria	66	17
Romania	233	51
Ukraine	572	128
UK	134	26
Spain	42	8
France	727	137
Germany	80	17
Netherlands	151	26
Denmark	159	32
Sweden	49	10
Morocco	95	20
Algeria	3419	707
Tunisia	114	23
Libya	942	122
Egypt	535	100
South Africa	1559	390
China	4746	1115
Mongolia	55	4
Thailand	22	5
Indonesia	303	46
India	584	96
Pakistan	586	105
Jordan	35	7
Turkey	163	24

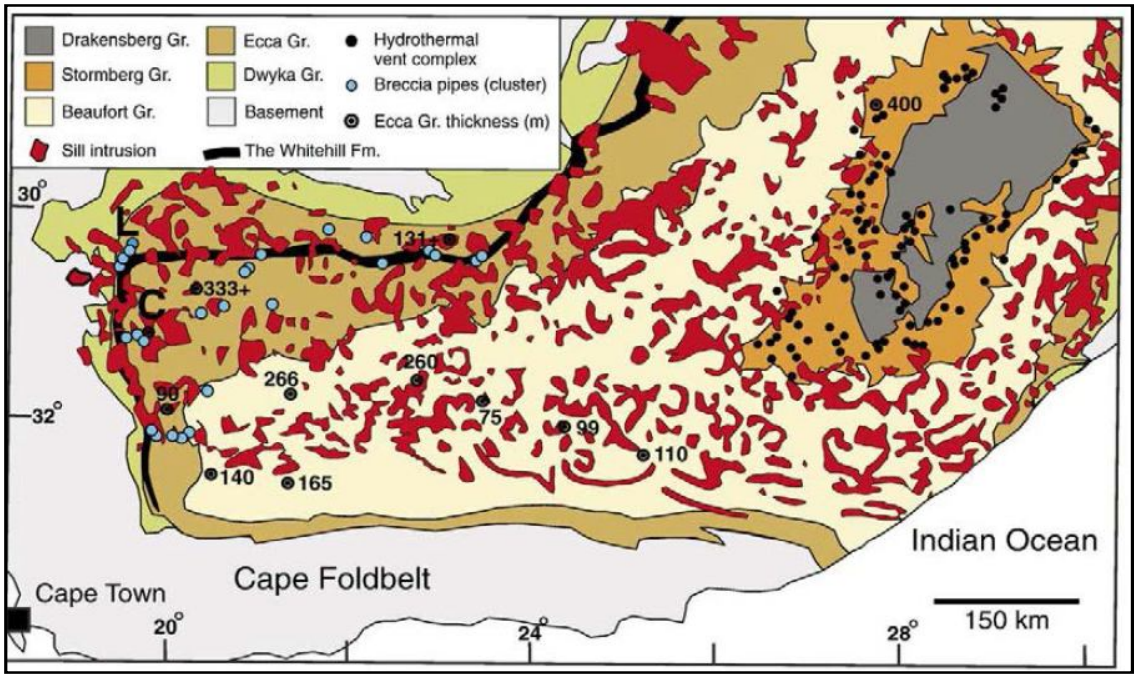

Figure 1-3: Map of Igneous Intrusions (Sill) within the Karoo Basin (EIA, 2013).

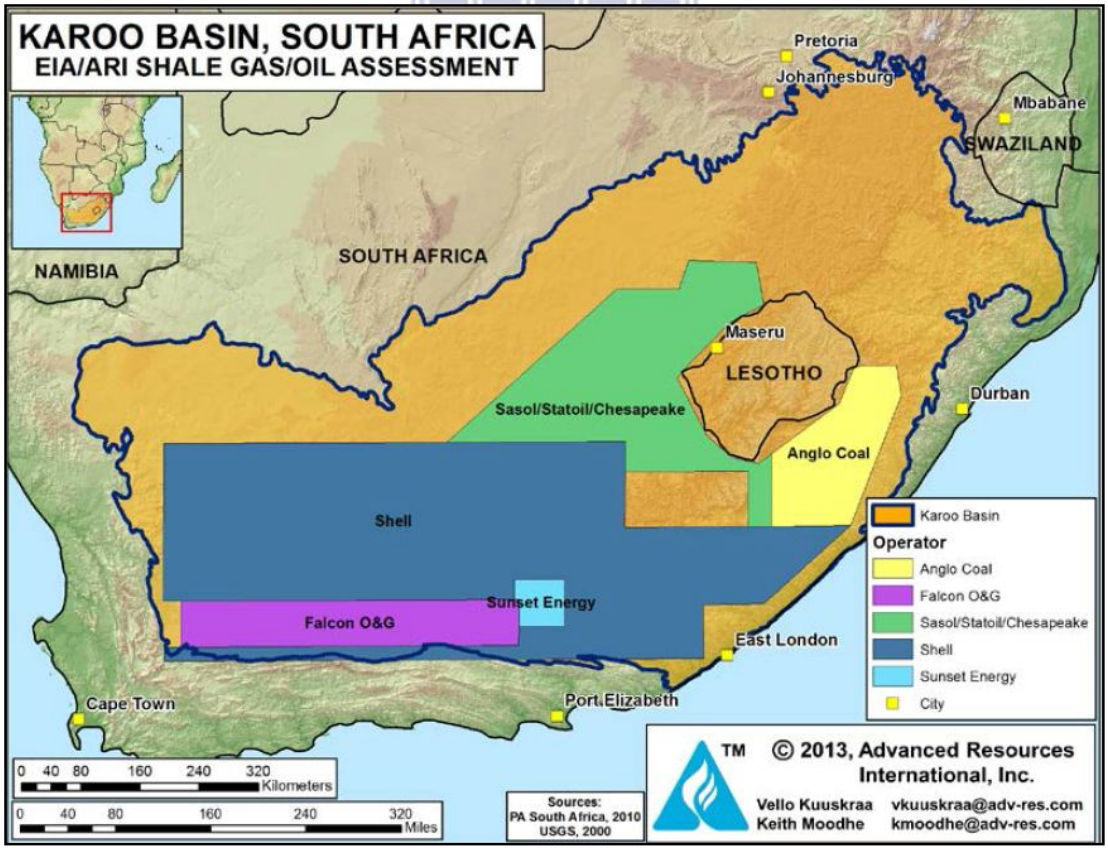

Figure 1-4: The Karoo Basin (South Africa) operator permits within the Karoo Basin indicating the regions where exploration will be conducted (EIA, 2013).

1.1.3 Contamination risks to water resources from shale gas development and hydraulic fracturing

1.1.3.1 Stray gas contamination to shallow aquifers

Leaking of natural gas from oil and gas wells created by hydraulic fracturing is referred to as stray-gas contamination. Stray-gas contamination in shallow aquifers is particularly worrisome due to more severe negative impacts than for instance on deep aquifers (Vengosh et al., 2014). The stray gas, as a rule consists of methane, propane, and ethane. The Division of Earth and Ocean Sciences at Duke University performed an elaborate study on this form of contamination (Vengosh et al., 2013).

From 2010 to 2014, this research group sampled over 600 shallow private wells across six states (Vengosh et al., 2013). Direct evidence obtained through these studies has shown stray-gas contamination occurs in shallow groundwater aquifers (Osborn et al., 2011; Jackson et al., 2013; Vengosh et al., 2013). The level of stray-gas contamination is directly related to the distance between shale-gas sites and wells (see figure 1-5). There is a direct correlation between elevated levels of stray gas in shallow water wells and the proximity to the shale-gas sites from these wells (Osborn et al., 2011; Jackson et al., 2013). The U.S. Department of Interior recommends immediate remediation for methane in water concentrations above 28 mg CH_4/L (Jackson et al., 2013).

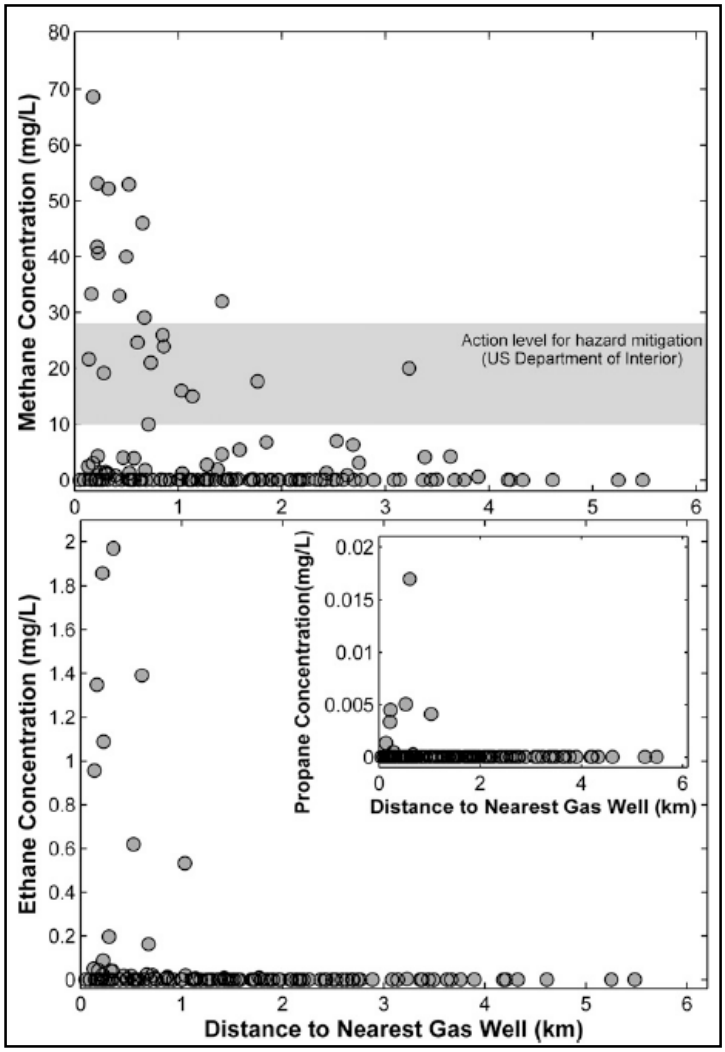

Figure 1-5: Results of concentration of methane (upper), ethane (lower) and propane (inset) measured in Pennsylvania in 2012. Vengosh et al., 2013

1.1.3.2 Production fluid and flow back contamination to surface water and shallow groundwater.

Contamination of surface water and shallow groundwater can occur through leaks, spills, and inadequate treatment of wastewater from hydraulic fracturing (Warner et al., 2013; Vengosh et al., 2014). The chemicals which could be found in the hydraulic fluid/wastewater in the United Sates (see table 1-1) include the following: Group 1 carcinogens (carcinogenic to humans) classified by the International Agency for Research on Cancer (IARC). Group 1 carcinogens in hydraulic-fracturing wastewater fluid are benzene, crystalline silica, formaldehyde, and radon (IARC, 2015). However it has to be mentioned that the hydraulic

fracturing cocktail differs from country to country based on national environmental regulations. It has to be emphasised that there exists different hydraulic fracturing cocktails and potential risks will be related to the content of the exact cocktail which was utilized. The Technologically Enhanced Naturally Occurring Radioactive Materials (TENORM) content within wastewater will depend on the geology in which the fracturing is conducted. It is of importance to avoid contamination by hydraulic fracturing wastewater to surrounding aquifers and consequently potential human or animal consumption.

1.1.3.3 Accumulation of toxic chemicals and TENORM in soil or stream sediments.

Another form of contamination is the potential accumulation of toxins and Technologically Enhanced Naturally Occurring Radioactive Material (TENORM) in soil and stream sediments near wastewater treatment facilities, reserve pits, and spill sites (Vengosh et al., 2014). Toxin accumulation can occur within sediments of downstream rivers from wastewater treatment facilities. These toxins consist of metals, salts, organic compounds, and TENORM which could build up in sediments, depending on a range of physicochemical conditions of the water. The Marcellus wastewaters (USA) contains elevated TENORM levels, especially radium (Rowan et al., 2011; Haluszczak et al., 2013; Warner et al., 2013; Vengosh et al., 2014).

South Africa is known as a mineral-rich country with a large mining sector, including an extensive amount of uranium resources (IAEA, 2009). South Africa's uranium reserves are predominantly allocated within the uranium provinces (see figure 1-6). Due to the elevated NORM content within the uranium provinces (see figure 1-6) and overlapping location with proposed shale gas development regions (see figure 1-4), and the high values of documented TENORM from the Marcellus wastewater, it can be assumed that elevated amounts of NORM will be observed from hydraulic-fracturing wastewater in the Karoo Basin. The natural radioactive materials expected to be observed are; ^{226}Ra, ^{228}Ra, ^{220}Rn, ^{222}Rn, ^{238}U and ^{232}Th.

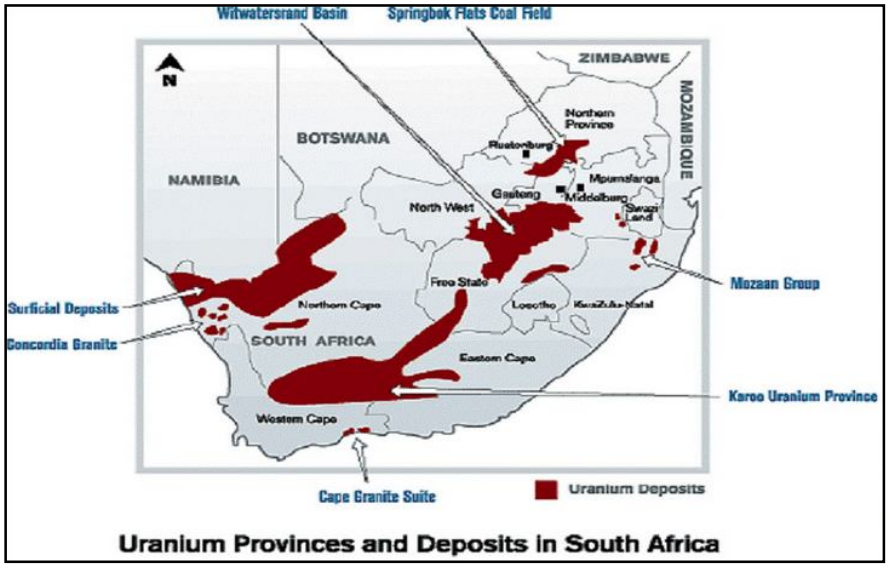

Figure 1-6: Uranium Provinces and Deposits in South Africa created by the South African Nuclear Energy Corporation (NECSA).

1.2 Motivation for this study

The prospect of unconventional shale gas development in the Karoo Basin (South Africa) has created the prerequisite to developing a regional radiological groundwater baseline. It is likely that there will be an increase in NORM levels in contaminated aquifers due to hydraulic fracturing in the Karoo Basin. The full-scale, long-term environmental effects of hydraulic fracturing are still largely unknown since this industry is relatively new. The largest potential risk due to hydraulic fracturing within Karoo Basin due to hydraulic fracturing will be water contamination (CSIR, 2016).

A limited number of studies have been conducted on radiological contamination of water resources due to the process of hydraulic fracturing. This study will be the most comprehensive characterization of radon-in-water within groundwater of the Karoo Basin to date (2016). Results from this study have been shared and were utilized by the Council for Scientific and Industrial Research (CSIR, South Africa) and Water Research Commission (WRC, South Africa). A study by the WRC released in the report (WRC, 2015; Kelley, 2016), titled, “The use of chemistry, isotopes and gases as indicators of deeper circulating groundwater in the Main Karoo Basin” made use of results from this study. A comprehensive study by the CSIR released in the report (CSIR, 2016), titled, “Shale Gas Development in the Central Karoo: A Scientific Assessment of the Opportunities and Risks” likewise made use of results from this study.

1.3 Aim of this study

The aim of this study is to develop a radiological groundwater baseline prior to potential shale gas development within the Karoo Basin (South Africa) by performing NORM characterization. Radon (^{222}Rn) was the NORM predominantly focused on in this study. However, radium (^{226}Ra and ^{228}Ra) and uranium (^{238}U) results are also included. A comprehensive baseline radon-in-water characterization for deep, mixed and shallow (see chapter 4) Karoo Basin groundwater aquifers were performed. Understanding baseline radon-in-water characterization according to spatial, temporal and source classification (deep, shallow or mixed) will provide additional knowledge on the nature of the baseline for radiological groundwater within the Karoo Basin.

CHAPTER 2 Background on radon

2.1 Introduction

Radioactivity, nuclear decay, or radioactive decay is the process by which a nucleus of an unstable atom dissipates energy by emitting radiation. In 1896 radioactivity was discovered by Henry Becquerel (Bauer and Westfall, 2011). Quantum theory states that it is not possible to predict as a function of time when the unstable nucleus will undergo nuclear decay on a single-atom level (stochastic process). Radioactivity is the distinct characteristic of unstable nuclear matter, which is not influenced by changes in its physical state or chemical nature. Main radiation sources include fast electrons (β decay, internal conversion and Auger electrons); heavy charged particles (α decay and spontaneous fission); electromagnetic radiation (γ rays, annihilation, Bremsstrahlung, synchrotron radiation and characteristic x-rays); and neutrons (Knoll, 2000). The radioactive isotopes, also are known as radionuclides, which were present during the formation of the Earth (^{238}U, ^{235}U, ^{232}Th, and ^{40}K) are called primordial radionuclides. The radionuclides synthesised by nuclear processes initiated by humans are referred to as anthropogenic (e.g. ^{90}Sr, ^{129}I, and ^{239}Pu).

In this chapter, a brief overview of fundamental concepts associated with nuclear decay is discussed: the exponential decay law; different types of radiation; radiation interaction with matter; and an overview of radon characteristics (nuclear properties, chemical properties, and transport mechanisms).

2.2 Radioactivity

On Earth naturally occurring radionuclides are located within the atmosphere, soil, rocks and groundwater as a decay series of uranium (^{238}U) and thorium (^{232}Th) with different levels of activity concentrations. By measuring associated characteristic radiation, a radionuclides' activity concentration can be quantitatively determined. As mentioned above, there are different types/modes of nuclear decay: alpha decay (α-decay); beta decay (β-decay); and gamma decay (γ-decay). A full description of all the different mechanisms of nuclear decay can be found in several textbooks (e.g. Bauer and Westfall, 2011; Knoll, 2000), although those with particular relevance to this thesis will be discussed in more detail.

One of the fundamental decay modes on which the quantitative analytical measurements of radon and thoron activity concentration are based on α-decay. The counting of α-particles with a particular energy (MeV) proves to be an efficient method for measuring radon activity concentration. The equation representing the α-decay mechanism (see figure 2-1) can be expressed as follow:

$$^{A}_{Z}X \rightarrow {}^{4}_{2}Y + {}^{A-4}_{Z-2}X' \qquad (2.1)$$

where a helium atom is also known as an α-particle ($^{4}_{2}He$) is emitted. Unstable heavy isotopes with A > 150 (Bauer and Westfall, 2011) are prone to undergo α-decay. Almost all α-particle energies (E_α) are limited to between 4 and 7 MeV (Bauer, 2011, see table 2-1). There is a strong correlation between the α-particle energy and the associated half-life of a parent radionuclide (see table 2-1). The α-particles with the greatest energy are those associated with the shortest half-life (Knoll, 2000; see table 2-1).

Table 2-1: Characteristics of different α-decay radionuclide sources. Table from Rytz (Rytz, 1973).

Source	Half-Life	Alpha Particle Kinetic Energy (with Uncertainty) in MeV		Percent Branching
^{148}Gd	93 y	3.182787	±0.000024	100
^{232}Th	1.4×10^{10} y	4.012	±0.005	77
		3.953	±0.008	23
^{238}U	4.5×10^{9} y	4.196	±0.004	77
		4.149	±0.005	23
^{235}U	7.1×10^{8} y	4.598	±0.002	4.6
		4.401	±0.002	56
		4.374	±0.002	6
		4.365	±0.002	12
		4.219	±0.002	6
^{236}U	2.4×10^{7} y	4.494	±0.003	74
		4.445	±0.005	26
^{230}Th	7.7×10^{4} y	4.6875	±0.0015	76.3
		4.6210	±0.0015	23.4
^{234}U	2.5×10^{5} y	4.7739	±0.0009	72
		4.7220	±0.0009	28
^{231}Pa	3.2×10^{4} y	5.0590	±0.0008	11
		5.0297	±0.0008	20
		5.0141	±0.0008	25.4
		4.9517	±0.0008	22.8
^{239}Pu	2.4×10^{4} y	5.1554	±0.0007	73.3
		5.1429	±0.0008	15.1
		5.1046	±0.0008	11.5
^{240}Pu	6.5×10^{3} y	5.16830	±0.00015	76
		5.12382	±0.00023	24
^{243}Am	7.4×10^{3} y	5.2754	±0.0010	87.4
		5.2335	±0.0010	11
^{210}Po	138 d	5.30451	±0.00007	99+
^{241}Am	433 y	5.48574	±0.00012	85.2
		5.44298	±0.00013	12.8
^{238}Pu	88 y	5.49921	±0.00020	71.1
		5.4565	±0.0004	28.7
^{244}Cm	18 y	5.80496	±0.00005	76.4
		5.762835	±0.000030	23.6
^{243}Cm	30 y	6.067	±0.003	1.5
		5.992	±0.002	5.7
		5.7847	±0.0009	73.2
		5.7415	±0.0009	11.5
^{242}Cm	163 d	6.11292	±0.00008	74
		6.06963	±0.00012	26
^{254m}Es	276 d	6.4288	±0.0015	93
^{253}Es	20.5 d	6.63273	±0.00005	90
		6.5916	±0.0002	6.6

The other nuclear decay process applicable to this thesis, apart from α-decay is γ-decay. Gamma decay influences energetic photons which are emitted when excited nuclei undergo transitions to a lower energy state. One of the typical mechanisms by which γ-radiation is produced is as a secondary result of β-decay (or electron capture) with sources like ^{22}Na, ^{57}Co, ^{60}Co and ^{137}Cs.

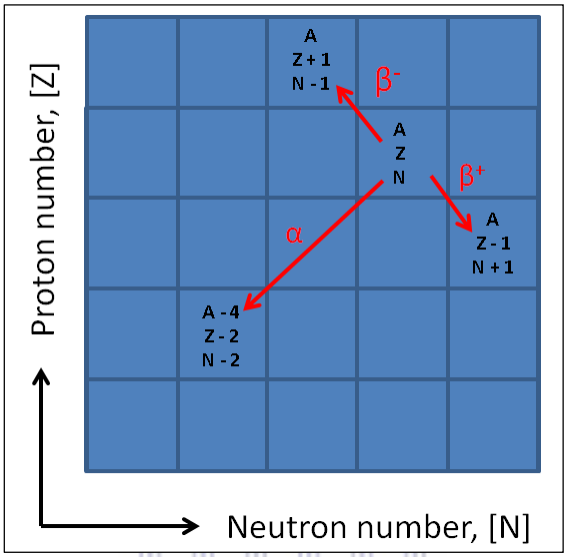

Figure 2-1: Transition diagram for nuclear decay modes (α, β^- and β^+) for a single parent atom, with neutron number (N), proton number (Z) and the mass number (A).

The radioactive decay (one decay chain) for an unstable radionuclide X_1 that decays into another X_2 can be expressed by the following general first-order differential equation (ODE):

$$A = -\frac{dN}{dt} = \lambda N \qquad (2\text{-}2)$$

where N is the nuclide population, dt – an increment of time, λ – the decay constant, and A – the total activity. The activity (A) of a radionuclide is the number of nuclear decays per second with the SI unit of becquerel (Bq). A solution to the first-order differential equation 2-2 is:

$$N(t) = N_o e^{-\lambda t} \qquad (2\text{-}3)$$

where N_o is the value of N at t = 0. For all times (t), it needs to hold that:

$$N_{X_1} + N_{X_2} = N_{total} \qquad (2\text{-}4)$$

and it can be shown that:

$$N_{X2} = N_{X1,t=o}(1 - e^{-\lambda t}) \quad (2\text{-}5)$$

A central aspect of the decay laws and a key characteristic of any radionuclide is its half-life ($t_{1/2}$). The half-life of a nuclide refers to the total amount of time it takes for exactly half of a given population of radionuclides (N) to decay by equation 2-3. The half-life equation for a single decay chain can be obtained from 2-3:

$$t_{1/2} = \frac{\ln(2)}{\lambda} \quad (2\text{-}6)$$

Radionuclides in general decay via a multiple range of nuclear decay modes. The ratio of exact number of nuclei that decay by a specific decay mode to the total amount of atoms decayed is referred to as the branching ratio (BR). Bateman's equations (see equation 2-9 and 2-10) describe how to model multiple (D) consecutive decay chains (unstable daughter products):

$$A_1 \rightarrow A_2 \rightarrow \cdots \rightarrow A_i \rightarrow \cdots \rightarrow A_D \quad (2\text{-}7)$$

which will generate the following first-order ODE:

$$\frac{dN_i}{dt} = \lambda_{i-1}N_{i-1} - \lambda_i N_i \ (i = 2, D) \quad (2\text{-}8)$$

The general solution to this recursive first-order ODE is given by Bateman's equations:

$$N_D(t) = \frac{N_1(0)}{\lambda_D}\sum_{i=1}^{D}\lambda_i c_i\, e^{-\lambda_i t} \quad (2\text{-}9)$$

with the expansion coefficient of:

$$c_i = \prod_{j=1,i\neq j}^{D}\frac{\lambda_j}{\lambda_j - \lambda_i} \quad (2\text{-}10)$$

Jerzy Cetnar calculated the total activity as a function of time for a multiple consecutive (multiple) decay chain using Bateman's equations (equations. 2-9 & 2-10). The calculation can be expressed as (Cetnar, 2006):

$$A(t) = \sum_{i=1}^{n}\lambda_i\alpha_i \exp[-\lambda_i t]\cdot\sum_{m=0}^{\mu_i}\frac{(\lambda_i t)^m}{m!}\cdot\Omega_{i,\mu_i-m} \quad (2\text{-}11)$$

where the following expansion coefficients are applicable

$$\alpha_i = \prod_{\substack{j=1,n \\ j\neq i}} \left(\frac{\lambda_j}{\lambda_j - \lambda_i}\right)^{m_j} \quad \Omega_{i,j} = \sum_{h_1=0}^{j}\sum_{h_2=0}^{j}\cdots\sum_{h_n=0}^{j} \times \prod_{\substack{k=1 \\ k\neq i}}^{n} \binom{h_k + \mu_k}{\mu_k} \left(\frac{\lambda_i}{\lambda_i - \lambda_k}\right)^{h_k} \delta\left(j, \sum_{\substack{l=0 \\ l\neq i}}^{n} h_l\right) \tag{2-12}$$

The International System of Units (SI) recommended unit to measure radioactive activity is becquerel (Bq). Another unit used for radioactive decay is Curie (Ci, 1 Ci = 3.7 x 10^{10} Bq), which is used in countries such as the United States.

2.3 Interaction of radiation with matter

The physics principles of the radiation interaction with matter underpin the fundamental design principles of radiation detectors. The probability of radiation interactions with matter are related to the concept of a reaction cross section.

2.3.1 Interaction of heavy charged particles with matter

Measuring radon-in-water activity concentrations is one of the primary metrology foci of this thesis. Heavy positively charged particles, such as an α-particle, predominantly interacts with matter through the Coulomb force (Knoll, 2000). As charged particles interact with matter, it will undergo Coulomb interaction with the medium's electrons. These surrounding electrons could consequently be excited to a higher energy orbital state or even emitted (ionization). The charged particles travel only within in a finite range in matter. More specifically α-particles from natural radioactivity do not travel more than a few μm (see figure 2-2).

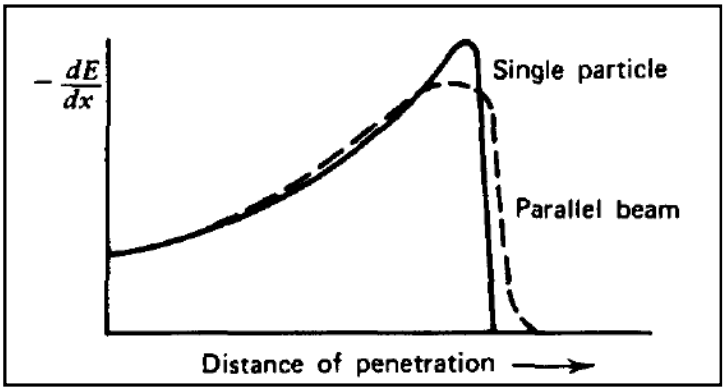

Figure 2-2: The specific energy dissipation along an alpha track of charged particle within matter which is also known as the Bragg curve (Knoll, 2000).

2.3.2 Interaction of γ-rays with matter

Both γ-rays and x-rays are electrically neutral and not subject to the Coulomb or nuclear forces. The photon interactions are long-ranged and not short-ranged interactions associated with heavy charged particles (see section 2.3.1). The γ-ray attenuation (good geometry) by matter can generally be expressed as:

$$I = I_0 e^{-\mu_l L} \tag{2-13}$$

where I_0 is the incident γ-ray intensity, μ_l is the attenuation coefficient (property of the absorber material), L is the thickness of the absorber material, and I is the emerging γ-ray intensity. Photons (γ-rays) can also move through matter without any interactions. The three predominant types of interaction with matter (see figure 2-5) will be discussed in the next sections.

2.3.2.1 Photoelectric effect

The photoelectric effect, also known as photoelectric absorption, was first proposed by Albert Einstein to establish the quantum mechanical nature of light. An atom's bound electron could potentially absorb an energetic incident photon and a free electron (photoelectron) emerges. The overall probability for photoelectric absorption (cross section, σ) of a material can be expressed as follow:

$$\sigma_{photoelectric} \propto \frac{Z^n}{E_\gamma^{3.5}}, \tag{2-14}$$

where n is between 4 and 5, Z is the atomic number (Z), and E_γ the incident photon energy (see figure 2-5).

2.3.2.2 Compton scattering

When an incident photon's energy (E_γ^i) exceeds the binding energy of the innermost atomic electrons, the probability (cross section) of the photoelectric absorption occurring will be surpassed by the probability of the photon being scattered. By making use of the conservation of energy and momentum principles combined with relativistic mechanics the following scattering equation can be established:

$$E_\gamma^f = \frac{E_\gamma^i}{1+\frac{E_\gamma^i}{m_0c^2}(1-cos\theta)}$$ (see figure 2-3) (2-15)

where m_0c^2 = 0.511 MeV (electron rest mass energy) and the photon's scattering angle (θ) can range from 0° to 180° (Compton edge).

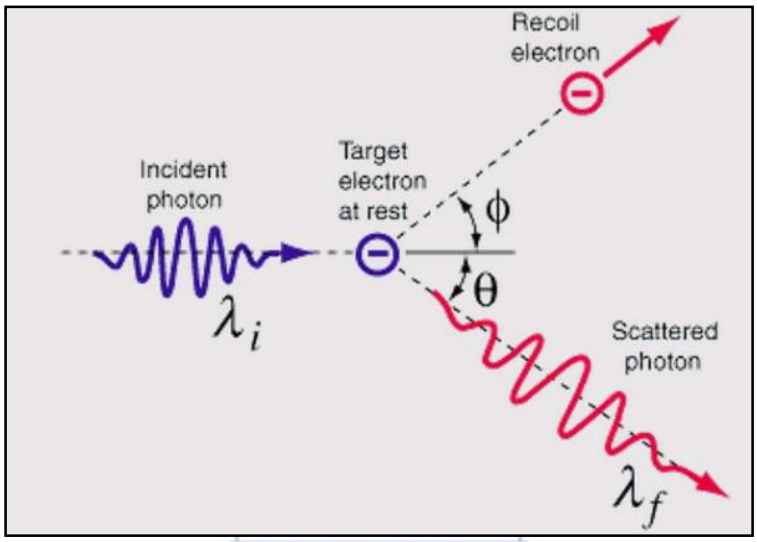

Figure 2-3: Illustration of the Compton scattering effect. An incident photon transfers a component of its energy to an electron which is in a bound orbital energy state and is scattered at an angle of θ.

The scattered photon's energy E_γ^f depends only on its scattering angle θ and its incident energy E_γ^i. The photon scattering angle of 0° will result in no energy transfer from the incident photon to the recoil electron and with the photon back scattered (θ = 180°, Compton edge), the largest amount of energy will be transferred. The backscattered photons will consequently create backscatter peak in γ-spectra (see figure 2-4).

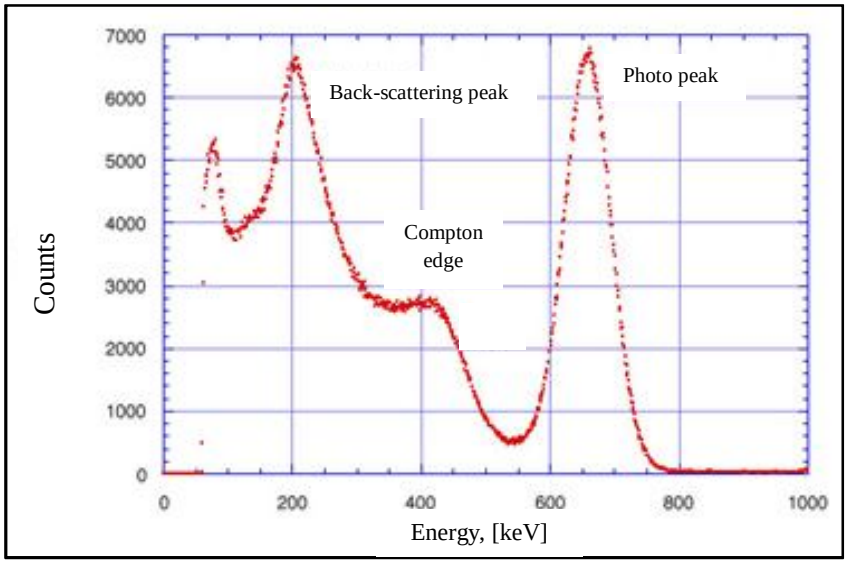

Figure 2-4: A γ-spectrum from a Cs-137 source illustrates the photo peak, Compton edge and backscattered peaks.

2.3.2.3 Pair Production

The pair production effect becomes energetically favourable when the incident photon energy exceeds the rest mass of two electrons (1.022 MeV). The pair production is governed by the mechanism where an incident photon (E > 1.022 MeV) interacts with the Coulomb field of a nucleus is converted to an electron (e^-) –positron (e^+) pair :

$$\gamma \rightarrow e^- + e^+ \qquad (2\text{-}16)$$

This electron-positron pair interacts with the absorption materials' electrons via the Coulomb force and one of the associated effects observed is breaking radiation (bremsstrahlung), which is the process where an electron interacts with the Coulomb field of an atom and undergoes a transition between two energy states, consequently emitting a photon.

Pair production is the predominant attenuation mechanism for photons with high energies (see figure 2-5). The pair production cross section for large energies can be expressed as:

$$\sigma_{pair} \propto Z^2 \ln\left(\frac{E_\gamma}{mc^2}\right) \qquad (2\text{-}17)$$

Thus pair production interaction rates (see eq. 2-17) proportional to the square of the atomic number (Z) of the interaction material. One of the key characteristics of the pair production is also the annihilation process:

$$e^- + e^+ \rightarrow \gamma + \gamma\,. \qquad (2\text{-}18)$$

An annihilation process occurs when the positron interacts with an electron, and the pair annihilates, due to the conservation of charge, energy and momentum; two identical back-to-back (180°) photons are created with the identical energy of 0.511 MeV.

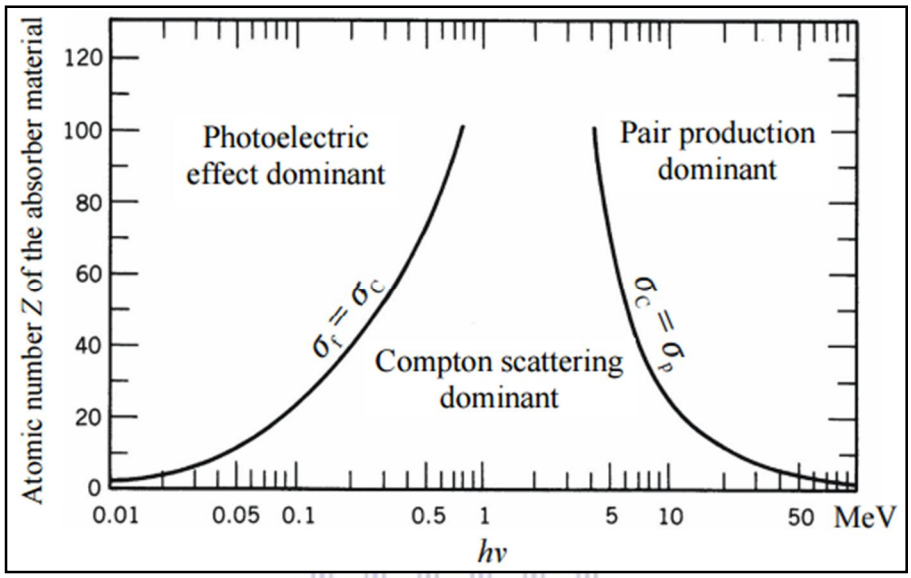

Figure 2-5: The interaction of γ-ray with matter and the associated dominant regions; photoelectric effect, Compton scattering and pair production.

For naturally occurring radioactive materials, the predominant γ-ray interaction with matter will be the photoelectric effect and Compton scattering based on its relatively low (100 keV to 1500 keV) photon energies (Firestone, 1996).

2.4 Radon Characteristics

2.4.1 Overview of radon in water

Radon (^{222}Rn half-life = 3.825 days) is a naturally occurring radionuclide which occurs as a noble gas which is relatively soluble in water. Hereinafter, radon or Rn will refer to ^{222}Rn isotope, unless otherwise specified. The three most prominent radionuclides of its 39 isotopes are ^{219}Rn (half-life = 3.96 s) known as actinium; ^{220}Rn (half-life = 55.6 s) known as thoron; and ^{222}Rn (half-life = 3.8235 d) known as radon. These will be discussed in section 2.4.3.

Radon (a NORM), and its daughter products (progeny) are prominent carcinogens (UNSCEAR, 2008) due to ionisation radiation exposure. The US Environmental Protection Agency (EPA) (EPA, 1993), International Commission on Radiological Protection (IRCP) (ICRP Publication 126, 2014), and the International Atomic Energy Agency, IAEA (IAEA, 2013) have all classified radon as the second leading cause of lung cancer.

There are numerous fields in which radon applications have been utilized, such as hydrology, seismology, atmospheric sciences, and medicine. Radon is utilized as a radionuclide tracer in hydrology to study groundwater discharge, geochemical exploration, the interaction between deep and shallow groundwater systems, and physical geological systems (Cable et al., 1996; Petitta et al., 2011; Santos and Bradley, 2011). Radon studies are performed within seismology to investigate the potential correlation between seismic activity and radon levels. The concept is to use it as an additional potential earthquake prediction system (Singh et al., 1999). Radon had been utilized in radiation therapy treatment for cancer (cervix, mouth, tongue, tonsils, rectum, bladder, etc.) and arthritis patients from 1940 to 1960 (Becker, 2004). Radon seeds (brachytherapy) with activities ranging from 1.85 mCi to 185 mCi were administrated during the abovementioned period (ORAU, 1999). Radon seeds were replaced in 1960 with ^{125}I, ^{198}Au, and ^{60}Co seeds which are the standard ionisation source used for brachytherapy in radiation therapy today (ORAU, 1999).

Radon-in-water activity concentration measurements in the Karoo Basin were performed with a DURRIDGE RAD7 detector (www.durridge.com). Due to the “short” half-life of radon (3.825 days), it is crucial to perform radon-in-water activity concentration measurements as soon as possible after sampling. It is thus preferable to have a mobile and accurate radon measuring system onsite to perform measurements rather than to send samples to an off-site laboratory.

Elevated radon-in-water activity concentrations have been extensively measured at a number of hot springs around the world (Vogiannis et al., 2004; Somlai et al., 2007; Botha et al., 2016). Some natural hot springs resorts have advertised radon for alleged therapeutic properties. Modern medicine does not claim that radon holds therapeutic properties; however, this possibility must not entirely be disregarded on the basis of radiation hormesis (Zdrojewicz, 2006). More studies in the field of radiobiology are needed to prove or reject the

claim of therapeutic properties from ionisation exposure of radon and associated daughter products (Zdrojewicz, 2006).

2.4.2 Nuclear properties

The isotopes of radon range from ^{193}Rn to ^{231}Rn (BNL, 2016) have predominantly α-, β^-- and β^+ decay modes (see table 2-2). The half-lives for these isotopes range from 245 ns (^{214m}Rn) up to 3.82 days (^{222}Rn, see table 2-2). The isotope of particular interest for this thesis is ^{222}Rn (radon). Radon is produced as part of the primordial occurring radioactive material (NORM) group (see figure 2-6, blue section) by the consecutive decay sequences starting with ^{238}U. Radon undergoes α-decay (5.59 MeV, 99.92%) with a half-life of about 3.82 days. Radon decay progeny (see figure 2-6, purple section) are of particular importance, as it serves as an indirect mechanism to measure radon and poses the largest effective public dose due to ionisation radiation exposure (WHO, 2009; ICRP, 2010). The radon decay products (RnDP) can generally be considered as the following: ^{218}Po (α-decay, $t_{1/2}$ = 3.10 min); ^{214}Pb (β/γ-decay, $t_{1/2}$ = 26.8 min); ^{214}Bi (β/γ-decay, $t_{1/2}$ = 19.9 min); and ^{214}Po (α-decay, $t_{1/2}$ = 164 µs). These radon in-air decay products initially exist as positively charged free ions. These ions will neutralise, while nano-sized clusters of both unattached RnDP (>10 nm) and RnDP attached to aerosols (10 to 1000 nm) could be produced (Goldstein and Hopke, 1985; Butterweck et al., 1992; Vaupotic, 2008).

The ratio between the activity concentration of equilibrium equivalent (EC) radon daughter products (RnDP) and radon (Rn) is known as the equilibrium factor (F). Consequently, the equilibrium factor (F) could have values between 0 and 1. The International Commission of Radiation Protection recommends general indoor and outdoor equilibrium factors of 0.4 and 0.8 (ICRP, 2010), respectively. In a realistic dynamic system, the activity concentrations of radon and its progeny vary significantly with space and time and, consequently, also the equilibrium factor (0.19 – 0.90, Yu et al., 2008).

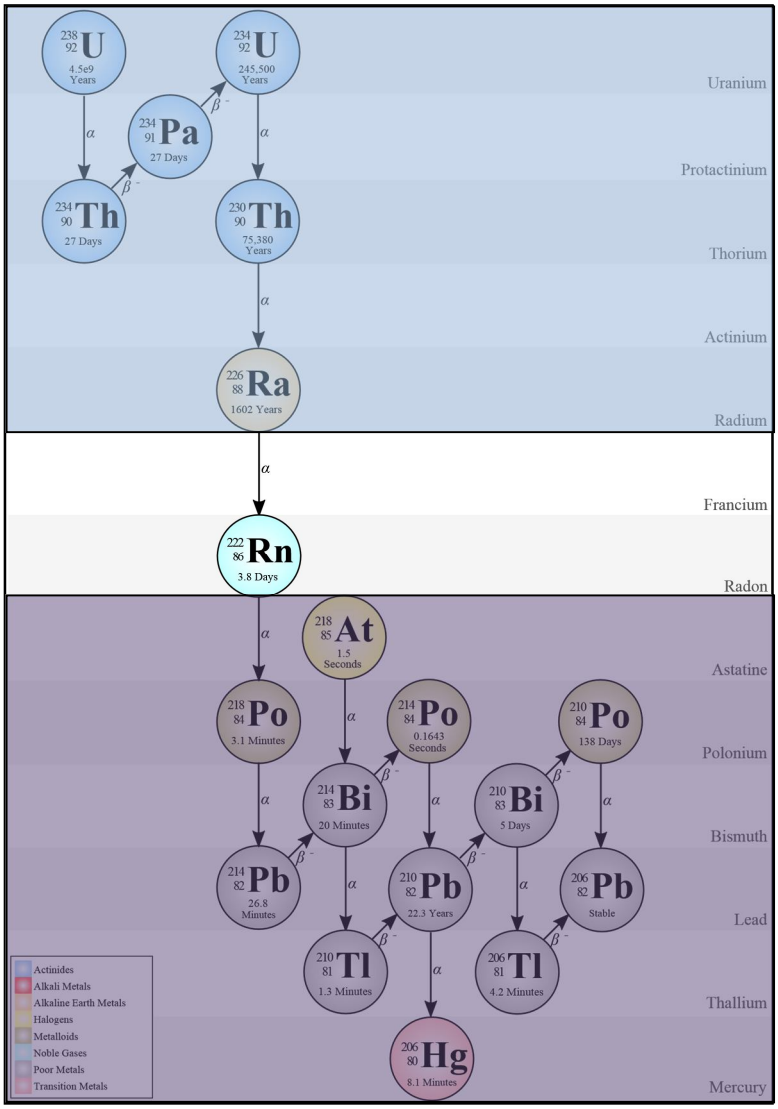

Figure 2-6: Natural α- and β-decay series of ^{238}U with each radionuclide's half-life shown.

Table 2-2: Table of the radionuclide isotopes of radon with the nuclear characteristics: decay modes, half-life and excitation energy (Audi, 2003; De Laeter, 2003; Wieser, 2006).

Radionuclide Symbol	Historic Name	Z(p)	N(n)	Isotopic mass (u)	Half-life	Decay Modes	Daughter Isotope
^{219}Rn	Actinon Actinium emanation	86	133	219.0094802 (27)	3.96 (1) s	α	^{215}Po
^{220}Rn	Thoron Thorium emanation	86	134	220.0113940 (24)	55.6 (1) s	α	^{216}Po
						$\beta^-\beta^-$ (rare)	^{220}Ra
^{221}Rn		86	135	221.015537 (6)	25.7 (5) min	β^- (78%)	^{221}Fr
						α (22%)	^{217}Po
^{222}Rn	Radon Radium emanation Emanation Emanon Niton	86	136	222.0175777 (25)	3.8235 (3) d	α	^{218}Po

2.4.3 Chemical and physical properties

Radon is a naturally occurring radioactive noble gas which is colourless, tasteless, and odourless. Radon's valence electron structure is occupied (noble gas) and will not react chemically. The non-magnetic monatomic gas has a high density of about 9.73 kg/m^3 at standard temperature and pressure and is soluble in water.

2.4.4 Transport mechanisms

Radon displaces in space and time either by diffusion or by carrier mediums. Consequently, these transport mechanisms are characterised and elaborated upon below:

2.4.3.1 Diffusion

Radon under standard temperature and pressure is in a gas phase. One of the fundamental mechanisms whereby radon moves as a function of space and time is diffusion. The geometric mean indoor radon in-air activity concentration is 45 Bq/m^3 (UNSCEAR, 2008).

Radon turbulent diffusion depends on a range of elements such as pedology (Kojima et al., 1999), geology (Ball et al., 1991) and atmospheric conditions (Porstendörfer et al., 2009). Diffusion is the progression of atoms/molecules from a region in space with high concentrations towards regions with lower concentrations as a function of time. The two main macroscopic parameters which govern diffusion are temperature and pressure defined with the Boltzmann's kinetics equations.

2.4.3.2 Movement of air masses

Air masses act as a carrier medium for radon (Crawford et al., 2009; Crawford et al., 2015). If radon displaces into the atmosphere, the atmospheric dynamics will act as a carrier system (see figure 2-7). The natural isotopic tracer is of particular use in atmospheric sciences (Crawford et al., 2015) and environmental sciences (Slemr, 2013; Crawford et al., 2015). Continental air masses contains up to a factor of three times more radon compared to oceanic air (Crawford et al., 2015), thus making radon a valuable natural radionuclide for air-mass classification (Brunke et al., 2002; Crawford et al., 2009).

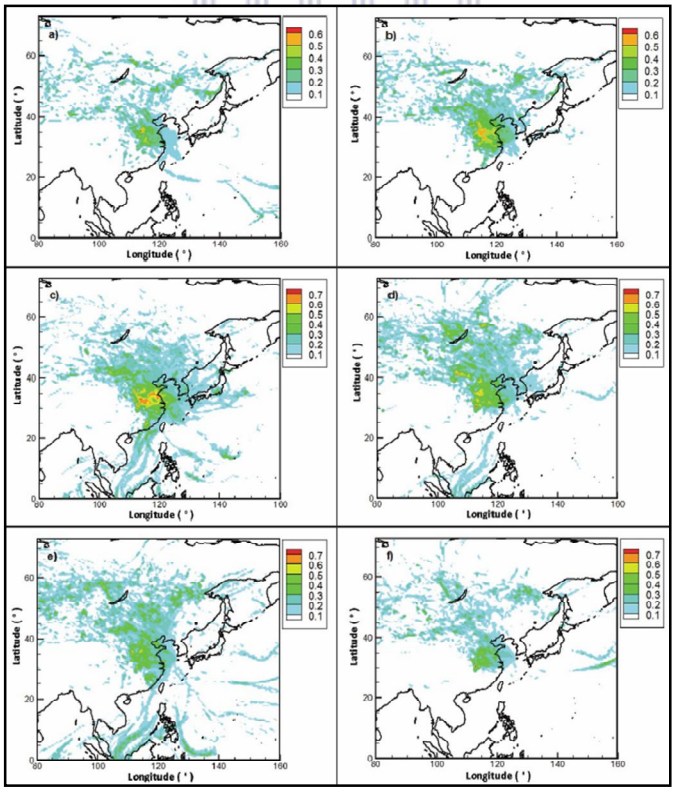

Figure 2-7: Seven days back trajectories incorporating radon in-air measurements for atmospheric pollution studies (Crawford et al., 2015).

2.4.3.3 Movement of soils and rocks

The displacement of soil and rock containing radon or radon-producing radionuclides (see figure 2-6, blue-tinted section) acts as a carrier medium. The movement of soils and rocks can be categorised as creep, slumping, flows, and fall (see figure 2-8). The unstable ^{226}Ra atom undergoes α-decay; when an α-particle is ejected with the ^{222}Rn atom, it occurs in the opposite direction (alpha recoil) with the distance of 0.02 to 0.07 µm (Durrani and Ilic, 1997). The alpha recoil mechanism acts as a radon emanation process to release it from the solid carrier medium such as rocks.

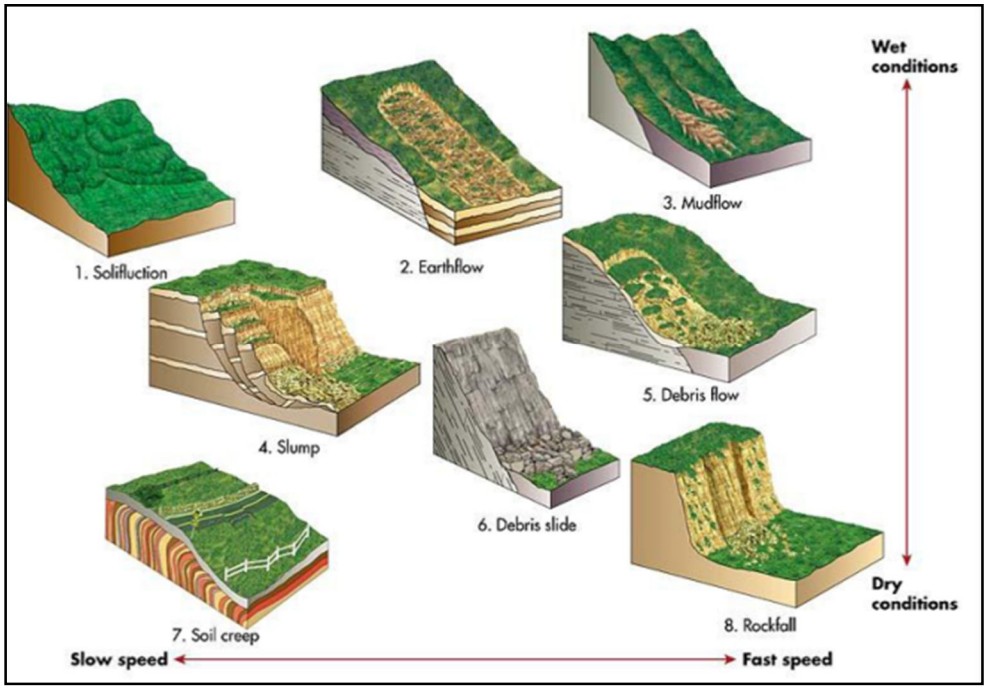

Figure 2-8: The mass movement of soils and rocks (erosion) down a slope (Study Blue, 2016).

2.4.3.4 Hydrology

Hydrology provides insight into how NORMs are transported within water bodies in nature. Radon-in-water could be in one of two potential states: supported or unsupported. A supported system is referred to when ^{226}Ra levels are present in a specified system and will produce radon. Unsupported are referring to a situation where no "new" radon can be produced within a particular system based on the fact that no to small amounts of ^{226}Ra is present.

The natural radionuclide activity levels of ^{238}U, ^{226}Ra, and ^{222}Rn in groundwater with granite geological structures are systematically higher than for gneiss/metasedimentary/metavolcanic rocks (Vinson et al., 2009). The mobility and absorption of radium in groundwater depends on the chemical properties, such as the following:

- pH (Vinson et al., 2009, Cecil, 1987; Dickson and Harczeg, 1992; Bolton, 2000; Szabo, 2005);
- salinity (Kraemer et al., 1984; Sturchio et al., 2001;Wood et al., 2004; Vinson et al., 2009);
- reducing conditions respect to barite ($BaSO_4$),(Szabo and Zapecza, 1987; Herczeg et al.,1988);
- microbial sulfate reduction affecting barite (Phillips et al., 2001; Martin et al., 2003);
- microbial Fe (III) reduction (Landa et al., 1991);
- supersaturation with respect to barite (Gilkeson et al., 1984; Grundl and Cape, 2006); and
- redox processes (Vinson et al., 2009).

In general, there exist a substantial disequilibrium (inverse proportionality) between uranium, radium and radon in groundwater because of geochemical conditions (Vinson et al., 2009). The disequilibrium between the mentioned natural radionuclides is especially prevalent when crystalline rocks are present (Vinson et al., 2009). For instance, the activity levels of uranium might be high, while being low in radium and radon (Asikainen, 1981b). Some studies indicated groundwater where radon-in-water activity levels are a magnitude higher compared to radium (King, 1982; Wanty et al., 1991) or high in radium in-water activity but low in uranium, particularly within anoxic waters (Andrews et al., 1989).

2.4.3.5 Technologically enhanced carrier systems

The technological processes associated with hydraulic fracturing to extract shale gas could also act as a mechanism to transport NORMs. Technologically enhanced naturally occurring radioactive material (TENORM) could be transported by hydraulic fracturing (see section 1.1.1) either by the retrieved wastewater or during the shale-gas extraction phase (see figure 1-1).

Production fluids extracted to ground level could contain natural radionuclides such as ^{220}Rn, ^{222}Rn, ^{226} Ra, ^{228}Ra, ^{234}Th, and ^{238}U, when the bedrock in which the hydraulic fracturing well and fractures was created, contains these NORMs. For example, the Marcellus hydraulic fracturing wastewater contains elevated levels of these NORM (Vengosh et al., 2014; Warner et al., 2013a; Warner et al., 2013b; Haluszczak et al., 2013; Rowan et al., 2011).

Shale gas extracted to the surface could act as the gas carrier medium, particularly for radon and thoron. If the bedrock surrounding the created fractures contains ^{226}Ra and ^{224}Ra, then it is likely that radon and thoron will be observed within the extracted shale gas, respectively.

CHAPTER 3 RADIONUCLIDE METROLOGY

Radon (^{222}Rn) was the principal NORM measured within groundwaters of the Karoo Basin. Two different measuring techniques were utilised to conduct radon-in-water activity concentration measurements: α-spectrometry (section 2.4) utilizing DURRIDGE RAD7 detectors and γ-spectrometry utilizing a hyper-pure germanium (HPGe) detector. This chapter describes the different experimental measurement setups, metrology methodologies, and detection optimisation methods of radon-in-water measurements. Additional subsequent measurement results were included in this study, namely elemental uranium concentrations and radium activity concentration (^{226}Ra and ^{228}Ra). In section 3.8 and 3.9 a brief overview of sampling and measurement techniques regarding these additional results is given.

3.1 Introduction

Radon in water, air, and solids can be measured either by direct or indirect nuclear decay mechanisms such as alpha (α), and gamma radiation (γ, see section 2.4.1). The indirect method of measuring radon refers to the detection of radon decay progeny (^{218}Po, ^{214}Pb, ^{214}Bi, ^{214}Po, ^{210}Pb, ^{210}Bi ^{210}Po, and more, see figure 2-6). The direct method of measuring radon refers to measuring α particles (E_α = 5.489 MeV). An indirect method of measuring radon-in-water was also applied during this study.

Due to the relatively short half-life of radon (3.82 days), the minimization of the duration between sampling and measurement is important, especially when working with low activity samples. In-situ measurement approach is therefore favoured. Measuring radon activity concentrations at an off-site laboratory is most favourable, if:

- the detection system has a low, lower level of detection (LLD);
- unsupported radon-in-water sample; and
- sample activity is above the LLD during the time of measurement (radioactive decay corrections can be applied).

The primary radon detector system utilized in this study was the α-spectrometry using a DURRIDGE RAD7 detector (see section 3.2). A γ-spectroscopy high-purity germanium

detector (HPGe-detector) at iThemba LABS was utilized to perform radon and radium in-water activity concentration measurements for this study.

3.2 RAD7 radon and thoron detection system

3.2.1. Introduction

Several types of commercial continuous radon (CR) detectors are available on the market. Almost the entire range relies on α-spectroscopy as the main radiation detection method. It's considerably challenging to maintain both a low background and high sensitivity for mobile β and γ CR detectors. The in-situ continuous radon (^{222}Rn) and thoron (^{220}Rn) measurement system, the RAD7, has five different measurement modes (see section 3.2.3).

The RAD7 detector can be combined with a range of additional equipment produced by the manufacturer, DURRIDGE. The RAD H2O kit and DRYSTICK ADS-3R were extensively used in this study. This is discussed in section 3.2.5 and 3.2.6, respectively.

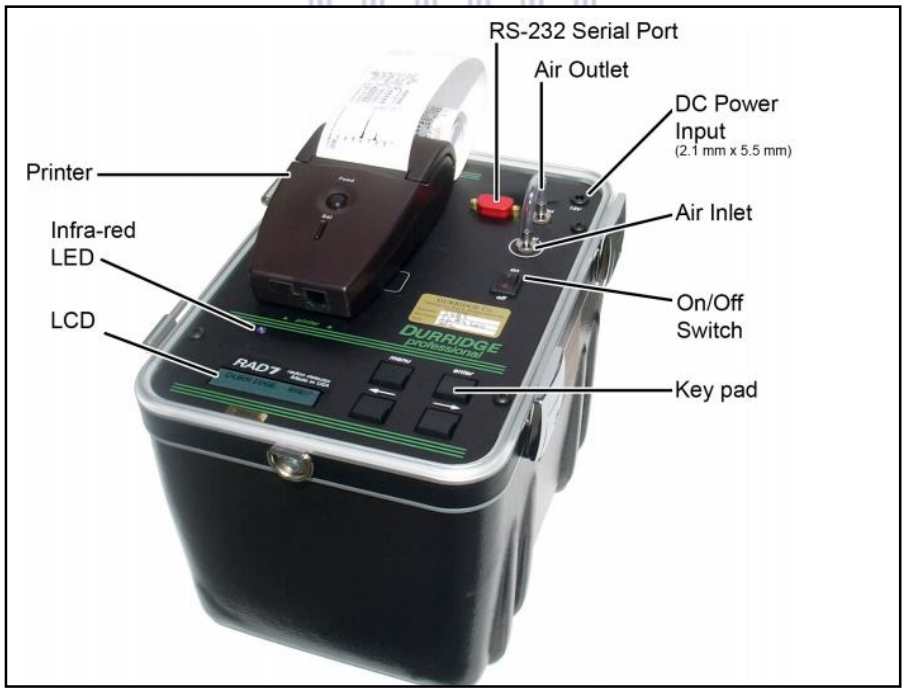

Figure 3-1: The RAD7 detector: radon and thoron activity concentration detection instrument with mobile infrared printer (RAD7, 2015).

3.2.2. Overview of the RAD7 detector

The RAD7's detection chamber (see figure 3-2) consists of a 0.7 L internal chamber coated with an electrical conductor and a solid-state planar silicon detector section. The RAD7 utilises ion-implantation technology by accelerating charged radon decay progeny onto a solid state planar silicon detector. The induced electrical field on the conductor accelerates the positively charged radon decay particles: ^{218}Po ($T_{1/2}$ = 3.05 min, E_{α} = 6.00 MeV) and ^{214}Po ($T_{1/2}$ = 164 µs, E_{α} = 7.69 MeV) onto a silicon detector unit. A carrier medium of ambient air with the relative air humidity (RH) of below 10% is used to transfer radon and decay progeny to the silicon detector (see section 3.2.5). The RAD7 detector is required to be calibrated every 12 to 15 months. The RAD7 detectors used in this study were all within the specified calibration window. A brief overview of the RAD7 detection system manufactured by DURRIDGE Company Inc. (RAD7, 2015):

Table 3-1: Metrology specifications of the RAD7 detector

Real-time α-spectrometry measurement
Passivated ion-implanted planar silicon detector
Radon concentration detection range: 4.0 - 750 000 Bq/m^3
Intrinisic background: 0.2 Bq/m^3 (or less)
Measurement accuracy: ± 5% (absolute)
Weight: 4.35 kg
Radon & thoron activity concentration measurements of air, water, soil, rock samples.

Figure 3-2: Inside components of RAD7 detector (side view) with the detection chamber visible in the centre. (Tan et al., 2014).

3.2.3. Measurement modes

The RAD7 detector system has five different measurement modes. The measurement duration are referred to as the cycle, the amount of times the cycle is repeated is referred to as the recycle. The measuring modes are as follows:

- **Sniff mode**: This mode is most applicable, if a rapid response time is required for real-time fast changing radon in-air activity concentration measurements; however, it in general compromises on statistical accuracy by measuring only the ^{218}Po decays (E_α = 6.00 MeV).
- **Normal mode:** Both the ^{218}Po (E_α = 6.00 MeV) and ^{214}Po (E_α = 7.69 MeV) decays are counted to determine the radon activity concentration with superior statistical accuracy and applicable to long-term continuous measurements. This mode can only be applied for measurement times larger than three hours, since equilibrium of longer-lived radon decay progeny is essential.
- **Auto mode:** Both the Sniff and Normal mode are utilized with the Auto mode. The Auto mode measurement is initiated with the Sniff mode and then the system switch to the Normal mode after three hours of continuous measurements.

- **Wat-40 mode:** This mode is designed specifically to measure radon activity concentrations in water samples. The Wat-40 mode measurements are performed with 40 mL vials. The default measuring sequence is discussed in section 3.2.6 and 3.4.
- **Wat-250 mode:** This mode is identical to the detection method described above; apart from that, a 250 mL and not a 40 mL glass container is used. A customised Wat-250 mode was mostly utilised for radon-in-water activity concentration measurements within this study and is discussed in section 3.2.6 and 3.5.

3.2.4. Data Acquisition and analyses

Automated data acquisition is controlled by a microprocessor on-board the RAD7. Real-time data analyses of results can be viewed on the RAD7 display unit and also on a PC by running the Capture software (figure 3-3). The signals generated by the detection of α-decays are binned into 200 energy channels based on associated α-energy (RAD7, 2015). The detection α-energy (E_α) for the system ranges from 0.00 to 10.00 MeV (E_α = 0.05 MeV per channel). The relevant E_α range for detection of radon and also thoron is from 6.00 to 9.00 MeV. The α-energy ranges are grouped into eight bins, evenly distributed "windows" for analysis (see figure 3-5).

Data analyses can be performed with the software package (Capture) created for the RAD7 detector (see figure 3-4). The main window consists of sub-windows: main analyses window with different measurement recycles (shaded red area), spectrum for selected points (blue area) and summary of measurement parameters and results (green area, see figure 3-4.) Capture can also be utilised as a multifunctional tool from which the entire detection system can be remotely operated (see figure 3-3).

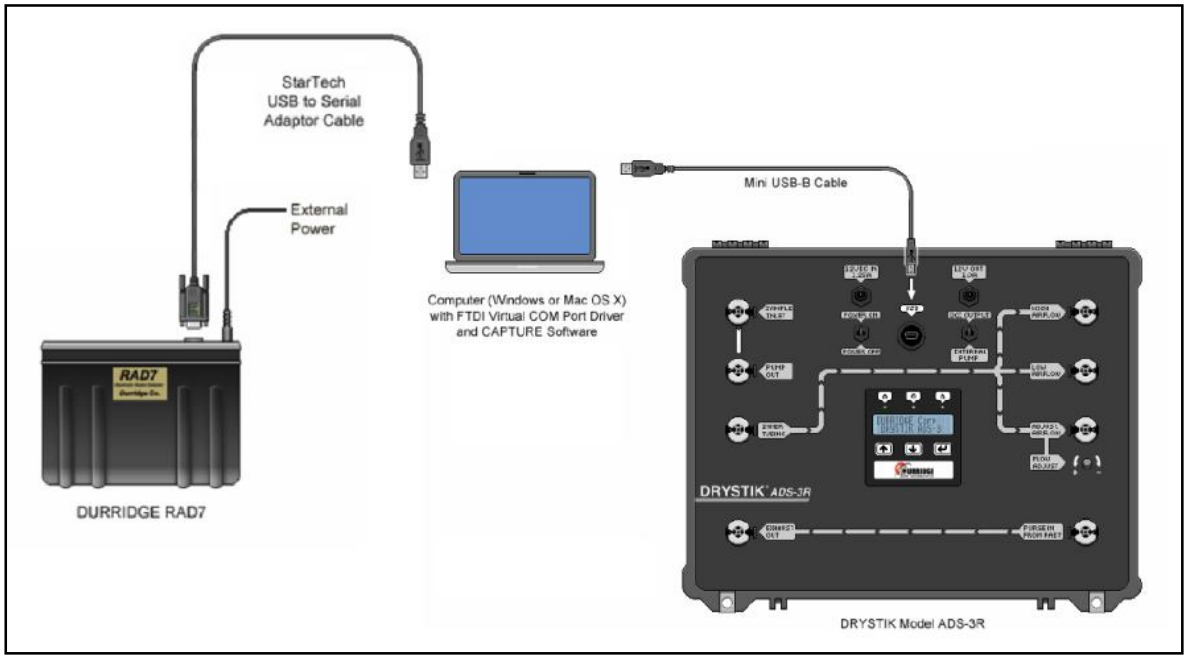

Figure 3-3: Setup configuration between computer (Capture Software), RAD7 detector/s and DRYSTICK ADS-3R unit (Capture, 2016).

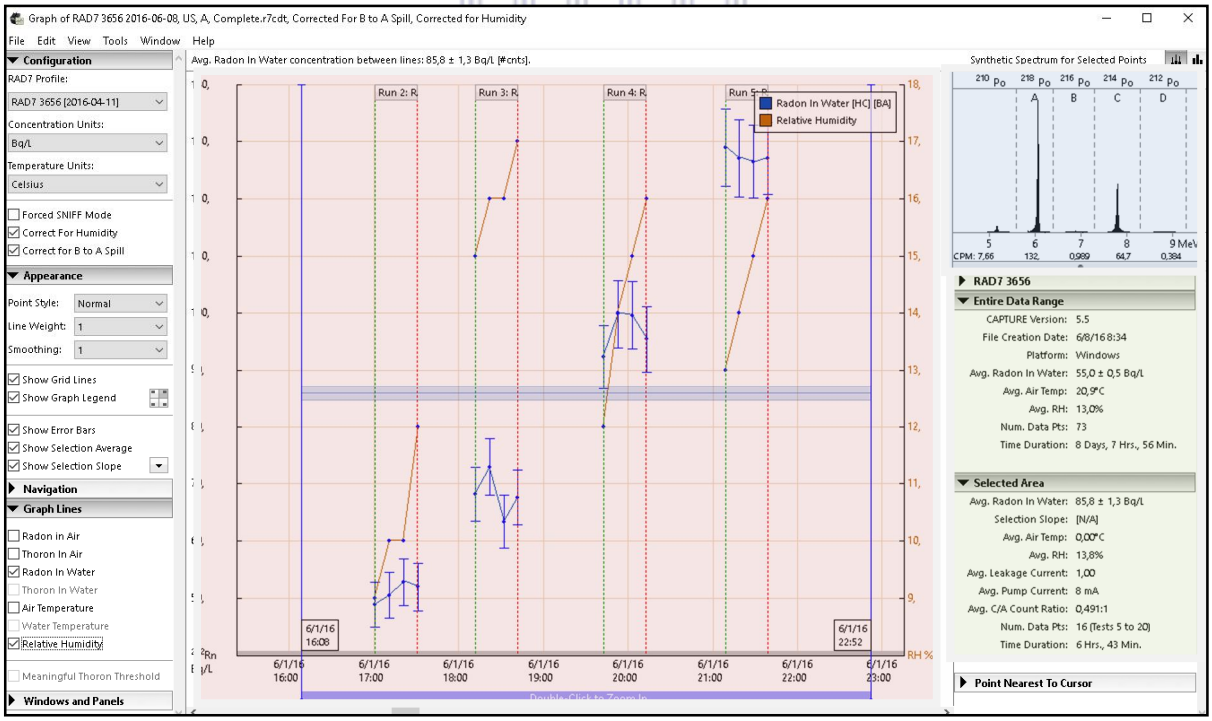

Figure 3-4: Data analyses making use of the Capture Software (screenshot).

Figure 3-5: Print-out of radon-in-water activity concentration measurement results (four recycles), measurement parameters (Relative Humidity (RH), detector chamber temperature and battery voltage (B)) and cumulative run spectrum making use of the infrared-printer (see figure 3-1).

The Capture software package is useful to obtain a brief, real-time overview of the measurement results and operational parameters. Nonetheless, more comprehensive data analyses were performed with a code developed in MATLAB (see Appendix; code 1 and code 2) and Microsoft Excel (see section 3.2.6). No radon activity concentration decay corrections have been performed within this study. The average duration between sampling and a radon measurement was averagely about 5 hours. By making use equation 2-3 and 2-6 (see section 2.2) to perform a decay correction and using, for instance, the highest observed radon-in-water activity concentration of 183 ± 18 Bq/L (see Appendix, table 1, S22) and the average decay duration of 5 hours (t). This sample (S22, F1) would have decayed by 7 Bq/L during the 5 hours of duration between sampling and measurement. Now taking into consideration that radon measurement uncertainty of 18 Bq/L, the decay correction of 7 Bq/L is thus not applicable. Thus the general rule was followed that if the radon decay correction was larger than the measurement uncertainty then a decay correction was made. Thus for all the radon activity concentration measurement, no decay corrections were performed. This is one of the advantages of having a mobile radon measurement system and being able to

perform measurements as soon as technically possible after sampling. As discussed two RAD7 detectors were used to measure an identical sample. The differences in the measured radon-in-water from the two detectors were almost always within measurement uncertainty (see Appendix, table 4). The representative radon-in-water activity concentration for a sample discussed in study was calculated by taking the average (mean) of the two radon-in-water measurements.

3.2.5. Practical aspects of RAD7 measurements

Purging is a crucial metrology component to ensure accurate and precise radon measurements when making use of the RAD7 detector system. The purging technique refers to making use of an internal air pump to inject ambient air into the detection system (chamber). Two different purging approaches can be followed: a closed-loop approach or an open-loop approach. With open-loop purging setup the air outlet (RAD7, see figure 3-1) or exhaust port (DRYSTICK, see figure 3-3) flows into the atmosphere. When the air outlet (RAD7, see figure 3-1) or exhaust port (DRYSTICK, see figure 3-3) are connected to the system's inlet port, it is referred to as closed-loop purging setup. The two main reasons for purging are described below.

In the scenario when radon measurements were made for samples with a high activity concentration (over 40 Bq/L), radon and associated decay progeny (see figure 2-6) will remain active within the detection chamber until it decays unless removed (purged) which will affect the accuracy of new measurements (RAD7, 2015). Based on section 3.2.3, one has to remove ^{222}Rn ($T_{1/2}$ = 3.82 days, E_α = 5.590 MeV), ^{218}Po ($T_{1/2}$ = 3.05 min, E_α = 6.00 MeV), and ^{214}Po ($T_{1/2}$ = 164 µs, E_α = 7.69 MeV) isotopes from previous measurements in the detection chamber. By making use of open-loop purging, the α-signature background removal process will be most efficient. In reality, both decay and open-loop purging are applied after a radon measurement is performed. In general, an open-loop purge is performed for a minimum of ten minutes before and after measurements. Before each measurement, the efficiency of the open-loop purge is verified by real-time analyses of the count rate in window A (^{218}Po) and window B (^{214}Po) (see figure 3-4). The intrinsic background of the long-lived radon daughter isotopes (^{210}Pb, $T_{1/2}$ = 22.3 years) should also be taken into consideration. The long-lived isotope ^{210}Pb ($T_{1/2}$ = 22.3 years) undergoes β-decay to ^{210}Bi ($T_{1/2}$ = 5 days) which progeny undergoes β-decay to ^{210}Po ($T_{1/2}$ = 138 days, E_α = 5.30 MeV). The β-decaying radon

progeny will have no effect on the radon measurements when making use of the RAD7 detector system.

The other functional aspect of purging is to remove the water (air moisture) within the measurement system, particularly within the detection chamber (see figure 3-2). Since α-decay has a localized decay track (around ten µm), the water content in the air can act as an attenuation medium during ion-implantation, which will affect the accuracy of measurements. Thus it is recommended that the relative humidity (RH) inside the detection chamber be kept below 10% during measurement, even though humidity corrections can be applied with recent changes to the Capture software (Capture, 2016). The closed-loop purging method is highly efficient in reducing the RH of the system; however not for removing the α-background. The three core components for reducing the RH in the RAD7 system are small desiccant drying tubes (figure 3-6 (B)), large laboratory desiccant drying tube (see figure 3-6, (A)), and the DRYSTICK (ADS-3R) unit (see figure 3-6, (A)).

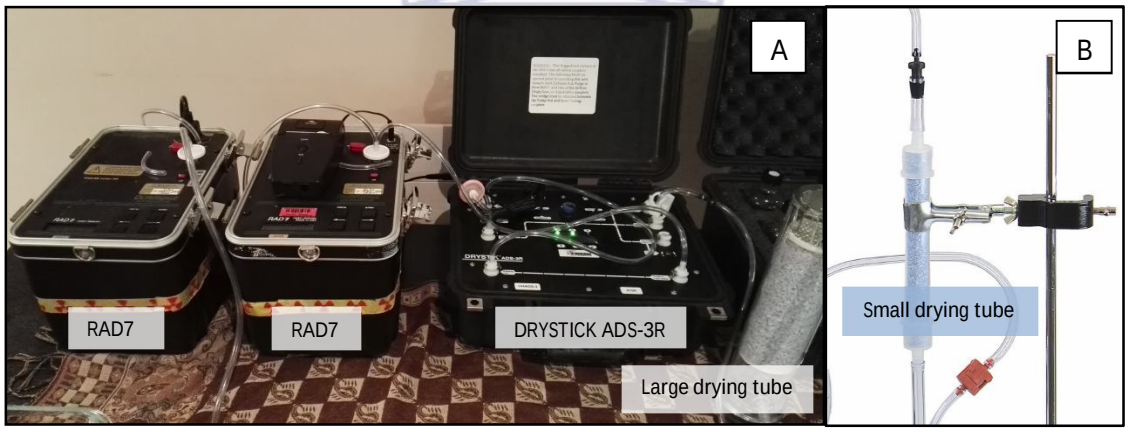

Figure 3-6: DURRIDGE manufactured components to reduce RAD7/s relative humidity (RH): DRYSTICK ADS-3R (A), large laboratory desiccant drying tube (A) and small desiccant drying tube (B).

The problems with desiccant drying tubes are that with long-term continuous measurements and high relative humidity conditions, the drying agent needs to be replenished on a regular basis. The DRYSTICK unit's primary function is to reduce RH by an active moisture exchange technology; Nafion ® membrane tubing (see figure 3-7). The DRYSTICK does not need to be replaced with regards to a drying agent during measurements even with high-flow rates (DRYSTICK, 2015). A secondary advantage of using this unit is the programmable Duty Cycle Controller (DCR), on which customised air-flow pumping protocols can be created. This programmable pumping protocol is not currently possible on the RAD7's

pumping system. It is important to ensure that when the DRYSTICK ADS-3R unit's air pump is used that the RAD7's internal air pump is switched off. The results from long-term (three days), hourly radon in-air activity concentration measurements to illustrate the effectiveness of the DRYSTICK ADS-3R are shown in figure 3-8. A RH average of 3.2% was obtained during this continuous three-day measurement. A DRYSTICK ADS-3R unit was utilised in this study for purging applications.

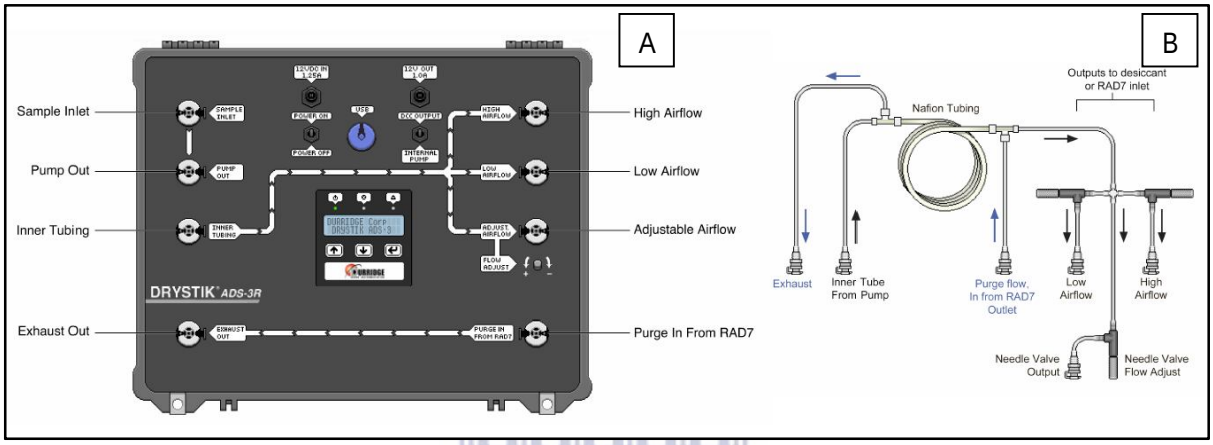

Figure 3-7: DRYSTICK ADS-3R instrument (A) and associated internal pump airflow structure (B) which was utilized in this study (DRYSTICK, 2015).

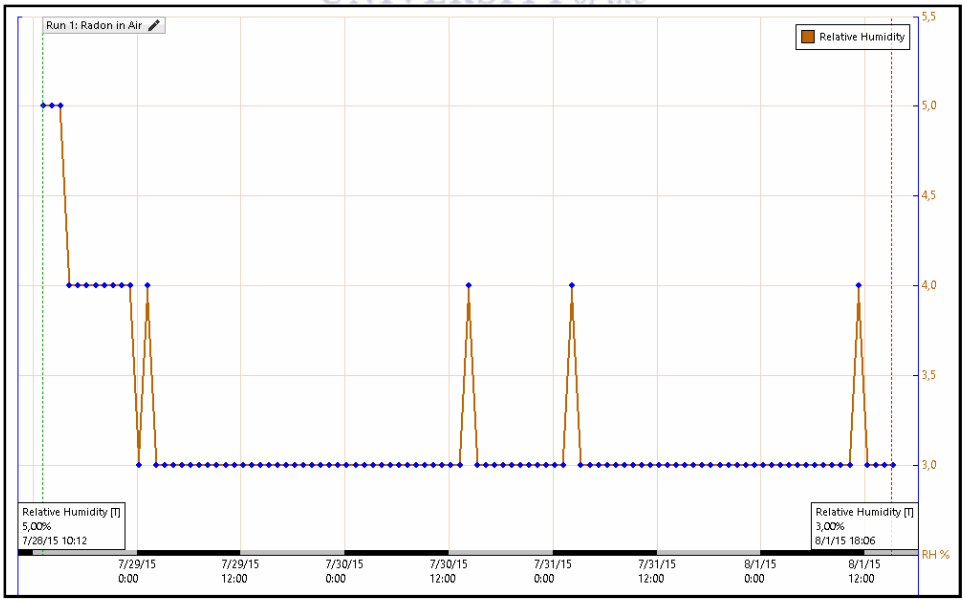

Figure 3-8: Radon detector chamber's relative humidity (RH) results for a three-day, hourly temporal resolution measurement making use of the DRYSTICK ADS-3R.

3.2.6. Radon-in-water measurement set-up

The radon-in-water measurements in this study were performed with three RAD7 detectors. On each of these field trips (F1 to F3), two RAD7 detectors were utilised at a given time (see figure 3-10). The experimental set-up utilised to do these measurements is illustrated in figures 3-9 and 3-10.

As mentioned above, the carrier medium for radon from samples (air/water/soil) to the RAD7 detection system is ambient air. The process of extracting the dissolved radon within a liquid sample such as water to the carrier medium is referred to as the aeration (see figure 3-9 (B)). The aerator assembly (B) has an adjustable glass frit height (RAD H2O, 2016) = a mm: 250 mL vial setup (a = 115 mm) and 40 mL vial setup (a = 40 mm). The aeration process takes place in the aerator assembly where the air is pumped through a glass frit (see figure 3-9 (B)). The turbulent air flow (bubbles) created by the frit (see figure 3-10) extracts the radon from the water into the air, from which it flows to the RAD7 detector for detection. By making use of the closed-loop radon extraction process (see figure 3-9 (A)), extraction efficiencies of (RAD7 air-pumping system) for a duration five minutes of aeration of 99% for the 40 mL vials and 94% for a 250 mL vials can be achieved (RAD H2O, 2016).

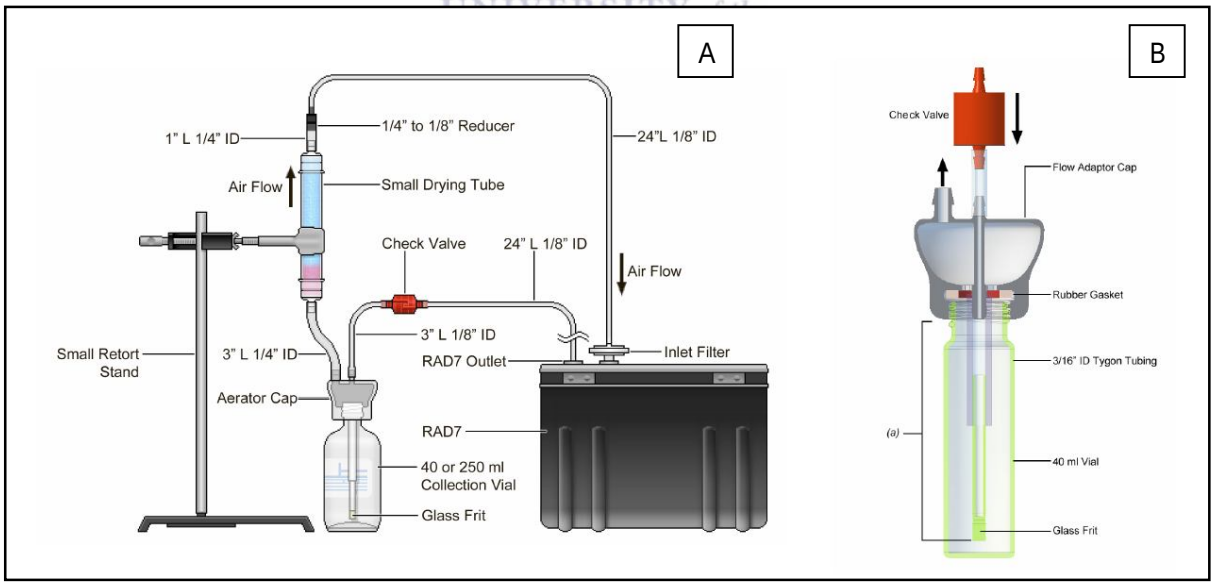

Figure 3-9: Conventional setup (A) utilized to conduct the radon-in-water activity concentration measurements (RAD H2O, 2016).

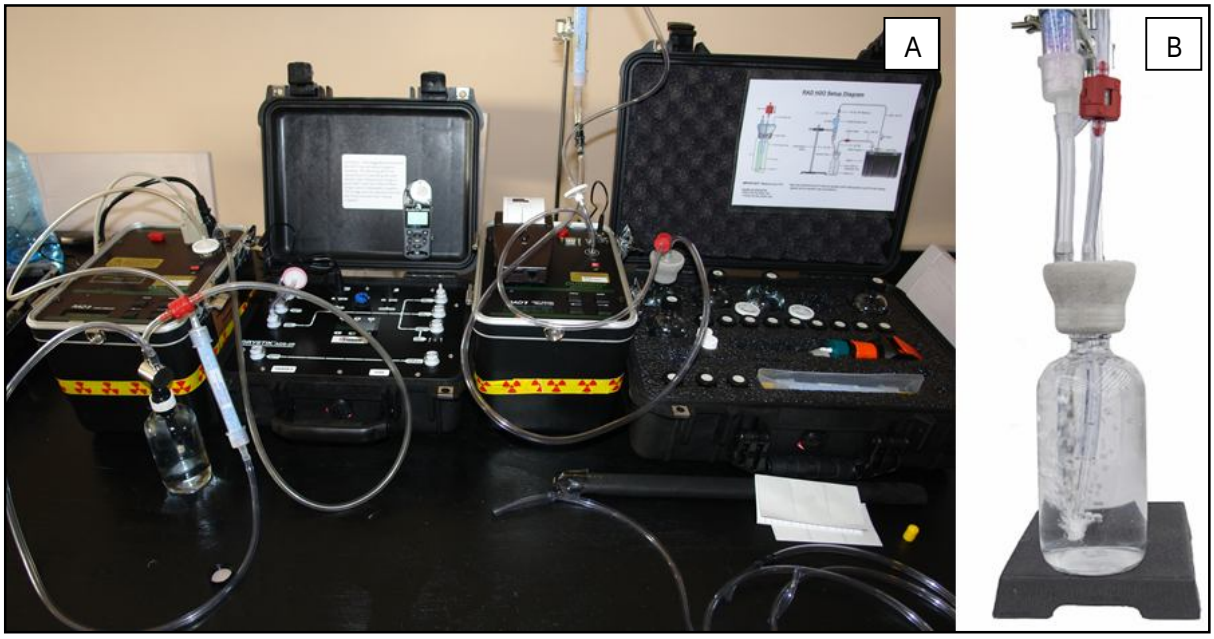

Figure 3-10: Experimental setup (A) to conduct the radon-in-water activity concentration measurements as illustrated in figure 3-9. Aeration process (B) in progress to extract the radon from the water to the air (carrier medium) for a 250 mL vial (RAD H2O, 2016).

The three RAD7 detectors which were used in the study:

- Det. A: RAD7 detector A (iThemba LABS equipment)
- Det. B: RAD7 detector B (University of the Western Cape equipment)
- Det. C: RAD7 detector C (Stellenbosch University equipment)

3.3 Measurement Uncertainties

Radioactive decay conforms to Poisson statistics, where the standard deviation (1 σ) is the square root of the total count. Poisson statistics underestimates the measurement uncertainty at low count rates (RAD7, 2015). To avoid this underestimate the calculation of the radon activity concentration's uncertainty are calculated with the RAD7 as follow:

$\sigma = 1 + \sqrt{N + 1}$, where N is the number of counts (RAD7, 2015). A large measurement uncertainty with the RAD7 is the result of trying to measure low radon activity concentration within a short measurement duration (cycle).

Based on the relatively small data sets in this study the uncertainty in the arithmetic mean (average or mean) was calculated as follow:

- Mean (x_{avg}): $x_{avg} = \frac{1}{N}\sum_{i=1}^{N} x_i$, where i = 1,2,…,N
- Range (R): $R = x_{max} - x_{min}$
- Uncertainty in the mean (Δx_{avg}): $\Delta x_{avg} = \frac{R}{2\sqrt{N}}$.

3.4 Sampling procedure

Water sampling for radon-in-water measurements is not a complicated task; nonetheless, if non-systematic and incorrect techniques are applied, it can affect the results by up to ± 20% (RAD H2O, 2016). The following order and systematic sampling procedure is recommended for taking multiple samples from the same source. This procedure was applied during the three measurements series (F1 to F3):

I. ensure the water source is as "fresh" as possible by adequate "bleeding" of the system to remove stagnant water. A standard approach utilized in the field of hydrology is to perform continuous electrical conductivity (EC) measurements (see figure 3-11) until a non-fluctuating reading is obtained and then proceed with sampling.
II. create a tubing system from the source (ex. borehole outlet) to produce and sustain a laminar flow.
III. flush the container and sampling vials with the water from the source to remove potential water from previous sampling sessions and also to ensure that all flushing water is drained.
IV. fill a container (see figure 3-12 (A)) with water using a laminar flow from the source and minimise the formation of bubbles i.e. reduce aeration.
V. immediately after the container has been filled, submerge the vials' top piece to just below the water surface level (tilted) in the container and fill the vials without creating bubbles. When the vials are filled to the top, submerge them completely underneath the water and seal adequately beneath the water surface (see figure 3-12, B).

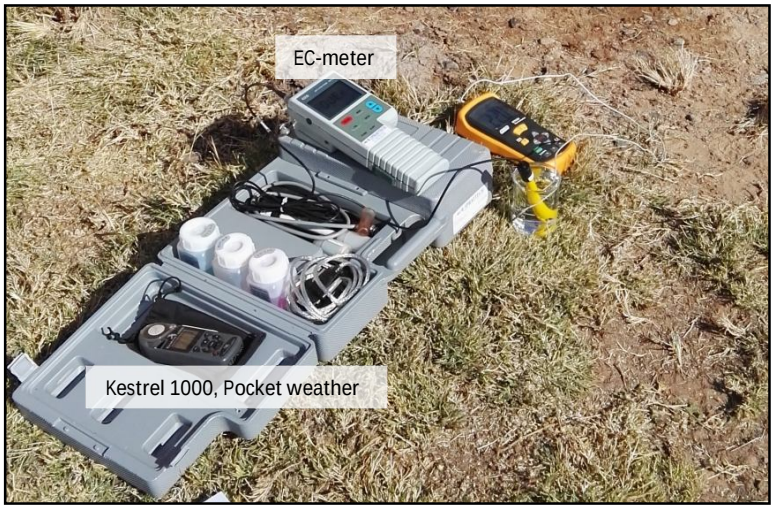

Figure 3-11: In-situ electrical (EC) conductivity measurement of water sample during pre-sampling stages by making use of the JENCO 6350 detection system and meteorological Kestrel 1000 detection system to measure air temperature.

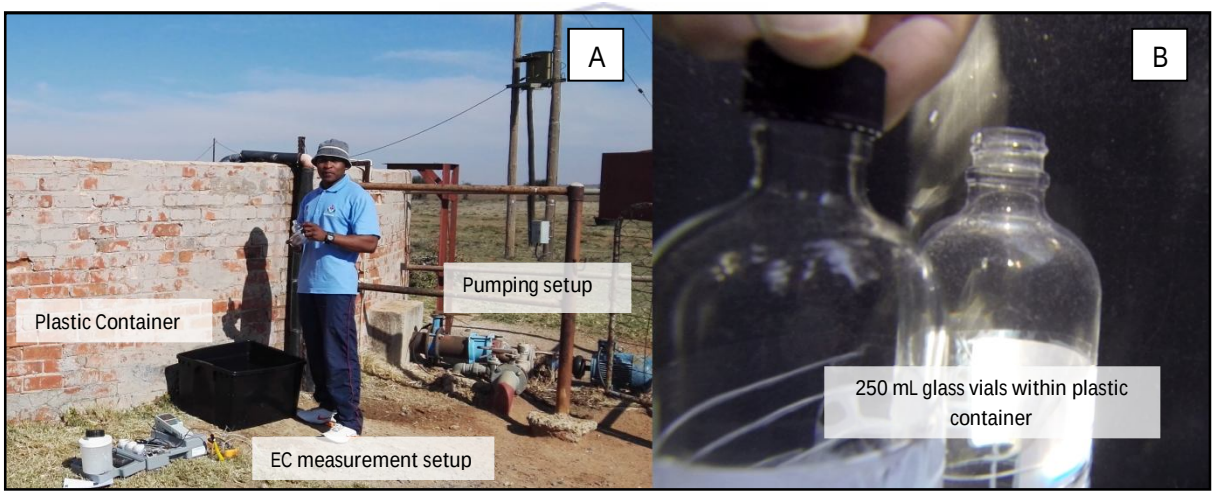

Figure 3-12: Sampling setup on-site (A) with the large black container filled which was used to fill the 250 mL glass vials (B), for radon-in-water activity concentration measurements.

A minimum of two 250 mL glass vials were filled per specific source or sampling location. The 250 mL vials were filled at the same time from the same container (source). The option is available to perform sampling also with the 40 mL glass vials. However larger sample sizes (250 mL vials) will produce a greater number of counts during measurement and consequently improve counting statistics (see section 3.7.1). The benefit of sampling in larger glass vials such as the 250 mL ones becomes important when a low radon activity concentration sample is measured (RAD H2O, 2016).

3.5 Measurement Protocol and Setup (F1)

As mentioned in section 3.2.3, the predominant mode utilised for the radon-in-water activity concentration measurements was the WAT-250 protocol. The WAT-250 protocol is a standard measurement sequence applied for the first measurement series (F1):

1. Pre-measurement purging: closed and open-loop between five and 15 minutes (added to the WAT-250 protocol)
2. Aeration for five minutes of the 250 mL glass vials during which a radon-in-water extraction efficiency of 94% can be delivered (see section 3.2.6)
3. An idling time for five minutes to achieve equilibrium between radon concentration in the water in the glass vial and air in the detection system
4. An idling time for five minutes to achieve equilibrium between ^{218}Pb and ^{222}Rn
5. Four runs (recycles) where five minutes of measurements (cycles) are performed
6. Post-measurement purging: open-loop between five and 15 minutes (added to the WAT-250 protocol)

The duration of a measurement (cycle) can be increased which will consequently improve the counting statistics. For the first field trip for measurement series (F1) a considerable number of sites (42) were sampled in a short time frame. The shortest technical measurement duration was consequently thus chosen. The complete radon-in-water measurement duration for a single sample is between 55 and 65 minutes.

3.6 Measurement protocol and set-up (F2)

During the second measurement series (F2) fewer samples per day had to be measured for radon. Thus, more time was available to increase the measurement duration (cycle) which improved the counting statistics. The following customised WAT-250 protocol was used for the second field trip (F2):

1. Pre-measurement purging: closed and open-loop between five and 15 minutes (added to the WAT-250 protocol)
2. Aeration for a duration of five minutes for the 250 mL glass vials
3. An idling time for five minutes to achieve equilibrium between radon in the water within the glass vial and the air in the detection system.

4. An idling time for five minutes to achieve equilibrium between ^{218}Pb and ^{222}Rn
5. Four cycles of 10 minute measurements
6. Post-measurement purging: open-loop between five and 15 minutes (added to the WAT-250 protocol)

3.7 Measurement protocol and set-up (F3)

The same customised measurement protocol (WAT-250) from the second field trip (see section 3.6) was used during the third field trip (F3) also with the increased 10 minute measurement duration (cycle).

3.8 Radon-in-water metrology optimisation

Radon-in-water measurements using the RAD7 detection system can be optimised by applying the following aspects:

3.8.1. Volume of sampling vials

The volume of the sampling vial is a parameter which affects the radon-in-water measurements. When the vial volume is very small (< 40 mL), less radon activity would be available for detection compared when for instance a larger volume vial size is sampled. With a scenario of a low radon activity sample (± 0.4 Bq/L) and a small volume vial (40 mL), the radon activity concentration could be below the lower level of detection (sensitivity) for the RAD7 (0.4 Bq/L). If the vial volume, however, becomes too large (above 2.5 L), then you have to be particularly careful to ensure that the aeration assembly can extract the radon from the water into the air (see figure 3-9).

A simple experiment was conducted using the standardized measurement protocol mentioned in section 3.4 (Wat-250 protocol) to analyse the effect of the vial size volume on the radon metrology. Water was sampled (source) from a tourist hot springs resort near Montagu (South Africa) which is known to contain elevated average radon-in-water activity concentration of 205 ± 6 Bq/L (Botha et al., 2016). The radon "rich" hot spring water was sampled at the same time in both 250 mL and 40 mL vials. Radon-in-water activity concentration measurements were performed at different times of the radioactive decay. The aim was to get an indication

how the different vial sizes affect the radon-in-water measurements at activity ranges (see figure 3-13).

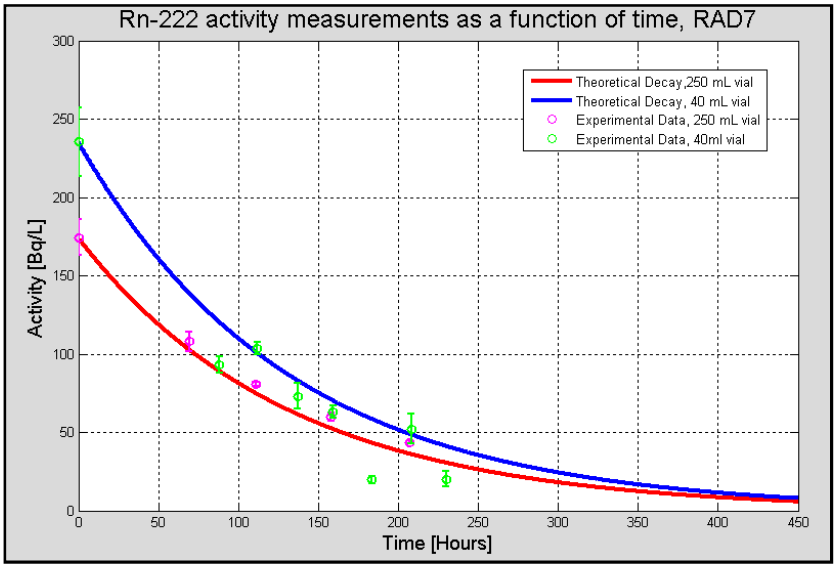

Figure 3-13: Results of the radon-in-water activity concentration measurements from the hot spring measured with 40 mL and 250 mL vial sizes which were measured at different stages of the decay process and the theoretically predicted activities making use of the decay equation (see equation 2-3).

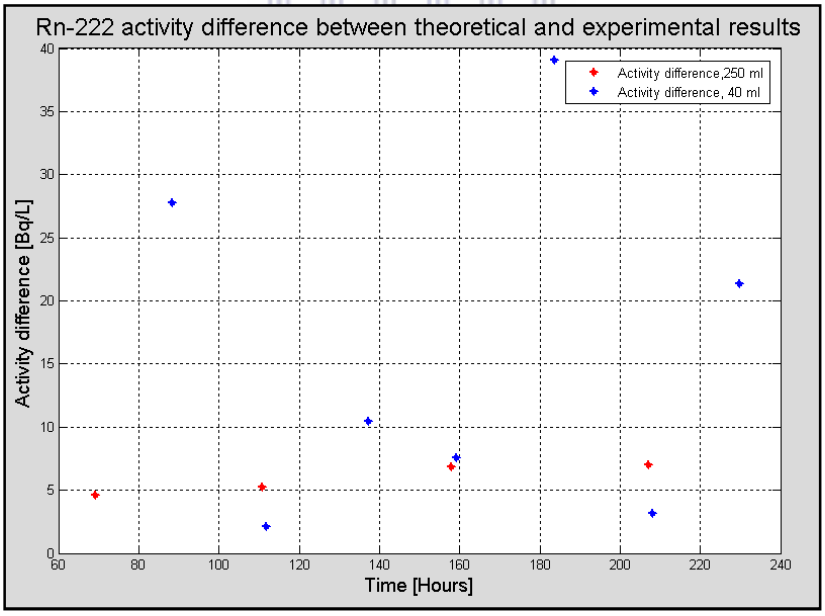

Figure 3-14: Results indicating the absolute difference between the theoretically predicted radon-in-water activity concentrations and the measured values for the 40 mL and 250 mL vial containers at the different stages of radioactive decay (see figure 3-13).

The absolute relative radon-in-water activity concentration fluctuations from the predicted exponential decay are much larger for the 40 ml vials than for the 250 ml vials (see figure 3-14). Based on the results of this experiment (see figure 3-13 and 3-14), it can be concluded that the measurement results with the 250 mL vials were more precise compared to those of the 40 mL vials. Both 40 mL and 250 mL vials are supplied in the H2O Kit manufactured by DURRIDGE Company Inc.

3.8.2. Minimization of the relative humidity

As mentioned in section 3.2.5 (purging applications), if quality radon measurements on to be achieved, then it is of important to keep RH as low as possible (below 10%). One of the key instruments that helped to achieve such favourable detection conditions was the DRYSTICK ADS-3R unit (see figure 3-8).

3.8.3. Increased measurement duration

In general, if the measurement duration is increased from the standard protocol (see section 3.4), then the quality of counting statistics (sensitivity) would also increase (decreased measurement uncertainty, see section 3.3). It is not always practically achievable, for instance when a large number of samples needs to be measured with a limited number of available detectors over a short period. By doubling the measurement duration (cycle), the counting statistics will be improved by a factor of $\sqrt{2}$ (RAD H2O, 2016).

Table 3-2: Measurement results performed by DURRIDGE Company Inc. as a quality control test by looking at different: detection methods, vial sizes and measurement durations taken from RAD H2O, 2016.

Method	RAD H_2O 40	RAD H_2O 250	Big Bottle System	Liquid Scintillation	Lucas Cell
Sample Size (mL)	40	250	2500	10	10
Sensitivity (cpm/pCi/L)	0.008	0.05	0.3	0.09	0.05
Background (cpm)	0.1*	0.1*	0.1*	15	0.25
2-sigma uncertainty at 300 pCi/L (in pCi/L)					
20-minute count	88	35		32	35
60-minute count	51	20	2.5	19	20
120-minute count	36	14	1.8	14	14
2-sigma uncertainty at 100 pCi/L (in pCi/L)					
20-minute count	53	20		24	20
60-minute count	31	12	1.5	14	12
120-minute count	22	8.5	1.1	10	8.5

Thus it is recommended to make the measurement duration (cycle) of the RAD7 detection system as long as practically achievable. Therefore, the measurement uncertainty will be minimised (see table 3-1). Practical aspects should, nonetheless, also be taken into consideration.

3.8.4. Measurement Quality Assurance

A variety of aspects has been introduced to ensure the quality of the radon activity concentration measurements:

- quality assurance tests before, during and after the measurement series were conducted. These tests include blank measurements (with hyper pure water), intercomparison measurements between the RAD7 detector (α-spectroscopy) and low background HPGe-detector (γ-spectroscopy).
- two independent measurements (split) for the same sample with two RAD7 detection systems for every measurement series (see Appendix table 4).
- general detection parameters optimization (see section 3.8).
- only measurement results obtained from calibrated RAD7 detectors were utilized in this study.

3.9 Uranium metrology

The elemental uranium in-water sampling and concentration measurements were performed by the hydrochemistry research team (Kelly, 2016). The acidified groundwater samples were measured for trace elements by making use of inductively coupled plasma mass spectrometry (ICP-MS) and atomic emission spectroscopy (AES). The ICP-MS/AES analytical elemental measurements were conducted with an Agilent 7700 (ICP-MS/AES) detection system at Stellenbosch University's Central Analytical Facilities (CAF).

3.10 Radium metrology

During the second measurement series (F2), radium (^{226}Ra and ^{228}Ra) in-water sampling and activity concentration measurements were conducted by the team of the Division of Earth and Ocean Sciences (Nicholas School of Environment) at Duke University (WRC, 2015). At a

particular site two 25 L containers were filled with the groundwater. The 50 L groundwater was then processed by letting it flow through a radium isotopes trapping device (see figure 3-15). Mn-oxide coated fibres act as a radium-isotopes trap. It is placed within two columns through which the water flows at a rate of < 1 L per minute (Vinson et al., 2008). The radium (^{226}Ra) in-water activity concentrations were measured with a DURRIDGE RAD7 detector (α-spectroscopy) after incubation of the MnO fibres for 20 days within a sealed glass column. The radium in-water activity concentrations (^{228}Ra) were measured with a Canberra HpGE detector (γ-spectroscopy) from a weighted count average associated with the 338 keV and 911 keV peaks of ^{228}Ac.

Figure 3-15: Radium isotopes filtering device making use of a gravity feed system and Mn-oxide coated fibbers.

CHAPTER 4 RADIONUCLIDE STUDY AREA

In this chapter the study area will be discussed (see table 4-1). Groundwater sampling was performed at 53 different locations spanning three provinces in the Karoo Basin (South Africa). The measurement locations spanned across a large area; some sites were 630 km apart from each other. The classification of the groundwater types was grouped into three different categories by the collaborating geochemistry research team (Kelley, 2016). The conventional perspective of defining aquifers according to the depth it originates from below the surface is not applicable. The hydrology parameters utilized to define the aquifer type were water temperature, ion chemistry (standard Stiff diagram), and radiocarbon content (Kelley, 2016). These parameters were used to define the shallow, mixed and deep aquifers. The mixed aquifers are defined as a combination of shallow and deep groundwater. Most aquifers sampled were classified as either a deep, mixed or shallow source; nonetheless, there were a limited number of aquifers not defined. The groundwater classification will be referred to as source or aquifer classification (deep, mixed, and shallow) in this study. Studying the potential connectivity of the deep and shallow sources connectivity is of importance and was consequently one of the main research aims of the geochemistry research collaborators. If hydraulic fracturing contamination occurs within deep aquifers then it will be likely to observe the contamination within the shallow sources if a connection between them exists. The mixed groundwater can be defined as an aquifer with connection between the deep and shallow sources. The sampling sites were labelled by site number and site name. The site number is specifically applicable to this study. However the site names are referring to the sites linked to the WRC report (Kelley, 2016; WRC, 2015).

It should be noted that the third measurement series (F3) coincides with the time when the area was experiencing extreme droughts. The South African Weather Service announced that 2015 was the driest year on record since meteorological measurements was started in 1904. This extreme drought is primarily due to a strong El Nino weather pattern, and the effects are persisting into 2016 (Bluden et al., 2015).

4.1 Introduction

The measurement series field trips for this study are summarised as follows:

Table 4-1: Schedule overview of three measurement series

First field trip (F1): summer 2014 (03-03-2014 to 13-03-2014) and 42 sampling sites
Second field trip (F2): winter 2014 (26-06-2014 to 09-06-2014) and 29 sampling sites (6 new sites)
Third field trip (F3): winter 2016 (01-06-2016 to 07-06-2016) and 15 sampling sites (3 new sites)

4.2 Study region description

4.2.1 Study Area Overview

Groundwater sampling (see figure 4-2) was performed at a total of 53 locations in eight different regions (see figure 4-1) in the Karoo Basin during three different measurement series. These sampling locations were chosen strategically based on source classification and regions earmarked for shale-gas development (see figure 1-4).

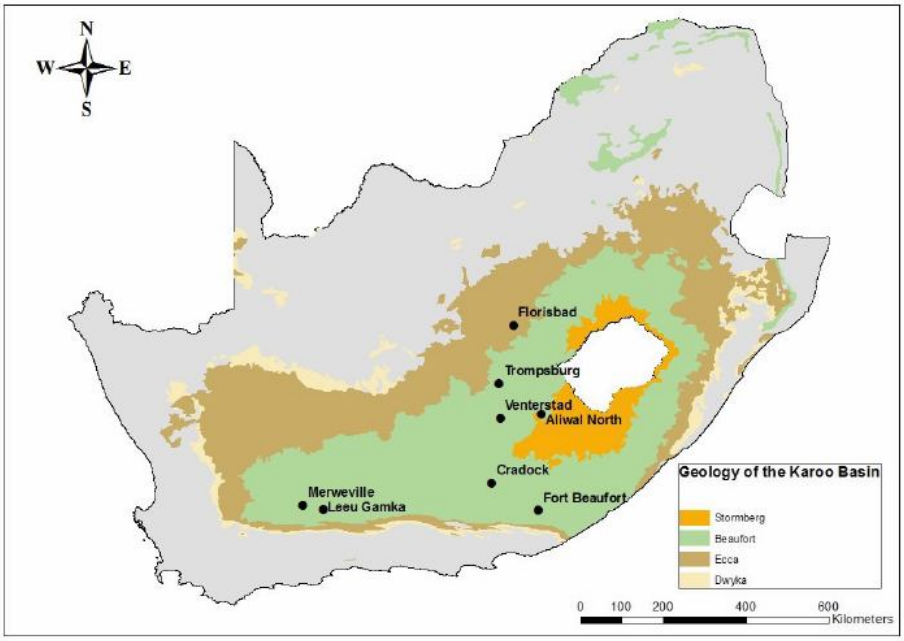

Figure 4-1: Map of South Africa and associated surrounding geological groups of the eight major sampling regions (Shapefiles provided by Council of Geoscience South Africa, Kelley, 2016).

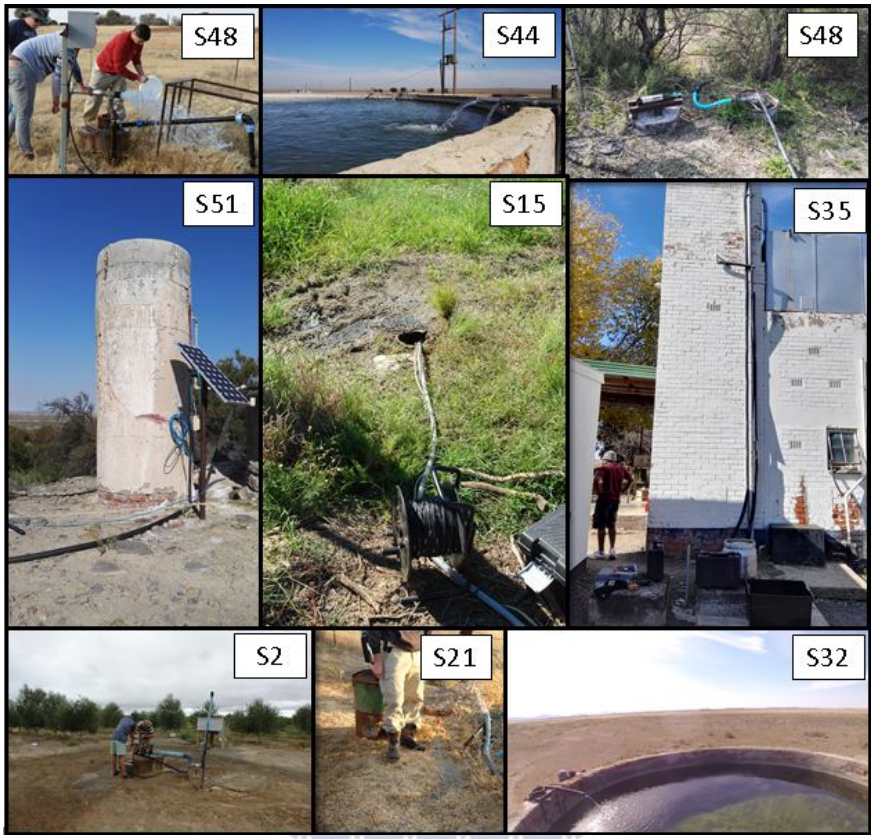

Figure 4-2**:** Images of sampling sites (see table 4.1 to 4.3) at which sampling was performed.

4.2.1.1 Merwewille

Merwewille is a small town situated in the Beaufort geological group of the Western Cape Province. This region is within the Karoo Uranium Province (see figure 1-6) with rich uranium deposits (IAEA, 2009). Work at the sampling sites (S) in this region was performed on a large, arid, privately owned farm (see figure 4-3) near Merwewille: S41 (MWB1), S42 (MWB2), S51, S52 and S53. The sampling sites are boreholes used for drinking water. Groundwater (shallow) sampling was performed during all three of the measurement series (F1 to F3) at this location.

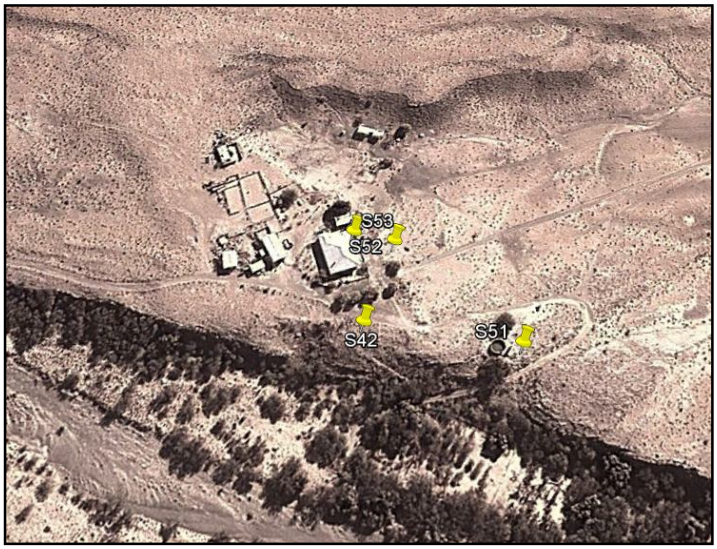

Figure 4-3: Satellite map of the Merweville sampling sites showing the arid environment (Google Earth, Imagery Date: 22-08-2013).

4.2.1.2 Leeu Gamka

Established in 1879, Leeu Gamka is a small town situated in the Beaufort geological group of the Western Cape Province (Central Karoo). This region is also situated in the Karoo Uranium Province (see figure 1-6). The sampling sites (S) within this region (see figure 4-4) were on two privately owned olive farms and a road construction camp: S2 (WP507), S3 (WP506), S4 (WP508), S5 (WP497), S6 (WP496), S7 (WP502) and S8 (WP505).

Figure 4-4: Satellite map of the Leeu Gamka sampling sites showing the surrounding agricultural activities (Google Earth, Imagery Date: 25-02-2016).

4.2.1.3 Fort Beaufort

Fort Beaufort is a town in the Beaufort geological group of the Eastern Cape Province (see figure 4-1). The sampling sites (S) in this region (see figure 4-5) were on privately owned

citrus farms: S15 (BFB1), and S16 (BFB2). Artesian groundwater is utilised predominantly for agricultural purposes. Site S15 (BFB1) is a deep source approximately 30 m from the source (eye) and 4.5 km away a mixed source S16 site (BFB2) with an approximately 100 m deep borehole. Sampling was performed at these sites only during the first measurement series (F1).

Figure 4-5: Satellite map of the Fort Beaufort sampling sites showing the surrounding agricultural activities (Google Earth, Imagery Date: 10-02-2016).

4.2.1.4 Cradock

Cradock is a town in the Beaufort geological group of the Eastern Cape Province (see figure 4-1) in the upper valley of the Great Fish River, established in 1816. The sampling sites (S) in this region (see figure 4-6) were on privately owned farms, a natural stream, and a hot spring resort: S9 (CRS1), S10 (DRB2), S11 (DRB3), S12 (DRB1), S13, and S14 (DRB4). Sampling was performed at a hot spring resort with an outdoor pool (S9, CRS1). These are not ideal sampling conditions (outdoor pool) for radon-in-water measurements because the inlet of the pool is beneath the water surface and mixing between the fresh recharge and pool water occurs. The shallow source boreholes S10 (DRB2), S11 (DRB3), and S12 (DRB1) are used for agricultural purposes. A natural stream (S13) was in the past (1999) used as a drinking source for the water-scarce Cradock area for approximately three years.

Figure 4-6: Satellite map of the Cradock sampling sites showing the surrounding agricultural activities (Google Earth, Imagery Date: 08-04-2016).

4.2.1.5 Aliwal North

Aliwal North is a town in the Stormberg geological group of the Eastern Cape Province on the Orange River established in 1849 (see figure 4-1). The sampling sites (S) in this region (see figure 4-7) included a hot spring resort (closed to the public) and privately owned farms: S18 (ANS1) – S20, S21 (ANBH1), and S50. Aliwal North was once famous for its hot spring resort that later became dilapidated and was finally closed off from the public in 2010. The thermal water is pumped from the source also known as the eye (S20) to different pools in the facility. Once again, these indoor (S18, ANS1) and outdoor pools (S17, ANS2) are not ideal for radon-in-water sampling, since the pool inlet is beneath the water surface. The deep groundwater site, S21 (ANBH1) on a privately owned farm outside Aliwal North, was used mainly for drinking water.

Figure 4-7: Satellite map of the Aliwal North sampling sites (Google Earth, Imagery Date: 31-03-2016).

4.2.1.6 Venterstad

Established in 1875, Venterstad is a town in the Beaufort geological group of the Karoo Basin within a close proximity to the Gariep Dam. The nine sampling sites (S) in this region (see figure 4-8) are on four privately owned farms: S22 (WVB3), S23 (DB11a), S24 (WVB1), S25 (RWB5), S26 (RWB1C), S28 (VBB1), S30 (LRB1), and S31 (LRB2). The deep, mixed, and shallow sources where sampling was performed are used for drinking water or agricultural purposes.

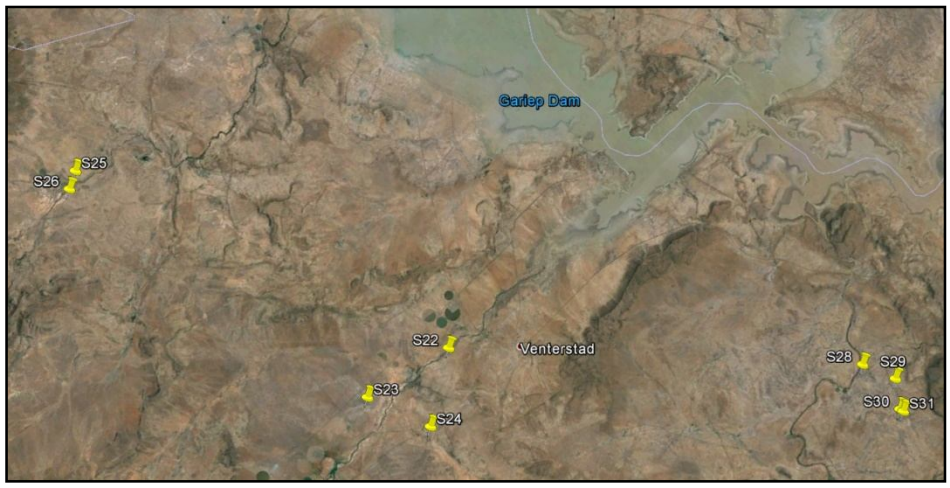

Figure 4-8: Satellite map of the Venterstad sampling sites around the Gariep Dam (Google Earth, Imagery Date: 20-02-2016).

4.2.1.7 Trompsburg

Established in 1891, Trompsburg is a town in the Beaufort geological group (see figure 4-1) of the Karoo Basin in the Free State Province. The two sampling sites (S) in this region (see figure 4-9) are on a large, privately owned Merino sheep farm: S32 (VFB1), S33 (VFB2), S34 (VFB3), and S35 (VFB4). The natural hot spring (S32, VFB1) is a deep aquifer, while the others (S33 to S35) are shallow aquifers. The water from these boreholes is utilised for drinking (S35) and (S32 to S34) for agricultural purposes.

Figure 4-9: Satellite map of the Trompsburg sampling sites showing the surrounding agricultural activities (Google Earth, Imagery Date: 2-10-2015).

4.2.1.8 Florisbad

Florisbad is a health resort (hot spring) approximately 45 kilometres northwest of Bloemfontein in the Ecca geological group of the Karoo Basin. Florisbad is also a popular archaeological and palaeontological site with an active research centre. The four sampling sites (S) in this region (see figure 4-10) are the Florisbad Spa (hot spring), Florisbad Resort, a privately owned farm, and salt pans: S37 (FLS1-37), S38 (FLS1-38), S39 (FLS1-39), S43 and S40 (FLB4). The water from the natural hot spring was in the past used for thermal pools that are no longer open to the public. The indoor hot spring pool (S37) inlet was beneath the surface of the water, making it less than ideal, as mentioned before, for radon-in-water measurement sampling. Water sampling (S39) was performed above the hot spring's eye/source, approximately six centimetres below the water surface. Thermal water from the indoor pool (S37) flows into an outdoor pool (S38) from which sampling was also performed.

Sampling was also performed on heavy saline water at a salt pan. It was not, however, measured for radon-in-water activity concentration given the high salinity (density) that is unfavourable for aeration with the RAD7. The sites from Florisbad are classified as deep sources. All water sampling within pools were performed at a depth of at least 6 cm below the water surface.

Figure 4-10: Satellite map of the Florisbad sampling sites showing the surrounding archaeological activities (Google Earth, Imagery Date: 07-06-2015).

4.2.2 First Measurements Series Study Area

The 41 deep, mixed, and shallow groundwater sampling sites chosen for the first measurement series (see figure 4-11) were strategically located within eight distinct regions (see figure 4-11) in the Karoo Basin based on the regions earmarked for potential unconventional shale gas development.

Table 4-2: Groundwater sampling sites and aquifer source classification for the first measurement series (F1, summer 2014).

Site number, [S]	Site name	Region	Sampling site specifics	Aquifer type
1	-	Prins Albert	Borehole (wind pump)	-
2	WP 507	Leeu Gamka	Borehole (in-situ pump)	Shallow
3	WP 506	Leeu Gamka	Borehole (in-situ pump)	Shallow
4	WP 508	Leeu Gamka	Borehole (in-situ pump), fast flow rate	Mixed
5	WP 497	Leeu Gamka	Borehole with fixed pump	Shallow
6	WP 496	Leeu Gamka	Borehole	Shallow
7	WP 502	Leeu Gamka	Borehole	Shallow
8	WP 505	Leeu Gamka	Borehole	Mixed
9	CRS1	Cradock	Spa outdoor pool (hot spring)	Deep
10	DRB2	Cradock	Borehole (wind pump)	Shallow
11	DRB3	Cradock	Artesian	-
12	DRB1	Cradock	Artesian	Shallow
13	-	Cradock	Stream, previous water supply for Cradock	Shallow
14	DRB4	Cradock	Borehole	Shallow
15	BFB1	Fort Beaufort	Artesian (hot spring)	Deep
16	BFB2	Fort Beaufort	Artesian	Mixed
17	ANS2	Aliwal North	Spa outdoor pool	Deep
18	ANS1	Aliwal North	Spa indoor pool (hot spring)	Deep
19	-	Aliwal North	Spa outdoor Olympic pool (far)	Deep
20	-	Aliwal North	Spa source (eye, hot spring)	Deep
21	ANBH1	Aliwal North	Borehole	Deep
22	WVB3	Venterstad	Borehole (wind pump)	Shallow
23	DB11a	Venterstad	Borehole (wind pump)	Shallow
24	WVB1	Venterstad	Borehole	Shallow
25	RWB5	Venterstad	Borehole	Shallow
26	RWB1c	Venterstad	Borehole (hot spring)	Mixed
27	RWB1c	Venterstad	Borehole	Mixed
28	VBB1	Venterstad	Borehole	Mixed
29	VBB2	Venterstad	Borehole	Shallow
30	LRB1	Venterstad	Borehole	Deep
31	LRB2	Venterstad	Borehole	Shallow
32	VFB1	Trompsburg	Artesian (hot spring)	Deep
33	VFB2	Trompsburg	Borehole	Shallow
34	VFB3	Trompsburg	Borehole	Shallow

35	VFB4	Trompsburg	Borehole	Shallow
37	FLS1-37	Florisbad	Spa indoor pool (eye, hot spring)	Deep
38	FLS1-38	Florisbad	Spa outdoor pool	Deep
39	FLS1-39	Florisbad	Indoor pool (surface)	Deep
40	FLB4	Florisbad	Borehole	Deep
41	MWB1	Merweville	Borehole	Shallow
42	MWB2	Merweville	Borehole	Shallow

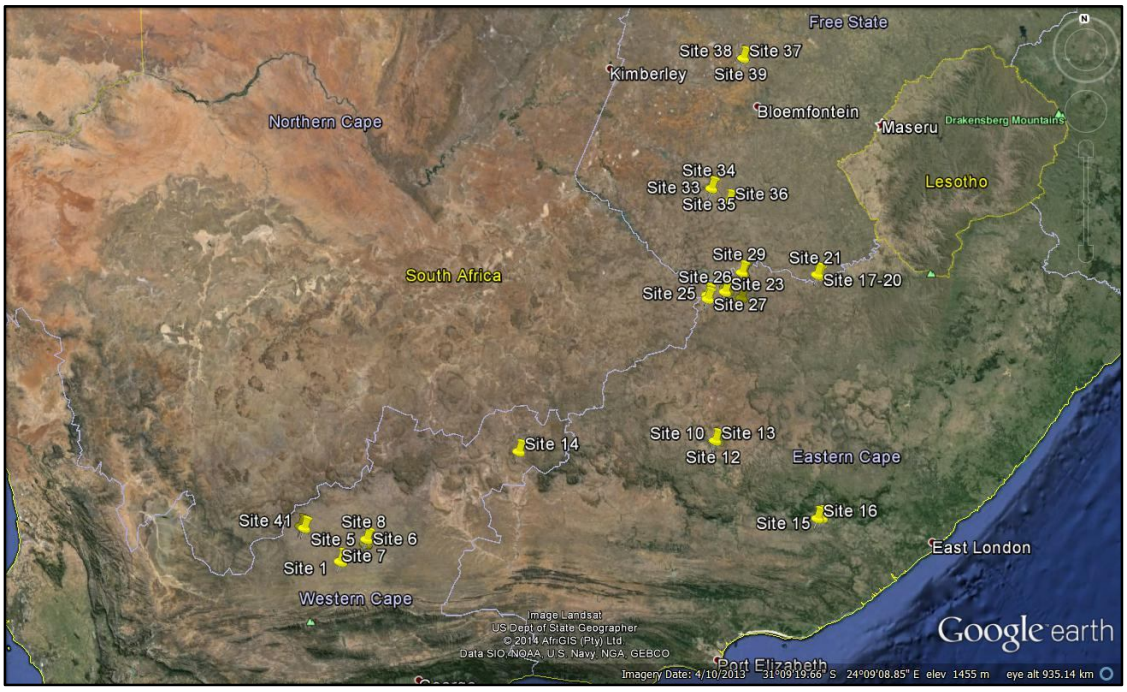

Figure 4-11: Satellite map of South Africa and the locations of the sampled sites from the first field trip (F1, summer).

4.2.3 Second Measurements Series Study Area

The second measurement series (F2) was conducted in the winter of 2014. Sampling was performed at 29 sites of which 6 of them were new sites (see table 4-2). From these 29 sites, eight were shallow sources, five were mixed sources, nine were deep sources and the rest were not classified according to source type.

Table 4-3: Groundwater sampling sites and aquifer source classification for the second measurement series (F2, winter 2014).

Site number, [S]	Site name	Region	Sampling site specifics	Aquifer type
1	-	Prins Albert	Borehole	-
4	WP508	Leeu Gamka	Borehole	Mixed
7	WP502	Leeu Gamka	Borehole	Shallow
8	WP505	Leeu Gamka	Borehole	Mixed
9	CRS1	Cradock	Spa outdoor pool (hot spring)	Deep
14	DRB4	Cradock	Borehole	Shallow
15	BFB1	Trompsburg	Artesian	Deep
16	BFB2	Trompsburg	Artesian	Mixed
18	ANS1	Aliwal North	Spa indoor pool (hot spring)	Deep
21	ANBH1	Aliwal North	Borehole	Deep
25	RWB5	Venterstad	Borehole	Shallow
26	RWB1C	Venterstad	Borehole (hot spring)	Mixed
28	VBB1	Venterstad	Borehole	Mixed
30	LRB1	Venterstad	Borehole	Deep
31	LRB2	Venterstad	Borehole	Shallow
32	VFB1	Trompsburg	Artesian (hot spring)	Deep
33	VFB2	Trompsburg	Borehole	Shallow
35	VFB4	Trompsburg	Borehole	Shallow
37	FLS1-37	Florisbad	Spa indoor pool (eye, hot spring)	Deep
38	FLS1-38	Florisbad	Spa outdoor pool	Deep
39	FLS1-39	Florisbad	Indoor pool (surface)	Deep
42	MWB2	Merweville	Borehole	Shallow
43	New	Soutpan (Bloemfontein)	Tap Water	-
44	New	Soutpan	Borehole	-
45	New	Soutpan	Borehole	-
46	New	Soutpan	Borehole	-
47	New	Soutpan	Borehole	-
48	New, FLB5	Soutpan	Borehole	-
49	RRB1(New)	Cradock	-	Shallow

4.2.4 Third Measurements Series Study Area

The third measurement series (F3) was conducted in the winter of 2016. Sampling was performed at 15 sites of which 3 were new sites (see table 4-3). Of these 15 sites, five were shallow sources, one was a mixed source, two were deep sources and seven were not classified according to the source type.

Table 4-4: Groundwater sampling sites and aquifer source classification for the third measurement series (F3, summer 2016).

Site number, [S]	Site name	Region	Sampling site specifics	Aquifer type
44	-	Soutpan-1 (Bloemfontein)	Borehole	-
45	-	Soutpan	Borehole	-
46	-	Soutpan	Borehole	-
48	-	Soutpan	Borehole	-
32	VFB1	Trompsburg	Artesian (hot spring)	Deep
33	VFB2	Trompsburg	Borehole	Shallow
35	VFB4	Trompsburg	Borehole	Shallow
50	New	Aliwal North	Borehole	Deep
25	RWB5	Venterstad	Borehole	Shallow
31	LRB2	Venterstad	Borehole	Shallow
28	VBB1	Venterstad	Borehole	Mixed
14	DRB4	Cradock	Borehole	Shallow
51	New	Merweville	Borehole	-
52	New	Merweville	Borehole	-
53	New	Merweville	Tap Water	-

CHAPTER 5 Results and discussion

In this chapter, the results of the Karoo Basin NORM groundwater baseline characterisation, with a focus on radon and additional radionuclides (^{226}Ra, ^{228}Ra, and ^{238}U), will be discussed. The groundwater sampling sites include boreholes, streams, hot springs (artesian), drinking taps, wind pumps, and solar pumps. The research work performed in this thesis was done in collaboration with a research team (Department of Earth Science, Stellenbosch University; Groundwater Africa; and the South African Water Research Commission) that focused on applying hydrochemistry and residence time constraints to distinguish groundwater systems in the Karoo Basin prior to shale-gas exploration (Kelley, 2016; WRC, 2015). The results of each of the measurement series' (F1 to F3) be discussed individually in the following sections (see section 5.1, 5.2 and 5.3) and collectively (see section 5.4).

5.1 First measurement series results

The first measurement series (F1) took place during summer of 2014 (see Appendix table 1). The radon-in-water activity concentration results on which groundwater classification has been performed are given in figure 5-1. In general radon-in-water activity concentrations for shallow sources are higher compared that of mixed and deep sources (see figure 5-1). The radon-in-water activity concentrations for deep groundwater sources were systematically the lowest (see figure 5-1). The mixed sources are an indication of a potential link (mixing) between the deep and shallow sources. Lower radon-in-water activity concentrations (< 30 Bq/L) are more frequent compared to higher levels during F1 (see figure 5-3). The mean radon-in-water activity concentration for the aquifers which were classified was 31.8 Bq/L (see figure 5-1). Interestingly the one deep source, S21 a borehole in Aliwal North had a significantly higher radon-in-water activity concentration of 56 ± 6 Bq/L compared to most deep sources (see figure 5-1). Similarly, the one mixed source, S28 a borehole in Venterstad had an unexpected higher radon-in-water activity concentration of 49 ± 9 Bq/L which is in the activity range of the deep sources.

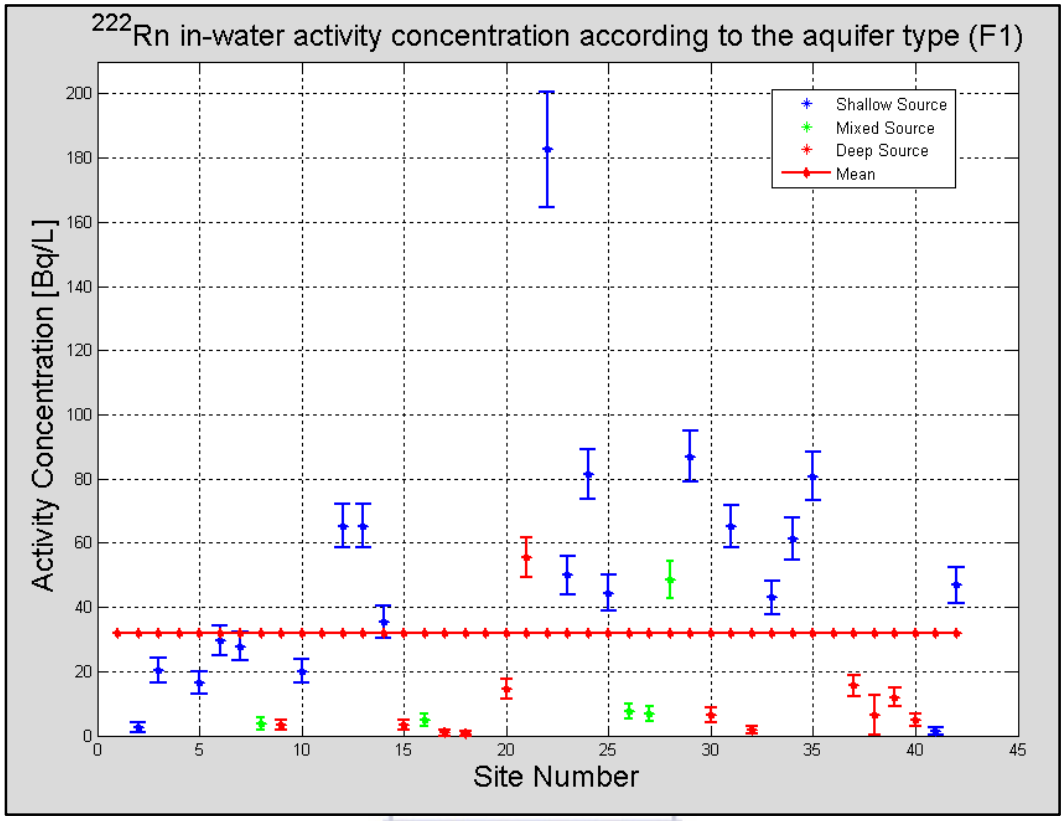

Figure 5-1: The results of the radon-in-water activity concentration grouped according to the aquifer classification (F1).

The shallow groundwater sources are associated with lower water temperatures (see figure 5-2). The radon-in-water activity concentration within groundwater of the Karoo Basin tends to decrease as the temperature increases (see figure 5-2). However, studies performed on radon in hot springs from around the world (see table 5-1) had mostly elevated (> 50 Bq/L) radon-in-water activity concentration (Botha et al., 2016; Vogiannis et al., 2004; Song et al., 2011). The hot springs in this study were all deep sources as expected. The hot springs radon-in-water activity concentration results for this study in the first measurement series are presented in (see table 5-5):

As mentioned in section 4.2, some sampling was performed from inlets allocated at the bottom of filled pools, making it challenging to sample a “fresh” sample without mixing with the stagnant pool water. Note that sampling circumstances at sites with underwater inlets will be referred to as unfavourable sampling conditions. The possibility exists that the radon-in-water activity concertation in reality is higher with unfavourable sampling conditions. The Karoo Basin hot springs (good sampling conditions) sites (S15, S20, S26 and S32) have a

significantly lower mean radon-in-water activity concentration of 6 ± 3 Bq/L compared to most hot springs from other countries (see table 5-1). For groundwater to be hot (> 22 °C), it most likely flowed from deep below the surface. It implies the water possibly flowed for a relatively long time underground which could explain the low radon levels since considerable time was available to undergo decay (see figure 5-11). A possible scenario why the hot springs radon-in-water levels in the Karoo Basin is low compared to what have been observed (see table 5-1) is due to a long flow duration from deep beneath the surface.

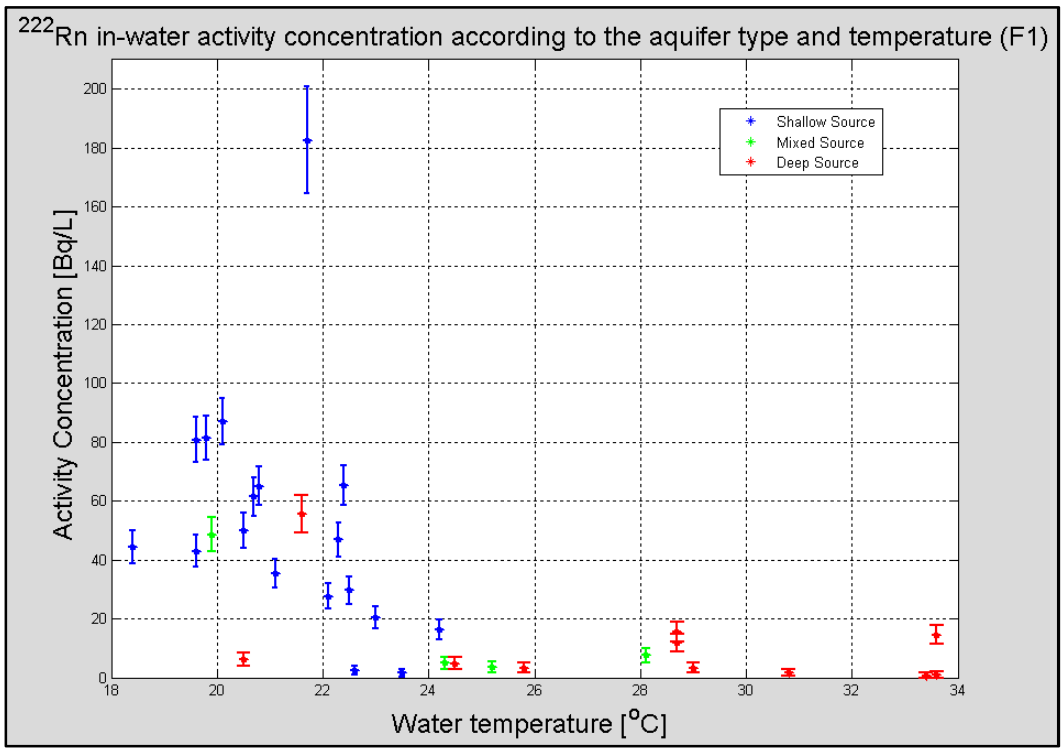

Figure 5-2: The results of the radon-in-water activity concentration according to the aquifer's water temperature (F1).

Table 5-1: Studies of radon-in-water activity concentrations within hot spring waters for various countries between 1993 and 2013 (Botha et al., 2016).

Location of hot spring	^{222}Rn water activity concentration measured, [Bq/L]	Measurement technique
Taiwan	0.6-5.6	Liquid scintillation counting
Jordan (Irbid Basin)	3.2-5.5	Passive
Greece (Lesvos Island, Polichnitos)	126-202	Alpha spectroscopy
Greece (Lesvos Island, Eftalou)	113–304	Alpha spectroscopy
Greece (Lesvos Island, Lisvori)	12–17	Alpha spectroscopy
Greece (Lesvos Island, Loutra Thermis)	13–22	Alpha spectroscopy
Poland (Marta)	104-326	Liquid scintillation counting
Lebanon	0.91-49.6	Passive
China (Guangdong)	66-206	Alpha spectroscopy
South Africa (Montagu)	188-223	Alpha spectroscopy and passive

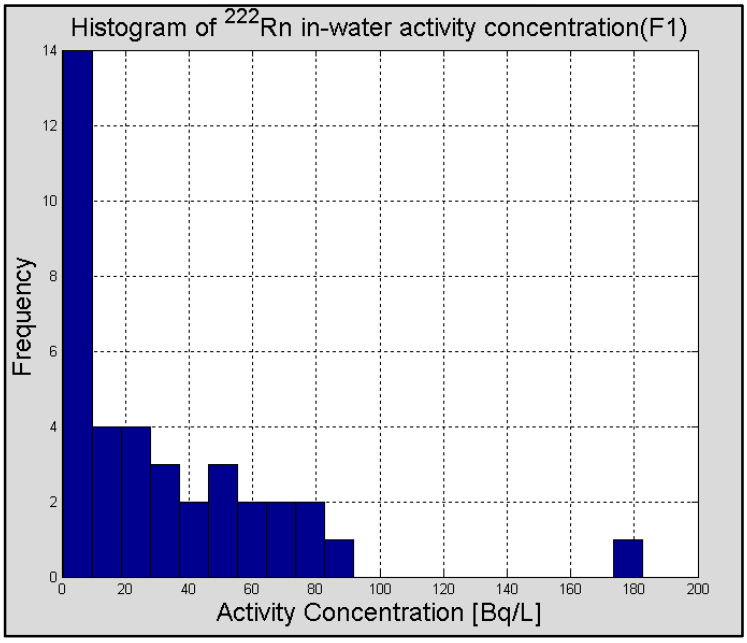

Figure 5-3: Histogram (10 bins) of radon-in-water activity concentration from the 42 sites (F1).

The groundwater sampled during the first measurement series had a pH range between 6.9 and 9.9 (see figure 5-4). Oddly, no radon-in-water activity concentration measurement events were observed for water with a pH between 8.5 to 9.5 (see figure 5-4). The highest radon-in-water activity concentrations were associated with the lower pH, 7 to 8.

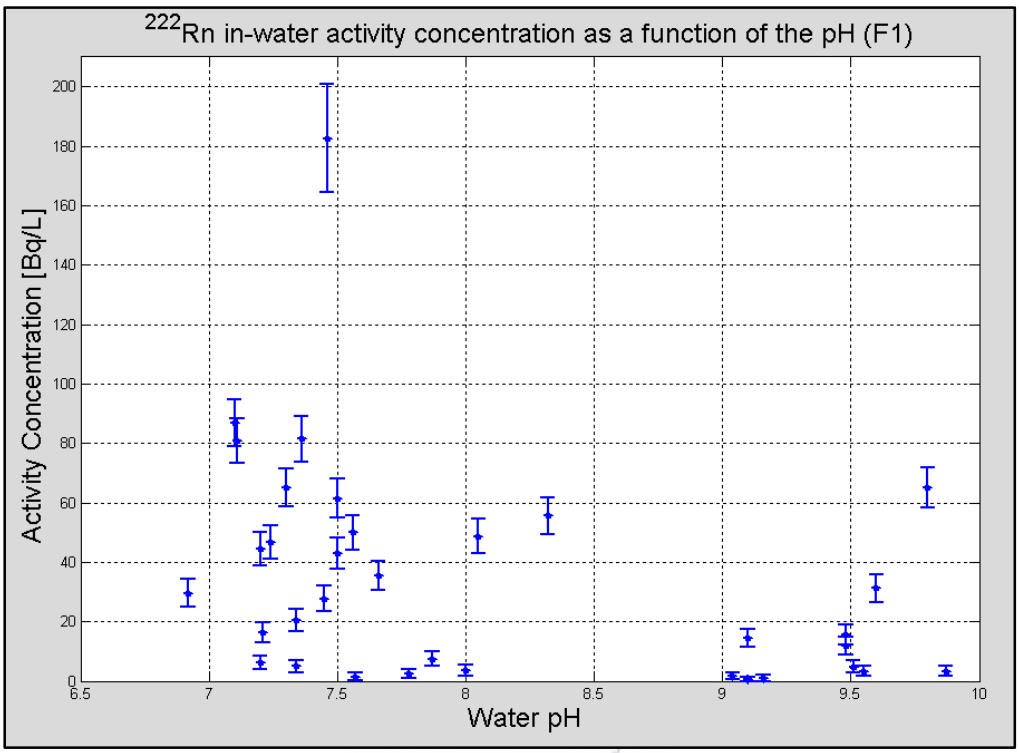

Figure 5-4: Radon-in-water activity concentration results according to the groundwater's pH (F1).

In most cases, there is an inverse proportionality (see section 2.4.3.4) between uranium, radium, and radon-in-water activity concentrations due to geochemical conditions (Vinson et al., 2009). The NORM inverse proportionality is also observed between elemental uranium and radon-in-water activity concentration (see figure 5-5).

The uranium in-water concentrations are systematically higher for shallow sources compared to the mixed and deep sources (figure 5-6). The baseline elemental uranium in-water concentration observed (F1) can be characterised as follows: range of 0.003 µg/L (S12, shallow source) to 21.9 µg/L (S14, shallow source) and mean of 4.5 ± 0.9 µg/L.

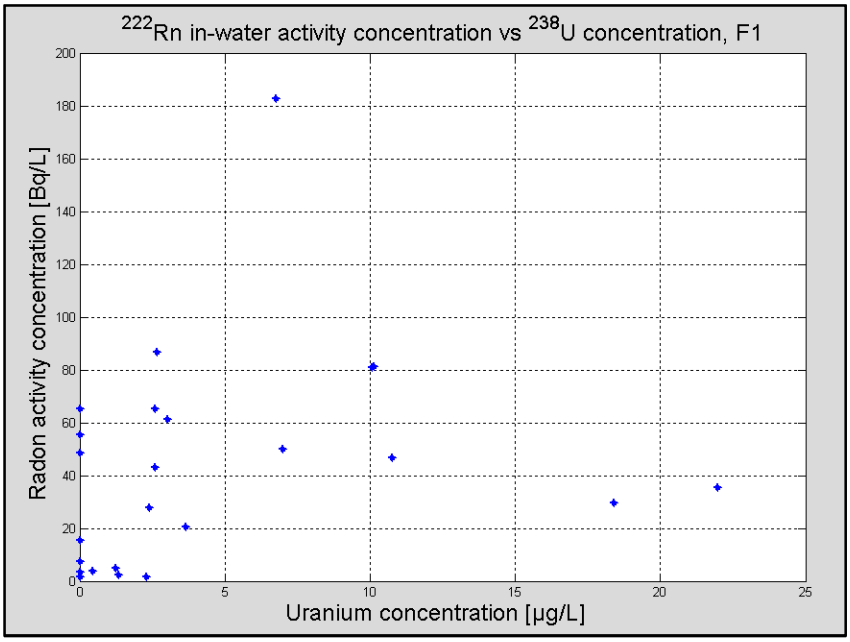

Figure 5-5: Results of radon-in-water activity concentration according to the elemental uranium concentration for all aquifers (F1).

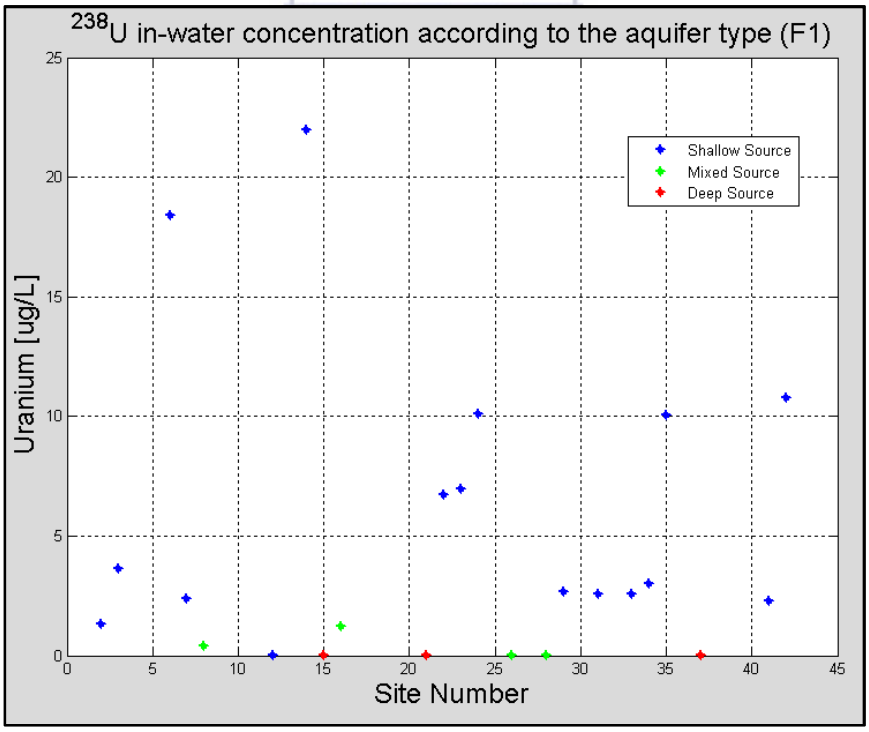

Figure 5-6: Results of uranium in-water concentration according to the aquifers classification (F1).

The number of radon-in-water activity concentration measurement points (events) is less as the EC increases (see figure 5-7). Also oddly, no radon-in-water activity concentration

measurement events were observed for water with an EC between 250 to 350 µS/cm (see figure 5-7).

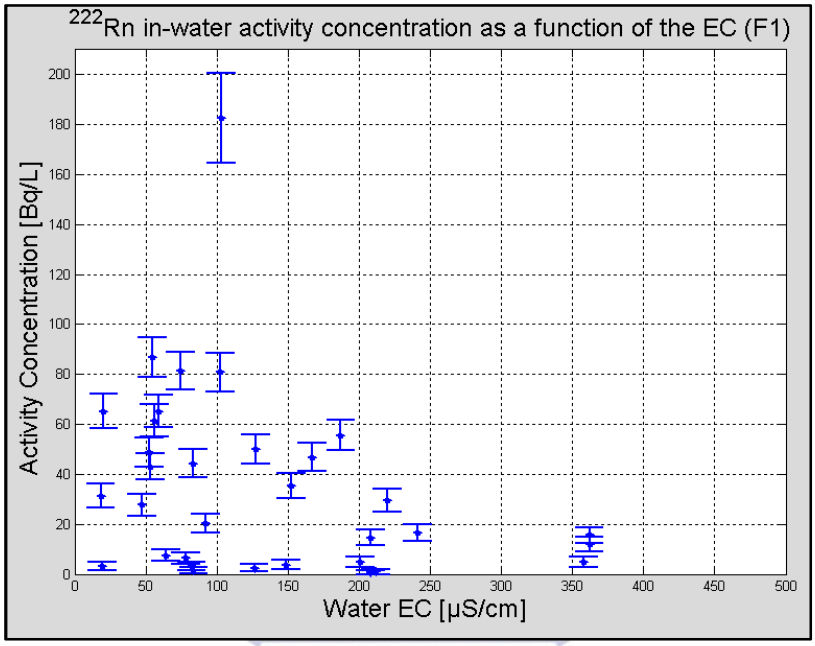

Figure 5-7: Results of radon-in-water activity concentration according to the groundwater's electrical conductivity (F1).

The baseline radon-in-water activity concentration in the Karoo Basin can be characterised by a mean of 32 ± 5 Bq/L for the first measurement series (F1). The highest to the lowest mean radon-in-water activity concentration for the different aquifer classifications were shallow groundwater sources (51 ± 11 Bq/L), mixed sources (14 ± 6 Bq/L), and deep sources (10 ± 3 Bq/L), respectively. The site-specific radon-in-water activity concentration characterisation[1] ranges from the lowest for the deep groundwater source S32 (VFB1: 1.6 ± 1.2 Bq/L) to the highest for the shallow source S22 (WVB3: 183 ± 18 Bq/L).

Table 5-2: Statistical results: radon-in-water activity concentration for different groundwater's source classification (F1).

Aquifer type	Mean radon-in-water activity, [Bq/L]
All types	32 ± 5
Shallow	51 ± 11
Mixed	14 ± 6
Deep	10 ± 3

[1] Results with unfavourable sampling conditions (mixing and aeration) and non-source classification data were not included.

5.2 Second Measurements Series Results

The second measurement series was conducted in the winter of 2014. The temporal inter-annual and seasonal effects will be discussed in this section (see Appendix table 2). A total of 20 sites from the first measurement series (summer, F1) were measured again for radon-in-water during the second measurement series (F2). Six new locations were added in the second measurements series. The site-specific radon-in-water activity concentration characterisation (see figure 5-8) for the second measurement series yields: a minimum of S1 (1.1 ± 0.7 Bq/L) to a maximum of S42 (MWB2: 165 ± 8 Bq/L). Note figure 5-8 represents both classified and sources which were not classified, thus it is an overview of all the radon-in-water activity concentration results for F2, independent of source classification.

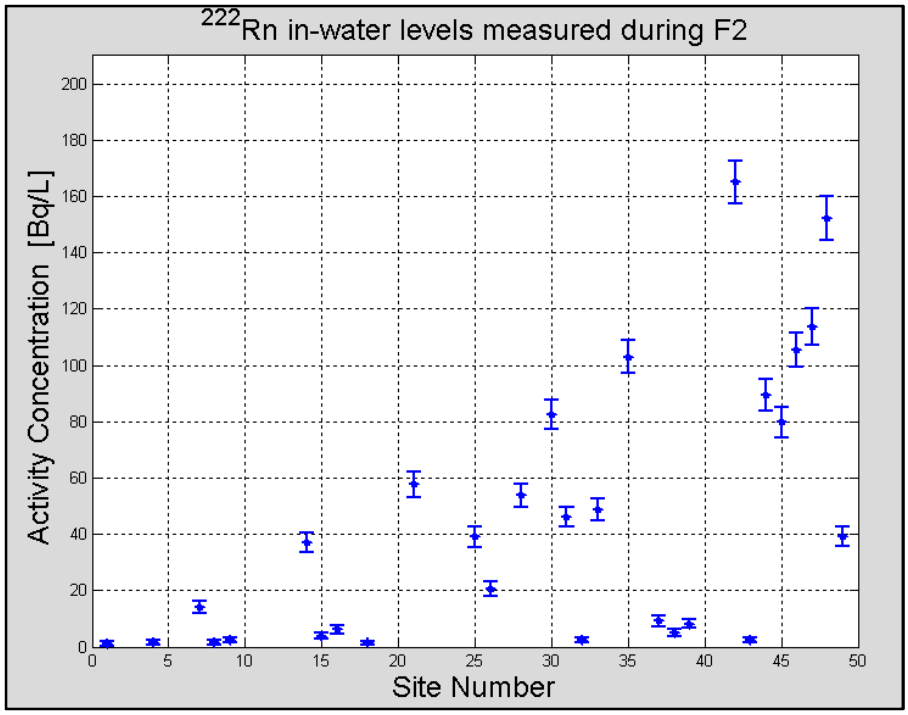

Figure 5-8: Radon-in-water activity concentrations results for the sampled sites (F2).

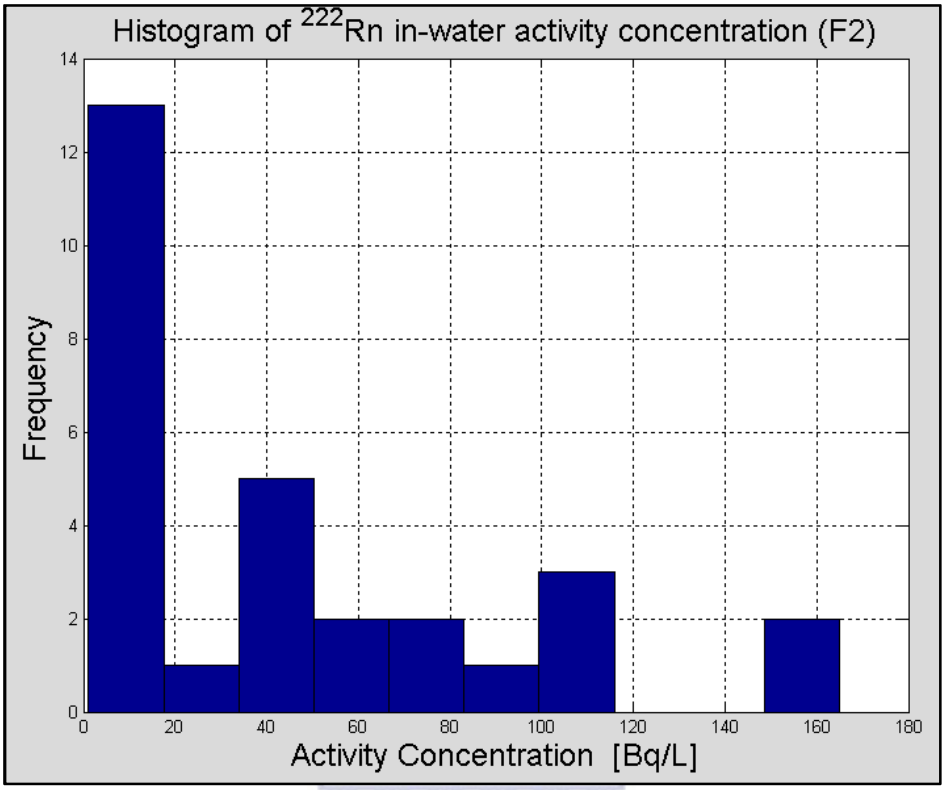

Figure 5-9: Histogram (10 bins) of radon-in-water activity concentration for the 29 sites during the second measurement series (F2).

Similar to the first measurement series (summer), the results from the second measurement series (winter) demonstrated higher radon-in-water activity concentration for shallow sources (see table 5-3) compared to mixed and deep sources (see figure 5-10). The deep source S30 (LRB1) had an elevated radon-in-water activity concentration of 82.4 ± 5.3 Bq/L. This is not a typically observed radon-in-water activity concentration for deep groundwater sources in the Karoo Basin (see table 5-2 and 5-3).

Shallow groundwater sources again have a systematically lower associated water temperature (see figure 5-2) as was observed for the first measurement series (see figure 5-11). The shallow aquifers have the highest radon-in-water activity concentration in the Karoo Basin. When reviewing only the shallow source's radon-in-water activity concentration results (blue data points, see figure 5-11), counterintuitively, one can see that the highest level (165 ± 7.5 Bq/L) is associated with the highest water temperature (21.5 °C). Results similarly (F1) indicate that radon-in-water activity concentration decreases as the water temperature increases (see figure 5-11) for the 2014 winter measurement series.

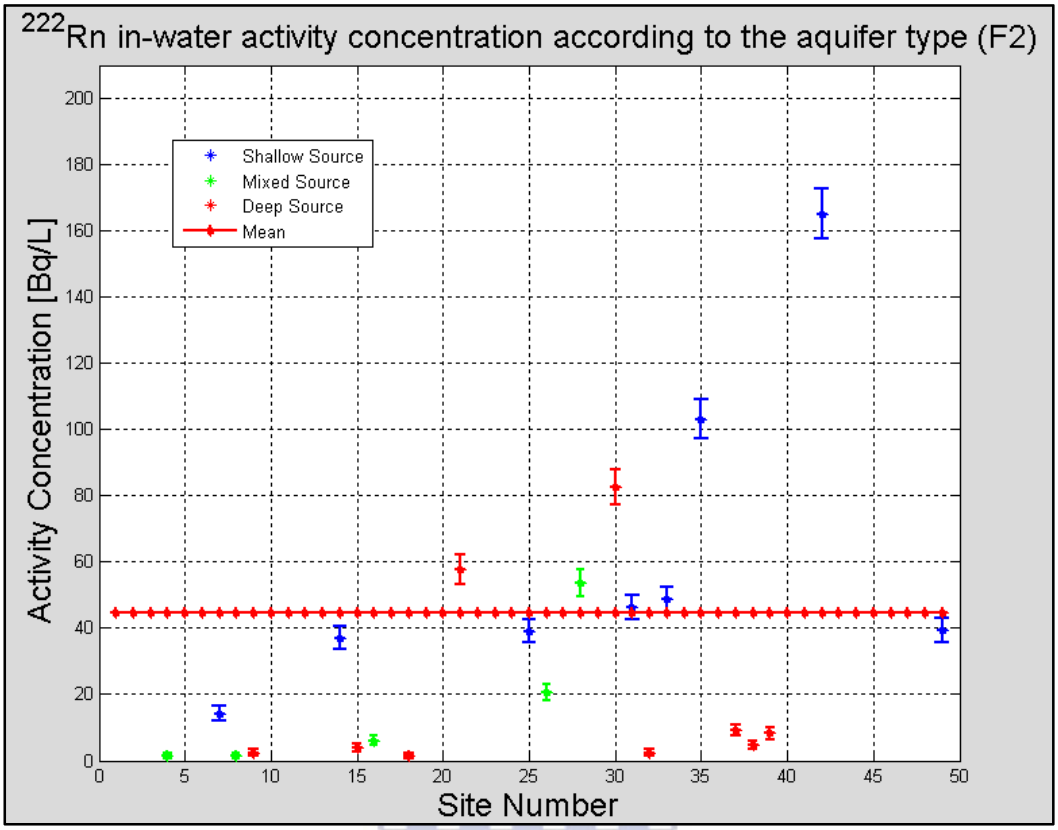

Figure 5-10: Radon-in-water activity concentration results according to source classification for 29 sites measured during the second measurement series (F2, winter).

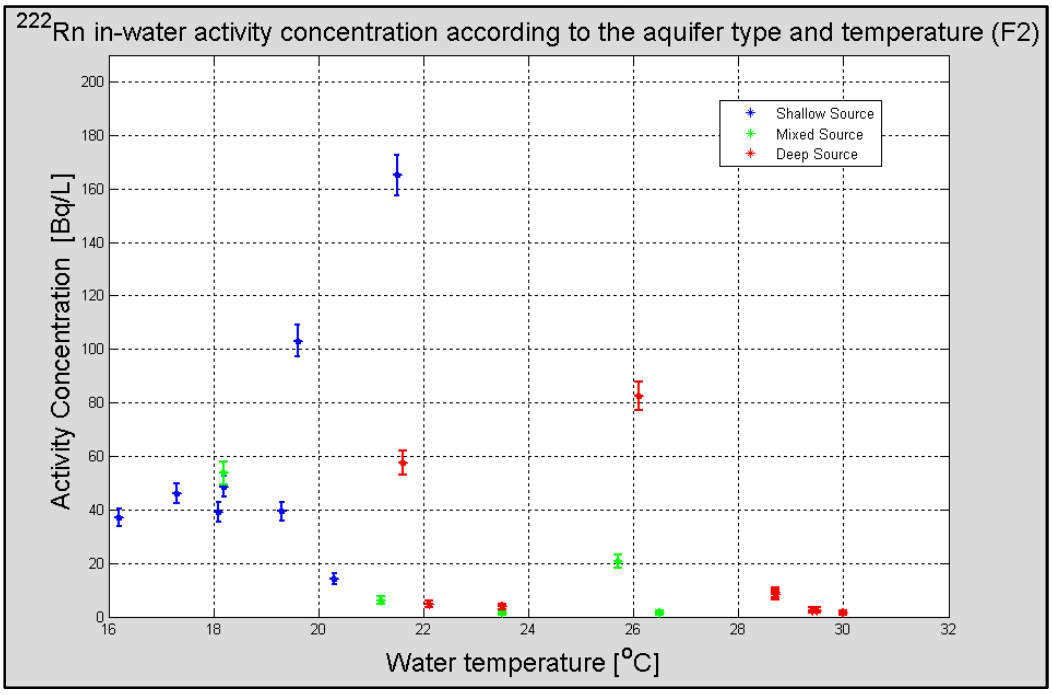

Figure 5-11: Radon-in-water activity concentration results according to the groundwater's temperature and source classification (F2).

Uranium in-water concentrations are consistently higher for shallow groundwater sources compared to the mixed and deep sources (figure 5-12). The baseline uranium in-water concentration observed in the Karoo Basin for winter 2014 can be characterised as follows: a minimum of 0.001 µg/L (S15, deep source), a maximum of 40.9 µg/L (S25, shallow source), and a mean of 4.5 ± 0.9 µg/L. A possible inverse proportionality between elemental uranium and radon-in-water activity concentration is furthermore observed for the winter 2014 measurement series (see figure 5-13). The higher radon-in-water concentrations are generally associated with the lower uranium in-water concentrations (see figure 5-13).

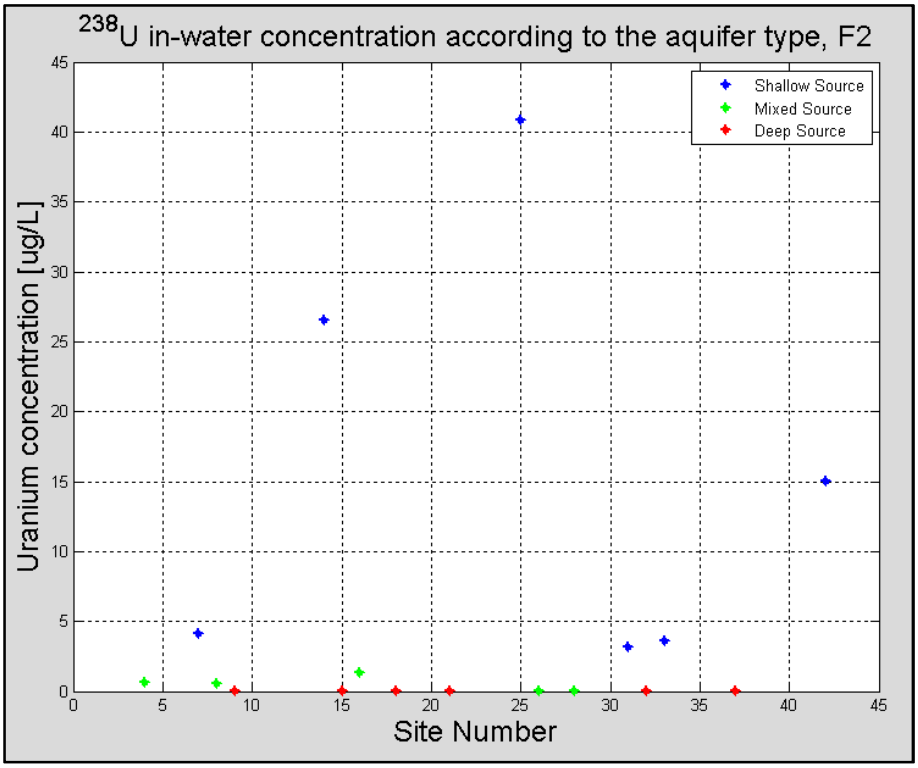

Figure 5-12: Uranium in-water concentration results at the different sites (F2).

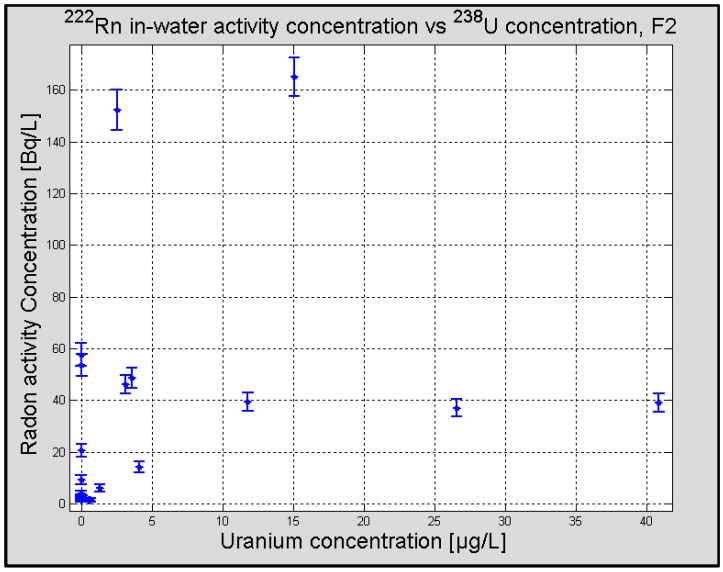

Figure 5-13: Results of radon-in-water activity concentration according to the elemental uranium concentration for all aquifers (F2).

The waters have a pH between 7.1 and 10.0 (see figure 5-14), thus can be considered to be alkaline (F2). There appears to be an inverse proportionality between the pH of the water and the radon-in-water activity concentration. Note that no radon-in-water activity concentration was measured for groundwater with a pH level between 8.5 to 9.5 (see figure 5-14); this was similarly observed during the previous measurement series (see figure 5-4).

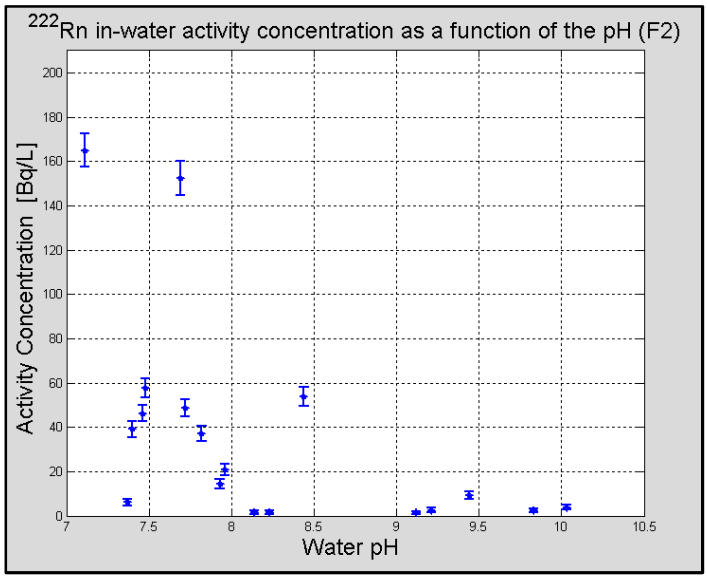

Figure 5-14: Radon-in-water activity concentration results according to the groundwater's pH.

The waters sampled for radon-in-water activity concentrations have an electrical conductivity (EC) between 21 µS/m and 362 µS/m for the second measurement series (see figure 5-15).

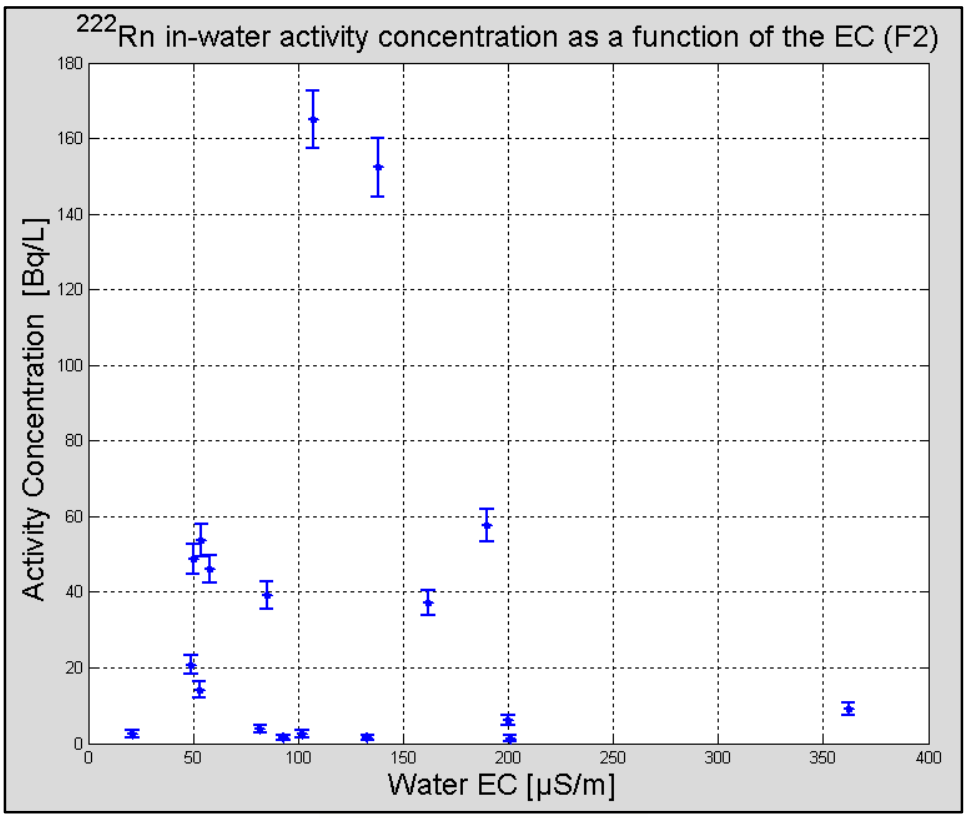

Figure 5-15: Results of radon-in-water activity concentration according to the groundwater's electrical conductivity (F2).

A key focus of the second measurement series was to study the temporal inter-annual effect on the radon-in-water in the Karoo Basin throughout 2014. The NORM in-water observations from the first and the second measurement series were generally almost indistinguishable. A period of about three months elapsed between F1 and F2 and with a change of seasons from summer to winter. The groundwater source with the smallest radon-in-water activity concentration fluctuations from F1 to F2 was expected to be the deep sources (see figure 5-16). Nonetheless, a substantial increase (76 Bq/L) of radon-in-water activity concentration for the deep source S30 (LRB1) was observed. The groundwater sources with the largest radon-in-water activity concentration fluctuations were the shallow aquifers (see figure 5-16, B). The largest site-specific radon-in-water activity concentration increase (118 Bq/L) from F1 to F2 is associated with the shallow aquifer S42 (MWB2) near Merweville.

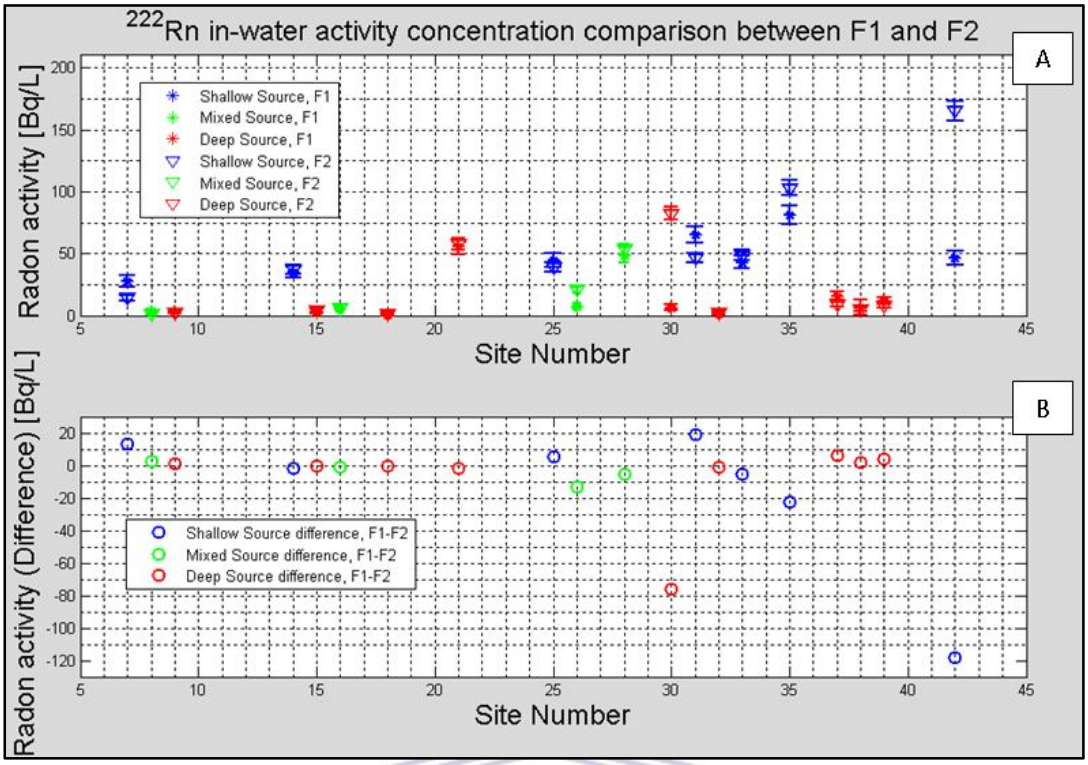

Figure 5-16: Inter-annual baseline characterization results (A) of radon-in-water activity concentration according to source classification (shallow/mixed/deep) and associated temporal differences (B) between F1 and F2.

The mean radon-in-water activity concentration increased from 32 ± 5 Bq/L to 44 ± 8 Bq/L from F1 (summer 2014) to F2 (winter 2014). The mean radon-in-water activity concentration (see table 5-3) characterisation during F2 is as follows: shallow sources (61 ± 22 Bq/L), deep sources (19 ± 6 Bq/L), and mixed sources (16 ± 8 Bq/L). The site-specific (see figure 5-8) radon-in-water characterisation [2] (F2) ranges from the lowest for the mixed groundwater source S8 (WP505: 1.5 ± 0.8 Bq/L) to the highest for the shallow source S42 (MWB2: 165 ± 8 Bq/L).

[2] Results with unfavourable sampling conditions (mixing and aeration) and non-source classification data were not included.

Table 5-3: Results for radon-in-water activity concentration according to the groundwater's classification type for the 29 sites (F2).

Aquifer type	Mean radon-in-water activity, [Bq/L]
All types	44 ± 8
Shallow	61 ± 22
Mixed	16 ± 8
Deep	19 ± 6

5.3 Third Measurements Series Results

In 2015, South Africa (Karoo Basin) experienced its worst drought in 112 years (Bluden et al., 2015) based on the average annual land rainfall according to the South African Weather Services. Studying the effects of the temporal changes and possible influence of droughts (Bluden et al., 2015) on the Karoo Basin radiological baseline were a particular focus in this section (see Appendix table 3). The radon-in-water activity concentration for F3 can be characterised by a minimum of 1.8 ± 0.8 Bq/L for the deep hot spring (S32, VFB1), maximum of 132 ± 7 Bq/L at the new site (S48), and a mean of 61 ± 16 Bq/L (see figure 5-17). The radon-in-water activity concentration histogram profile for the F3 (see figure 5-18) has a higher mid activity frequency range compared to the lower section predominance in the previous two measurements series (see figure 5-3 and figure 5-9).

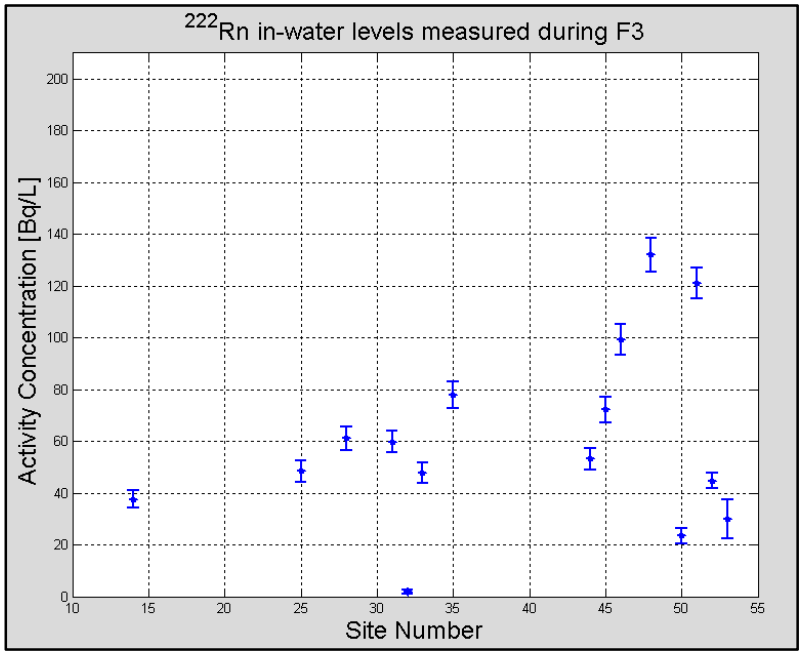

Figure 5-17: Radon-in-water activity concentration results according to the sampled sites (F3).

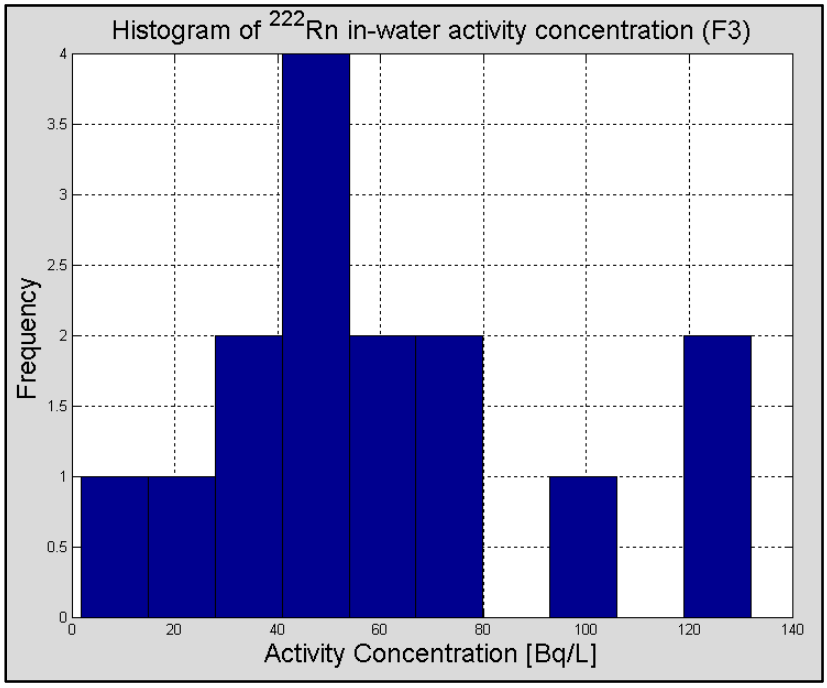

Figure 5-18: Histogram (10 bins) of radon-in-water activity concentration (F3).

Similar to F1 and F2 (see figure 5-1 and figure 5-10), the results from F3 (winter) indicate that radon-in-water activity concentration for shallow groundwater sources is systematically higher (see table 5-3) than for mixed and deep sources (see figure 5-10). The collective (F1 to F3) results of the baseline radon-in-water characterisation are discussed in section 5.4.

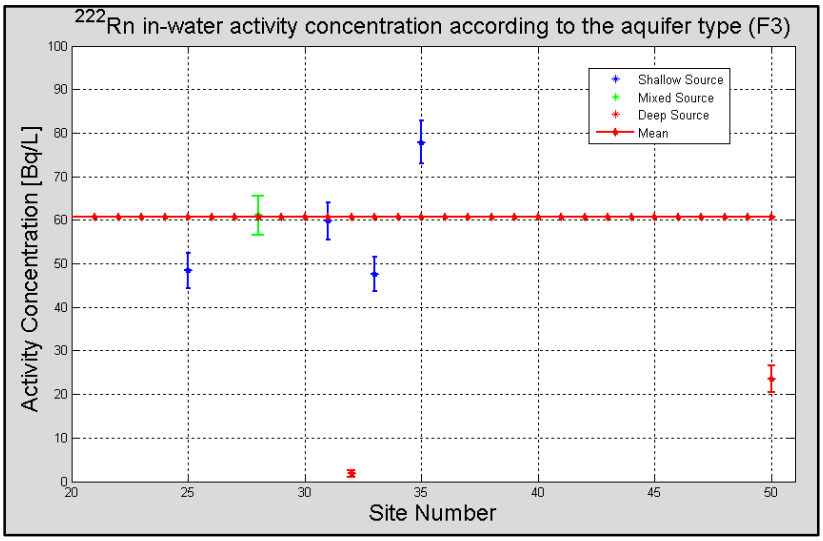

Figure 5-19: Results of radon-in-water activity concentration according to aquifer classification (F3).

The groundwater's EC ranges from 41 µS/m to 238 µS/m (F3). The majority of the measured radon events are associated with an EC between 100 µS/m and 150 µS/m (see figure 5-20). The groundwater's pH ranges from 4.7 to 11.3 (F3). The vast majority of the measured radon results have an associated pH between 4.7 and 6.3 (see figure 5-21).

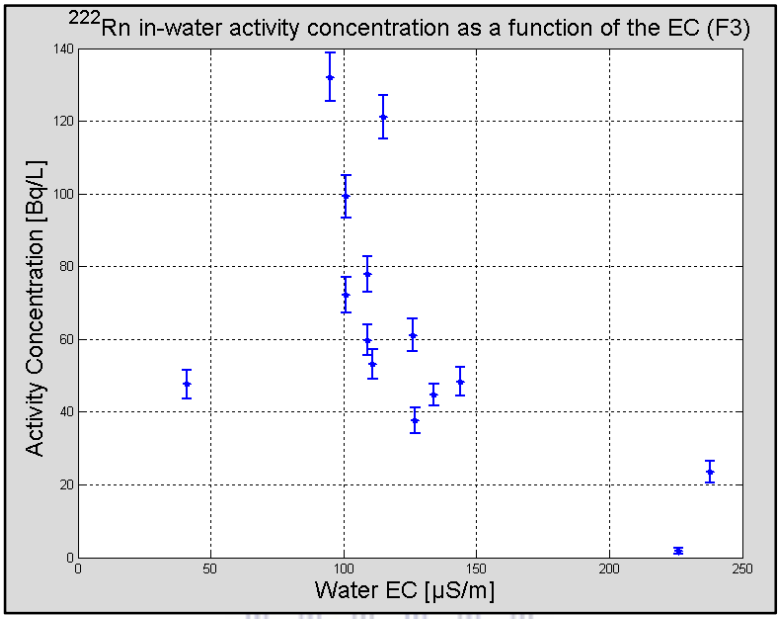

Figure 5-20: Radon-in-water activity concentration results according to the groundwater's electrical conductivity (EC).

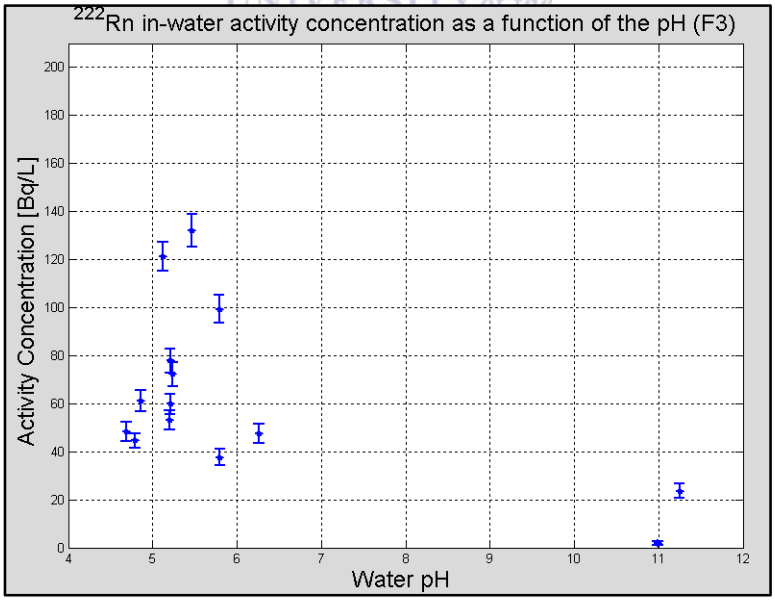

Figure 5-21: Radon-in-water activity concentration results according to the groundwater's pH.

The results of radon-in-water activity concentration plotted as a function of the groundwater source classification and temperature is illustrated in figure 5-22 (F3). The radon-in-water

activity concentrations for the shallow sources with lower water temperatures are systematically higher compared to those of the mixed and deep sources with higher associated water temperatures.

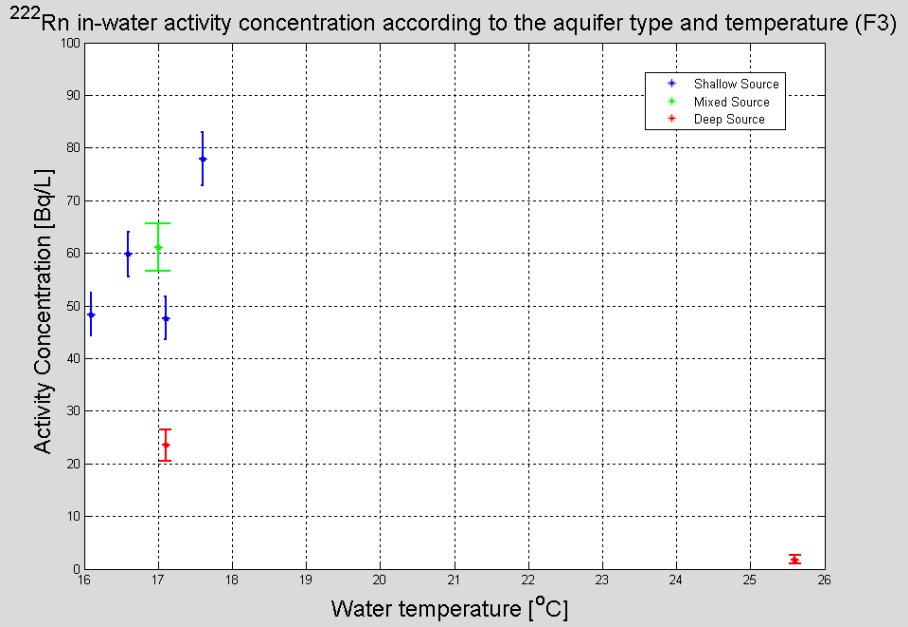

Figure 5-22: Results (F3) of radon-in-water activity concentration according to the groundwater's temperature and classification type (shallow/mixed/deep).

The baseline radon-in-water activity concentration from the 15 groundwater sites can be characterised by a mean of 61 ± 16 Bq/L for F3 during winter of 2016. The mean radon-in-water activity concentrations (see table 5-4) observed during the third measurement series were 58 ± 29 Bq/L for shallow sources and 12 ± 9 Bq/L deep sources with. Only one mixed source measurement was performed during F3 and was thus not included in the statistical analyses (see table 5-4). No uranium in-water concentration measurements were performed during F3. The site-specific (see figure 5-17) radon-in-water activity concentration characterisation[3] (F3) ranges from the lowest for the deep artesian hot spring source S32 (VFB1: 1.8 ± 0.8 Bq/L) to the highest for the presumed shallow source S48 (132 ± 6.7 Bq/L).

[3] Results with unfavourable sampling conditions (mixing and aeration) and non-source classification data were not included.

Table 5-4: Results (statistical) of radon-in-water activity concentration according to the groundwater's source classification for the 15 sites (F3).

Aquifer type	Mean radon-in-water activity, [Bq/L]
All types	61 ± 16
Shallow	58 ± 29
Mixed (one data point)	61 ± 5
Deep	12 ± 9

5.4 Collective overview and associated baseline system

The groundwater baseline NORM model for the Karoo Basin includes the results from the first measurement series (F1) to the third measurement series (F3). This baseline data will be discussed in this section to give a comprehensive overview of the radiological nature of aquifers in the Karoo Basin.

The general characterisation of the elemental uranium in-water concentration of the Karoo Basin for this study ranged from below detection level to 40.9 µg/L (see figure 5-23, A). The site with the highest elemental uranium in-water concentration (40.9 µg/L) was recorded during F2 at S25 (RWB5) which is situated about 16 kilometres from the Gariep Dam (Eastern Cape Province). This groundwater source (S25, RWB5) is utilized for drinking purposes, which is of concern since the recommended guidelines for uranium concentration in drinking water should not exceed 30.0 µg/L (WHO, 2011). The uranium in-water concentration was the highest for shallow sources compared to mixed and deep sources (see figure 5-23). An increase of up to 4.6 µg/L for elemental uranium in-water concentration was observed from F1 to F2 for the shallow sources (see figure 5-23, B). No or small increases were observed for the uranium in-water concentration in mixed and deep sources from F1 to F2 (see figure 5-23).

A possible inverse proportionality (disequilibrium) between radon-in-water activity and uranium in-water concentration (see figure 5-24) was observed, similar to other studies for example by Vinson et al., 2009.

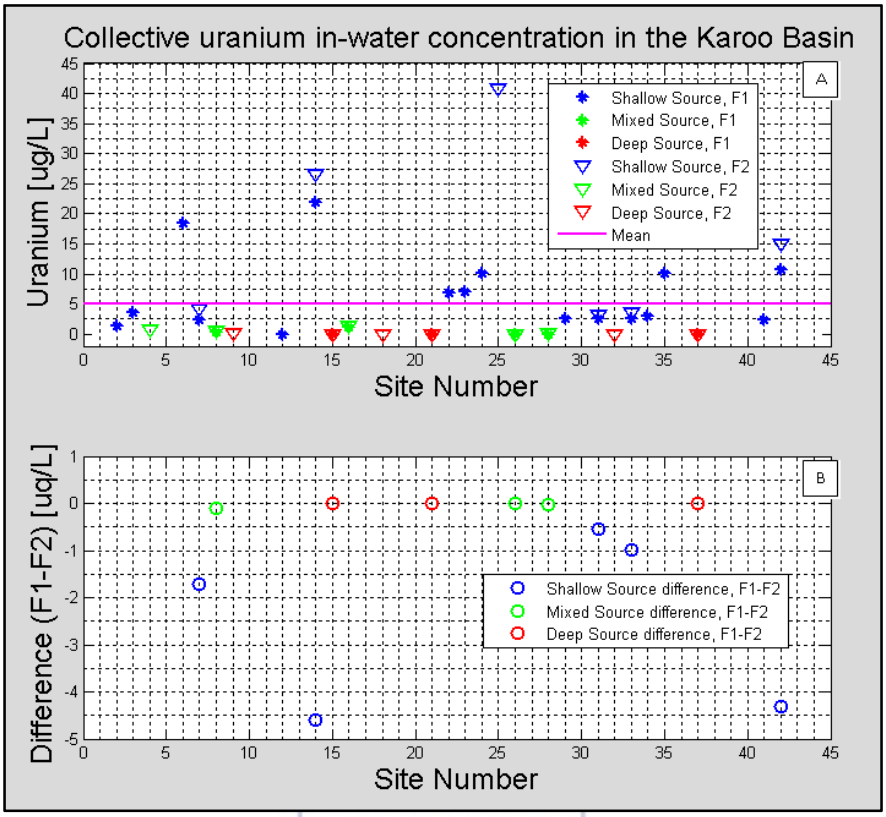

Figure 5-23: Characterization results (A) of uranium in-water concentration according to the groundwater's source classification and associated inter-annual temporal differences (B) between F1 and F2.

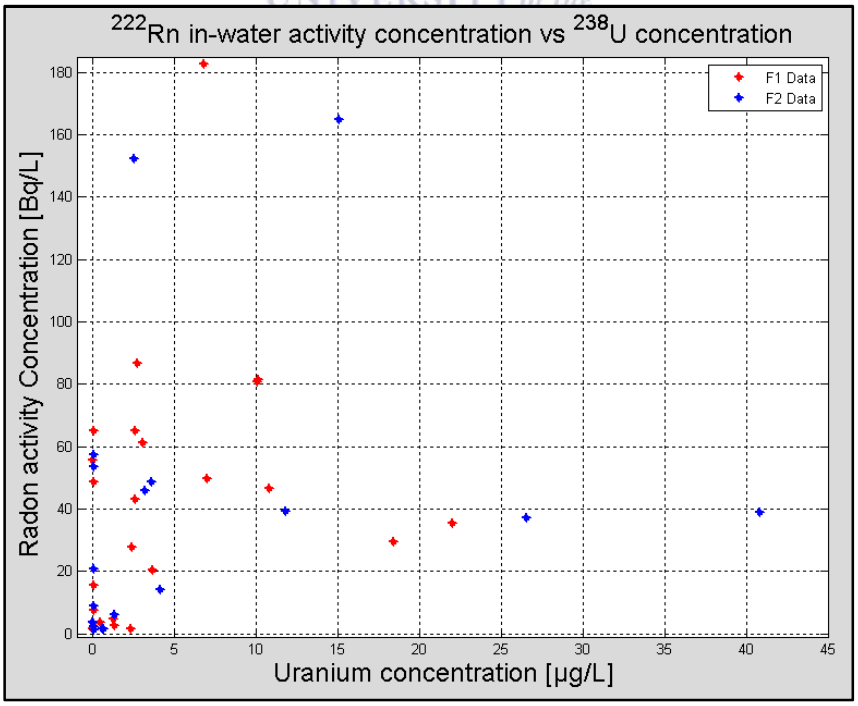

Figure 5-24: Collective (F1 & F2) characterization of the radon-in-water activity concentration and uranium in-water concentration.

The shallow aquifers have an overall higher radon-in-water activity concentration compared to mixed and deep aquifers (see figure 5-25 and table 5-7). The mean radon-in-water activity concentration (see table 5-7) for the shallow aquifers (55 ± 10 Bq/L) was two to three times higher than that of the mixed (20 ± 6 Bq/L) and deep aquifers (14 ± 3 Bq/L). The mean radon-in-water activity concentration characterisation for mixed (20 ± 6 Bq/L) and deep (14 ± 3 Bq/L) groundwater sources was almost identical within measurement uncertainty (see table 5-7). The European Union (EU) proposed a radon referenced action level for radon in drinking water of 100 Bq/L (EU, 2011). Seven sites had radon-in-water activity concentrations above the EU referenced level, S22, S35, S42, S46, S47, S48 and S51(See Appendix table 1,2 and 3).

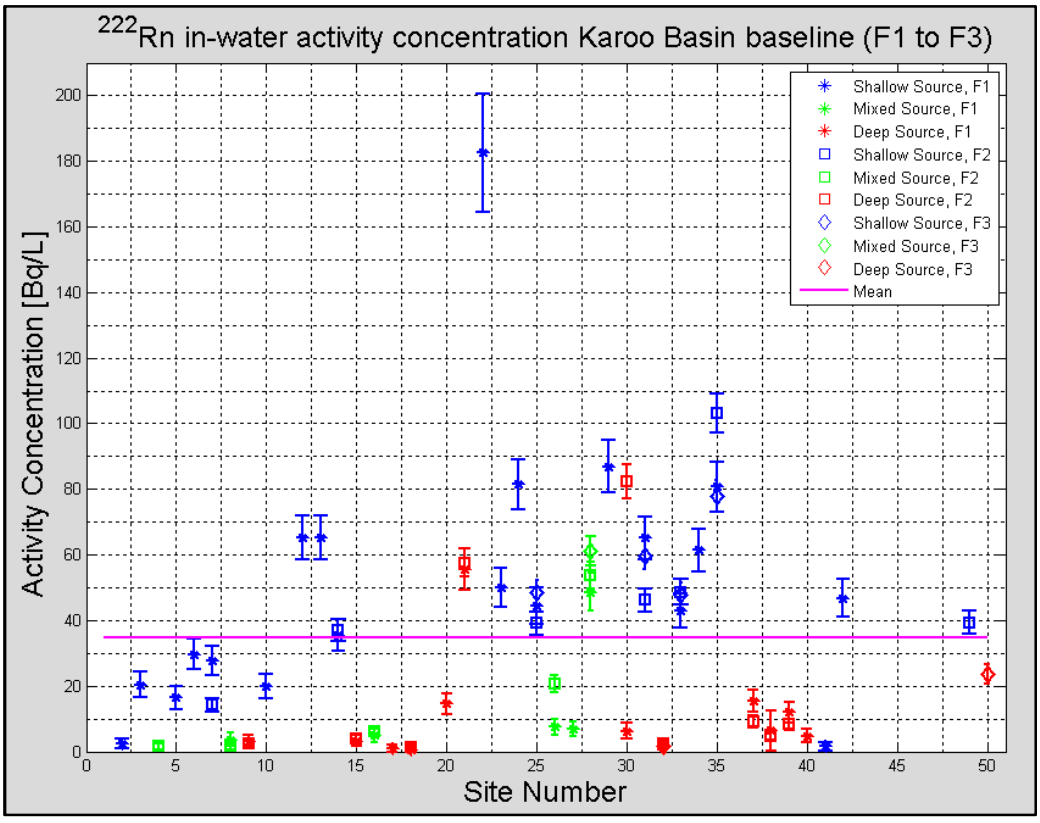

Figure 5-25: Collective results of radon-in-water activity concentration according to the groundwater's source classification (F1 to F3).

For the three measurement series, shallow aquifers are associated with relatively lower water temperatures of below 23 °C (see figure 5-26), which as mentioned, are higher in radon activity concentrations. The deep aquifers have a higher relative water temperature of above

23 °C (see figure 5-26), which is associated with lower radon-in-water activity concentrations. As stated before (see section 5.1), this observation is counterintuitive, as previous studies have shown that warmer groundwater, such as hot springs, have elevated radon-in-water activity concentrations (Vogiannis et al., 2004; Song et al., 2011; Botha et al., 2016).

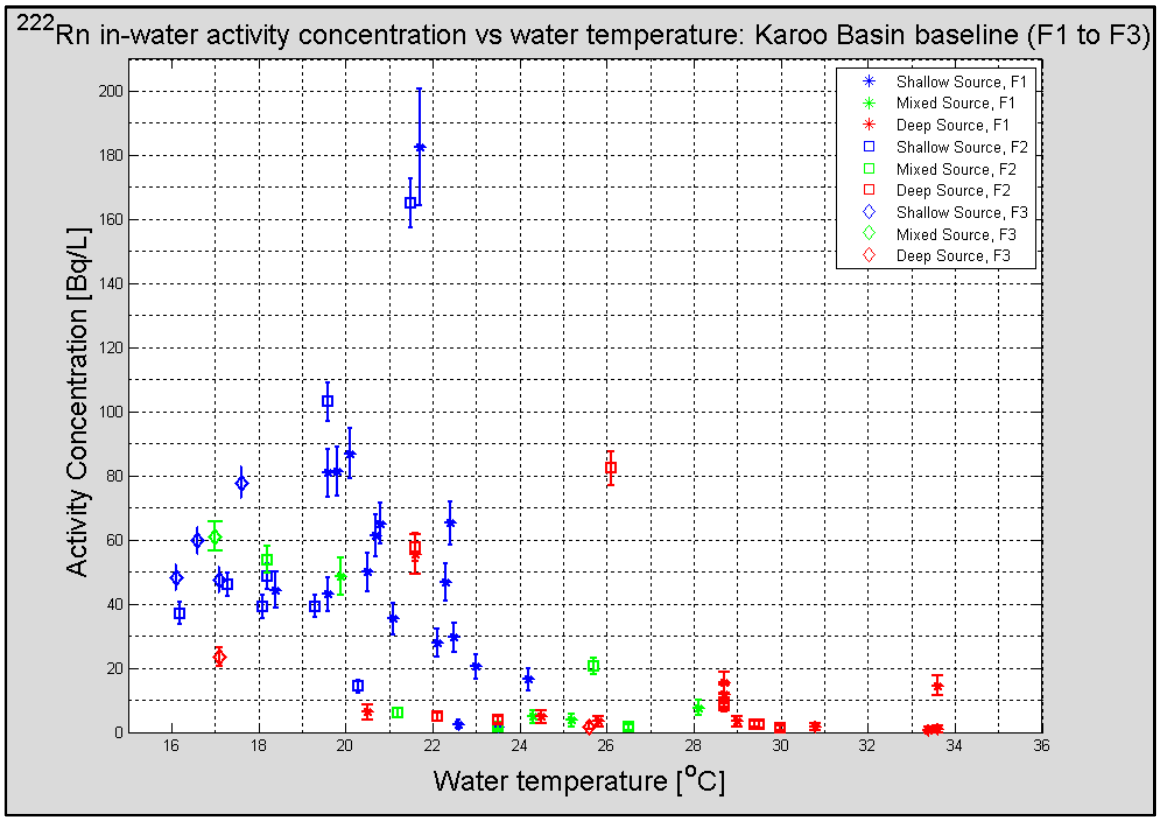

Figure 5-26: Collective results of radon-in-water activity concentration as a function of the groundwater's temperature and source classification (F1 to F3).

The highest radon-in-water activity concentration measured from a hot spring (see table 5-5) during this study was 26 ± 3 Bq/L (S26, F2) compared to a higher mean (long-term) of 205 ± 6 Bq/L measured at another study in Montagu (Botha et al., 2016). For the hot spring S32, (VFB1, deep source) radon-in-water activity concentrations remained constant to within measurement uncertainty during all three of the measurement series (see table 5-5). The hot spring S37 (FLS1, mixed), however, showed a decrease in the radon-in-water activity concentration from the F1 to F2.

Table 5-5: Collective hot springs radon-in-water activity concentration results for the Karoo Basin.

Sites classification	Sampling quality	Radon-in-water activity concentration, F1, [Bq/L]	Radon-in-water activity concentration, F2, [Bq/L]	Radon-in-water activity concentration, F3, [Bq/L]
S9 (CRS1), Deep Source	Not good	3 ± 2	2 ± 1	-
S15 (BFB1), Deep Source	Good	3 ± 2	4 ± 1	-
S18 (ANS1), Deep Source	Not good	1 ± 1	1 ± 1	-
S20, Deep Source	Good	2 ± 1	-	-
S26 (RWB1c), Mixed Source	Good	8 ± 2	26 ± 3	-
S32 (VFB1), Deep Source	Good	2 ± 1	2 ± 1	2 ± 1
S37 (FLS1), Deep Source	Not good	16 ± 3	9 ± 2	-

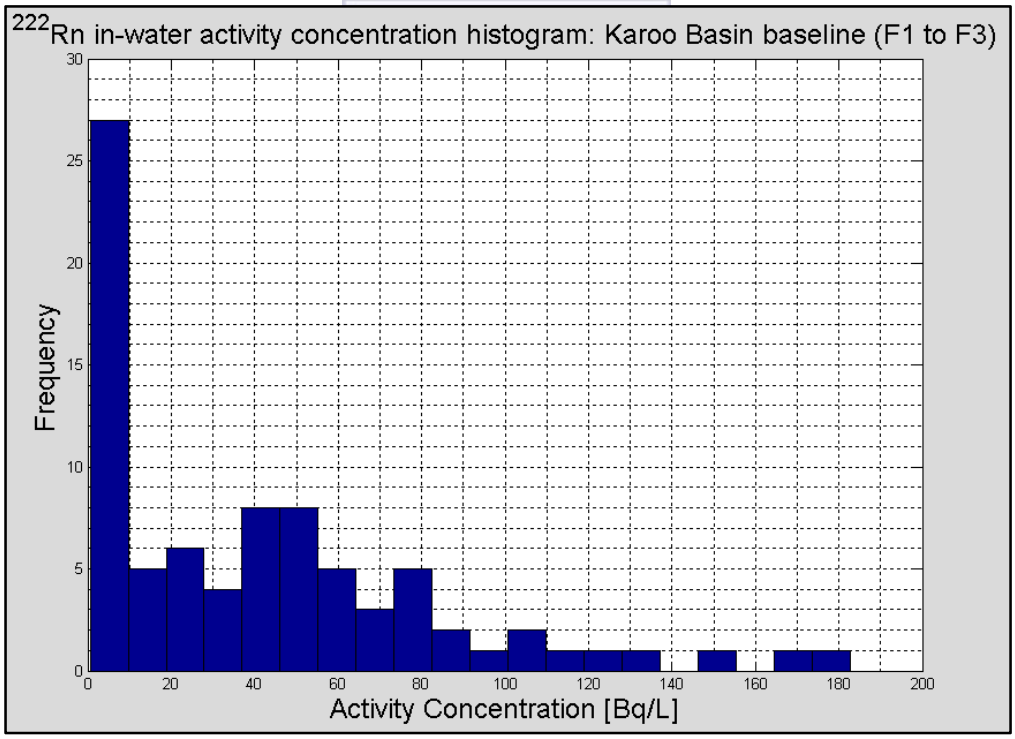

Figure 5-27: Collective histogram (20 bins) of radon-in-water activity concentration.

The baseline radon-in-water activity concentration for the Karoo basin can be characterised by a minimum 0.6 ± 0.9 Bq/L, maximum 183 ± 18 Bq/L, and mean 41 ± 5 Bq/L based on 86 measurements (see table 5-6).

Table 5-6: Collective baseline radon-in-water activity concentration results from F1 to F3.

Description	Radon-in-water activity, [Bq/L]
Minimum	0.6 ± 0.9
Maximum	183 ± 18
Mean	41 ± 5
Median	28
Data points	86

Table 5-7: Collective radon-in-water activity concentration statistical results according to the groundwater's source classification from F1 to F3.

Aquifer type	Minimum radon-in-water activity, [Bq/L]	Maximum radon-in-water activity, [Bq/L]	Mean radon-in-water activity, [Bq/L]	Median radon-in-water activity, [Bq/L]	Data points
Shallow	2 ± 1	183 ± 18	55 ± 10	47	32
Mixed	2 ± 1	61 ± 5	20 ± 6	7	11
Deep	1 ± 1	82 ± 5	14 ± 3	5	23

South Africa as a whole experienced a record drought from 2015 to 2016 (Bluden et al., 2015), and this should be taken into consideration as a factor which changed from F2 to F3. The lower annual rainfall could have an effect on the NORM levels within aquifers of the Karoo Basin. The mean radon-in-water activity concentration for all types of aquifers did undoubtedly increase during the period of the drought (see table 5-8). Nonetheless, it cannot conclusively be stated that radon-in-water in the Karoo Basin increased due to the intense droughts.

In total there were six aquifers on which measurements were performed for all of the measurement series (see figure 5-28). A particular challenge was that certain boreholes became unavailable from one measurement series to another. This is also why some new aquifers were measured for successive fieldtrips. Some boreholes got internally blocked, and one particular very deep borehole at Merweville depends on natural pressure for pumping

which is not always available. For these six aquifers the largest radon-in-water activity concentration change was observed for the shallow aquifer S35 (VFB4), namely 22 Bq/L (see figure 5-28, A). The radon-in-water activity concentrations for the shallow and mixed aquifers fluctuate over time (see figure 5-28, B). However, the radon-in-water activity concentrations for this deep aquifer, S32 did not change during the time the study was conducted (see figure 5-28, B).

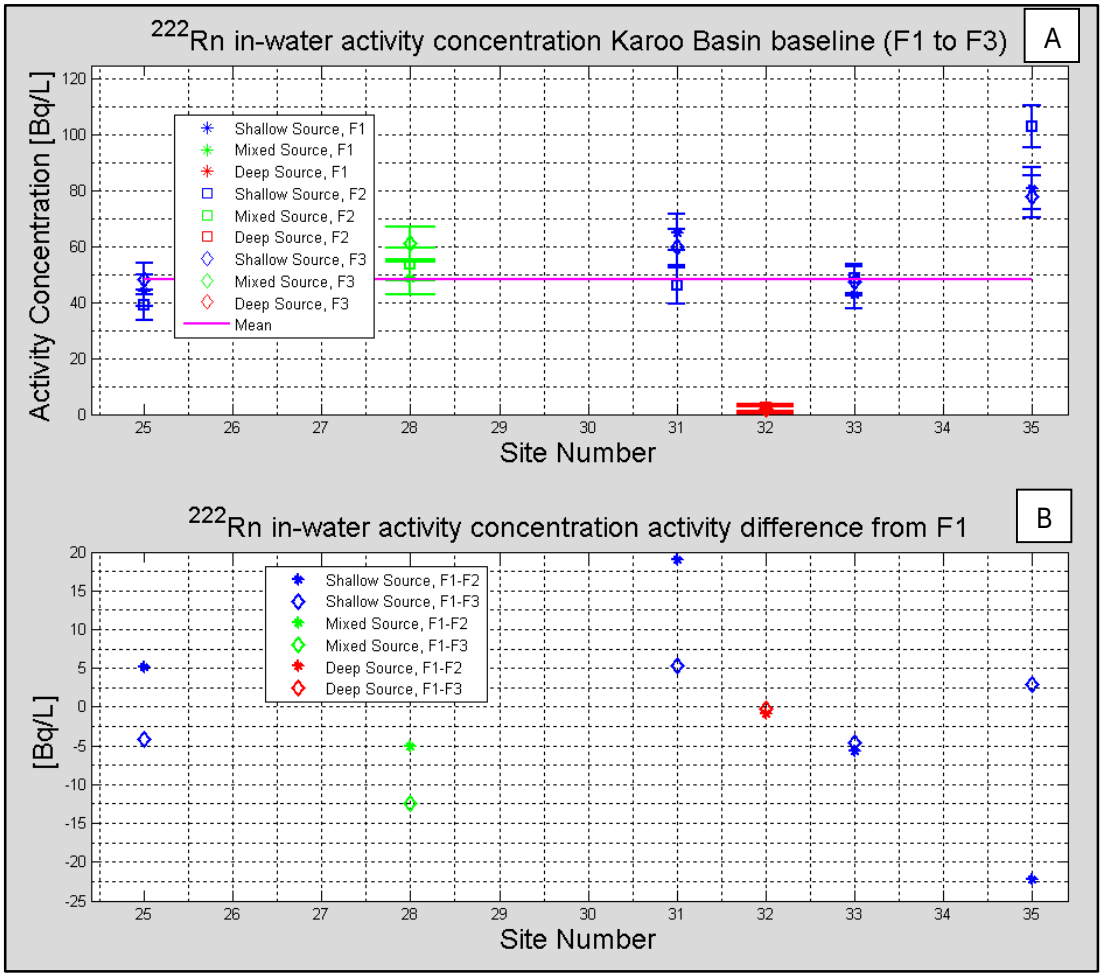

Figure 5-28: Collective (F1 to F3) comparison results of radon-in-water activity concentration according to the groundwater's source classification.

A consistent mean increase of about 12 Bq/L from F1 to F2 and furthermore 15 Bq/L from F2 to F3 was observed for the collective aquifers' radon-in-water activity concentration (see table 5-8). The mean radon-in-water activity concentrations for all the aquifers increased seasonally from the summer measurement series (F1) to the winter measurement series (F2) in 2014 (see table 5-8). Comparing the mean radon-in-water activity concentration from the

winter of 2014 (F2) to the winter of 2016 (F3); one can see a clear increase in the collective results, no change within measurement uncertainties for the shallow sources, and a decrease for the deep sources (see table 5-8). The seasonal effects (rain fall) are a contributing natural factor which could influence the radon-in-water levels in the groundwater of the Karoo Basin.

Table 5-8: Collective mean radon-in-water activity concentration statistical results according to the groundwater's classification (shallow/mixed/deep).

Mean radon-in-water activity for the different measurement series, [Bq/L]			
Aquifer type	**F1**	**F2**	**F3**
All types	32 ± 5	44 ± 8	61 ± 16
Shallow	51 ± 11	61 ± 22	58 ± 29
Mixed	14 ± 6	16 ± 8	-
Deep	10 ± 3	19 ± 6	12 ± 9

Radium (^{226}Ra and ^{228}Ra) in-water activity concentration measurements were performed during the second measurement series (see section 3.10). The ^{228}Ra/^{226}Ra in-water activity concentration ratio is a radionuclide signature to identify water contamination caused by unconventional shale-gas wastewater (Vengosh et al., 2014; Warner et al., 2014). The geologically specific ^{228}Ra/^{226}Ra ratios typically range from 0.15 to 4.25 for fractured crystalline rock (Vinson et al., 2008). Typical ^{228}Ra/^{226}Ra ratios (see figure 5-29) observed from unconventional shale-gas wastewater in the Marcellus formation are of the order of 0.1 to 0.3 (Warner et al., 2014). Due to low radium in-water activity concentrations only six of the 29 locations had detectable levels. For these six aquifers the radium (^{226}Ra) in-water activity concentration in the Karoo Basin had a minimum of 0.002 Bq/L, mean of 0.005 ± 0.001 Bq/L and a maximum of 0.008 Bq/L (see table 5-9). The baseline radium (^{228}Ra) in-water activity concentration in the Karoo Basin had a minimum of 0.004 Bq/L, mean of 0.010 ± 0.002 Bq/L and maximum of 0.015 Bq/L (see table 5-9). The ^{228}Ra/^{226}Ra ratio in the Karoo Basin can be characterised (see table 5-9) with a minimum of 0.93, a mean of 3.26 ± 1.33, and a maximum of 6.49 (WRC, 2015).

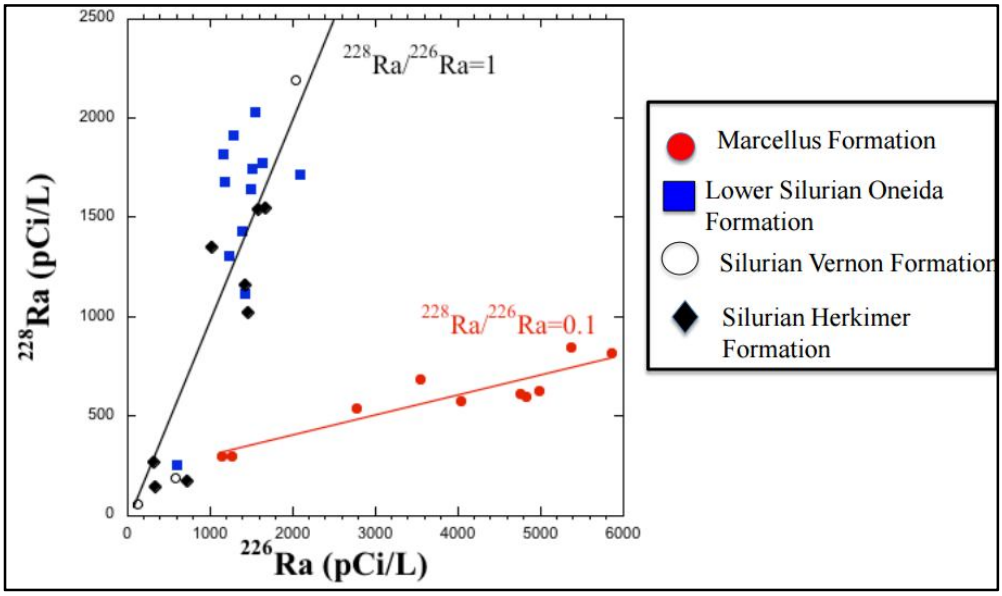

Figure 5-29: The $^{228}Ra/^{226}Ra$ ratio from Marcellus brines (unconventional shale gas) and other oil and gas (conventional) produced waters (Warner et al., 2014).

The disequilibrium between certain NORMs (^{226}Ra, ^{222}Rn and ^{238}U) has been discussed and becomes evident again. The disequilibrium between ^{222}Rn and ^{226}Ra in the aquifers of the Karoo Basin is evident based on the very low activity concentrations of the ^{226}Ra compared to ^{222}Rn (see table 5-9).

The mean $^{228}Ra/^{226}Ra$ ratios (see table 5-9) interestingly was also the highest for the shallow aquifers (4.8 ± 1.3) compared to the mixed and shallow aquifers (2.1 ± 0.4). Similarly, the higher radon-in-water activity concentration and elemental uranium concentration are from the shallow aquifers. Due to the unique geology of the Karoo Basin (see figure 1-3), the $^{228}Ra/^{226}Ra$ ratio should likewise be unique. Interestingly, the mean $^{228}Ra/^{226}Ra$ ratio for the six aquifers of the Karoo Basin was 3.3 ± 1.2 which is higher than that observed at other aquifers in the Marcellus Basin (Warner et al., 2014).

Table 5-9: Radium (^{226}Ra and ^{228}Ra) in-water activity concentration results and associated radon-in-water activity concentration from the second measurement series (WRC, 2015).

Sites number and classification	Ra-226 in-water activity concentration, [Bq/L]	Ra-228 in-water activity concentration, [Bq/L]	Ra-228/Ra-226	Radon-in-water activity concentration, [Bq/L]
S15 (BFB1), Deep Source	0.002	0.004	2.63	3.8
S18 (ANS1), Deep Source	0.008	0.012	1.62	1.3
S28 (VBB1), Mixed Source	0.007	0.006	0.93	53.7
S7 (WP 502), Shallow Source	0.002	0.012	6.94	14.2
S33 (VFB2), Shallow Source	0.002	0.01	5.05	48.6
S42 (MWB2), Shallow Source	0.006	0.015	2.39	165

CHAPTER 6 GENERAL CONCLUSION

6.1 Introduction

The main objective of this study was to develop a radon in-groundwater baseline reference database (see table 6-1) for the Karoo Basin prior to unconventional shale-gas developments and to characterise it. The legacy of hydraulic fracturing on the environment and human health are not very well studied over the last two decades since it has been implemented on an industrial scale. Baseline radon characterisation within aquifers of the Karoo Basin could further aid research on radiological health risks related to chronic TENORM or NORM exposure, as well as a radioisotope tracer (Hydrology). This study is a pioneering NORM (radon) in-groundwater characterisation of the semi-arid Karoo Basin.

Radon is the second leading cause of lung cancer after smoking (WHO, 2009; IAEA, 2014). Inhalation of radon can present up to an order of magnitude larger ionising radiation dose compared to ingestion (USNRC, 1999). Chronic ingestion of water with elevated radon levels poses associated health risks for humans (IAEA, 2014) consequently, 100 Bq/L was recommended as the maximum level for public drinking water (EU, 2001; WHO, 2011). A guideline was made by the WHO that uranium concentration in- public drinking water should not exceed 30.0 µg/L (WHO, 2011).

Hydraulic fracturing is conducted at various depths below the surface; however, most are performed at a depth of 2500 m (Jackson et al., 2015). Monitoring deep aquifer resources are thus of particular importance for strategic NORM monitoring. If water contamination occurs due to hydraulic fracturing, deep groundwater sources will most likely be affected the most severely (see figure 1-1). Emphasis was placed in this section on the results of the deep aquifers nonetheless based on that shallow, mixed and deep aquifers could potentially be connected, it will also be discussed. A key focus of the collaborative research (see section 4-1) is to study the potential linkage between deep and shallow sources (WRC, 2015; Kelley, 2016).

A brief overview of the study:

Table 6-1: An overview of the radiological survey for the groundwaters from the Karoo Basin performed in this study.

Conducted from 2014 to 2016 with three measurement series (F1, F2 and F3)
86 measurements of radon in-water
Supplemantary ^{238}U, ^{226}Ra, and ^{228}Ra measurements (F1 and F2)
53 different aquifers sampled from in the Karoo Basin
Studied 14 deep aquifers, 6 mixed aquifers, 21 shallow aquifers, 6 hot springs and other aquifers which were unclassifed

The baseline radon-in-water activity concentration characterisation in this study (see table 5-6) yields: a minimum of 0.6 ± 0.9 Bq/L, a maximum of 183 ± 18 Bq/L, and a mean of 41 ± 5 Bq/L. The majority of the aquifers (see figure 5-27) had relatively low radon-in-water activity concentration (< 30 Bq/L). The shallow aquifers (see table 5-7) systematically had the highest mean radon-in-water activity concentration (55 ± 10 Bq/L) compared to mixed (20 ± 6 Bq/L) and deep aquifers (14 ± 3 Bq/L). The measurement of radon-in-water activity concentration presents a way to indicate the type of aquifer within the Karoo Basin (see figure 5-26).

Consequently, less ionizing radiation exposure will occur to individuals drinking water from deep aquifers compared to consumption from mixed and especially shallow aquifers within the Karoo Basin. In total seven aquifers had radon-in-water activity concentrations above (see figure 5-4 and figure 5-8) the recommended WHO level for public drinking water of 100 Bq/L (WHO, 2011). Three of them are known for certain to be shallow aquifers (S22, S35 and S42) while the others (S46, S47, S48 and S51) have not been classified but are most likely to be shallow saline aquifers.

It is imperative to study the temporal nature of radon-in-water. A change in NORM activity concentration over time within aquifers in the Karoo Basin could be caused by natural and/or anthropogenic factors. During the time frame of this study no hydraulic fracturing activities were conducted, creating an ideal opportunity for a baseline conditions. Fluctuations in the

NORM results from this study cannot be contributed due to local industrial processes. However, climate change cannot be entirely disregarded as having no indirect effect (rainfall). Fluctuations of radon-in-water activity concentrations during the time frame of this study for deep aquifers were undetectable to very small (see table 5-8, figure 5-25 and figure 5-28). However, considerable fluctuations of radon-in-water can be confirmed for mixed and shallow aquifers (see table 5-8, figure 5-25 and figure 5-28). The radon-in-water fluctuating nature (shallow aquifers) was observed seasonally (see figure 5-16) and annually (see table 5-8 and figure 5-28) bases. A noticeable increase in the collective mean radon-in-water activity concentration from the first (32 ± 5 Bq/L), second (44 ± 8 Bq/L) to third (61 ± 16 Bq/L) measurement series was observed (see table 5-8). The increase in the collective mean radon-in-water activity concentration could be due to the record nationwide drought in 2015 (Bluden et al., 2015).

The elemental uranium levels within aquifers of the Karoo Basin can characterised by a minimum of below detection limit, a maximum of 41 µg/L, and a collective mean of 5.1 ± 0.8 µg/L. One location (S15) had a uranium in-water concentration above the recommended drinking water guideline of 30.0 µg/L (WHO, 2011). Similar for the radon-in-water results, shallow groundwater sources systematically had the highest uranium in-water concentrations when compared to mixed and deep sources (see figure 5-23). An inverse relationship exists between the radon-in-water activity concentration and uranium in-water concentration (see figure 5-24).

The baseline $^{228}Ra/^{226}Ra$ ratio for the Karoo Basin can be characterized by a minimum of 0.93, a mean of 3.26 ± 1.33, and a maximum of 6.49 (WRC, 2015). These $^{228}Ra/^{226}Ra$ ratios can be used as an analytical isotopic method to indicate whether contamination occurred due to unconventional shale-gas wastewater (Vengosh et al., 2014; Warner et al., 2014). The radium (^{228}Ra and ^{226}Ra) in-water activity concentrations were very low with a maximum of 0.015 Bq/L for ^{228}Ra, (see table 5-9). Studying baseline radon-in-water characterization according to spatial, temporal and aquifer classification offered a perspective on the radiological nature of groundwater within the Karoo Basin.

6.2 Recommended future work

Further investigation and continuing radiological characterisation of groundwaters will enhance our understanding of potential radiological contamination due to unconventional shale-gas development in the Karoo Basin. Future work could include the following:

- expand radiological baseline database with additional strategic measurement locations,
- develop and improve ultra-low radium (^{228}Ra and ^{226}Ra) in-water activity concentration measurement capabilities,
- develop an advanced underwater source (inlet) radon sampling system,
- expand study to perform an in-depth demographics study of chronic NORM exposure associated with health risks due to consumption of elevated levels of NORM,
- utilize the results from this study to extend the measurement of radon-in-water activity concentration within hot springs to most areas in South Africa.

REFERENCES

Andrews, J.N., Ford, D.J., Hussain, N., Trivedi, D., Youngman, M.J. 1989. Natural radioelement solution by circulating groundwaters in the Stripa granite, Geochimica et Cosmochimica Acta 53, 1791–1802, https://doi.org/10.1016/0016-7037(89)90300-1.

Asikainen, M., 1981b. State of disequilibrium between U-238, U-234, Ra-226, and Rn-222 in groundwater from bedrock, Geochimica et Cosmochimica Acta 45, 201–206.

Audi, G., Wapstra, A.H., Thibault, C.J. Blachot, Bersillon, O. 2003. The NUBASE evaluation of nuclear and decay properties, Nuclear Physics A 729: 3–128.

Bauer, W., Westfall, G.D., 2011, University Physics with Modern Physics, International Edition 2011, ISBN 978-007-131366-7, pg. 1334

Ball, T.K., Cameron, T.B., Colman, T.B., Roberts, P.D., 1991. Behaviour of radon in the geological environment: a review. Quart. J. Eng. Geol. Hydrogeol. 24, 169e182. doi: 10.1144/GSL.QJEG.1991.024.02.01.

Becker, K., 2004, One century of radon therapy, Int. J. Low Radiation, Vol. 1, No. 3, page 334.

Blunden, J. and D. S. Arndt, Eds., 2016. State of the Climate in 2015. Bull. Amer. Meteor. Soc., 97 (8), S1–S275, doi: 10.1175/2016BAMSStateoftheClimate.

BNL, 2016, A., Interactive Chart of Nuclides. National Nuclear Data Center: Brookhaven National Laboratory, Retrieved 2016-02-09.

Botha, R., Newman, R.T., Maleka, P.P. 2016. Radon levels measured at a touristic thermal spa resort in Montagu (South Africa) and associated effective doses, Health Phys. 2016 Sep;111(3): 281-9. doi: 10.1097/HP.0000000000000527.

Bolton, D.W., 2000. Occurrence and distribution of radium, gross alpha-particle activity, and gross-beta particle activity in ground water in the Magothy Formation and Potomac Group aquifers, upper Chesapeake Bay area, Maryland. Maryland Geological Survey, Report of Investigations, vol. 70.

Brunke, E.G, Labuschagne, C., Parker, B., Van der Spuy, D., Whittlestone, S., 2002. Cape Point GAW Station 222Rn detector: factors affecting sensitivity and accuracy, Atmospheric Environment, 36 (2002) 2257–2262.

Butterweck, G., Porstendörfer, J., Reineking, A., Kesten, J., 1992. Unattached fraction and the aerosol size distribution of the radon progeny in a natural cave and mine atmosphere, Radiat. Prot. Dosimetry 45:167–170.

Cable, J. E., Burnett, W.C., Chanton J. P., Weatherly, G.L.,1996, Estimating groundwater discharge into the north eastern Gulf of Mexico using radon-222, Earth and Planetary Science Letters, Volume 144, Issues 3–4, November 1996, pp. 591-604, doi: 10.1016/S0012-821X(96)00173-2.

Capture, 2016. Capture RAD7 data acquisition and analyses manual for Windows and OS X, DURRIDGE Company Inc., Revision: 20 May 2016.

Cetnar, J, 2006. General solution to Bateman equation for nuclear transmutations, Annals of Nuclear Energy 33 (7), 640–645, doi: 10.1016/j.anucene.2006.02.004.

Cecil, L.D., Smith, R.C., Reilly, M.A., Rose, A.W., 1987. Radium-228 and radium-226 in ground water of the Chickies Formation, southeastern Pennsylvania. In: Graves, B. (Ed.), Radon, Radium, and Other Radioactivity in Ground Water. Lewis Publishers, Chelsea, MI, pp. 437–447.

Charlez, Ph. A., 1997, Rock Mechanics: Petroleum Applications. Paris: Editions Technip. p. 239. ISBN 9782710805861.

Crawford, J, Zahorowski, W., Cohen, D.D., 2009. A new metric space incorporating radon-222 for generation of back trajectory clusters in atmospheric pollution studies, Atmospheric Environment 43 (2009) 371–381, doi: 10.1016/j.atmosenv.2008.09.073.

Crawford, J., Chambers, S., Kang, K., C-H., Kang, Griffiths, A., Kim, W-H., 2015. Analysis of a decade of Asian outflow of PM10 and TSP to Gosan, Korea; also incorporating Radon–222, Atmospheric Pollution Research 6(2015)529-539, doi: 10.5094/APR.2015.059.

CSIR, 2016. Shale Gas Development in the Central Karoo: A Scientific Assessment of the Opportunities and Risks. Accessed on 24-11-2016, Online Source: http://seasgd.csir.co.za/wp-content/uploads/2016/11/SGD-Scientific-Assessment-Binder1_LOW-RES_INCL-ADDENDA_21Nov2016.pdf

De Laeter, J.R., Bohlke, J.K.,de Bievre, P., Hidaka, H., Peiser, H.S., Rosman, J.R., Taylor, P.D.P, 2003, Atomic weights of the elements, Review 2000 (IUPAC Technical Report), Pure and Applied Chemistry 75 (6): 683–800. doi: 10.1351/pac200375060683.

Dickson, B.L., Herczeg, A.L., 1992. Naturally-occurring radionuclides in acid-saline groundwaters around Lake Tyrrell, Victoria, Australia. Chemical Geology 96, 95–114.

DOE, 2013, South Africa Yearbook 2012/2013, Department of Energy (DOE), http://www.gcis.gov.za/sites/www.gcis.gov.za/files/docs/resourcecentre/yearbook/2012/08%20Energy%20.pdf, online accessed on the 31-10-2016.

Durrani, S.A. and Ilic, R., 1997. Radon Measurements by Etched Track Detectors, World Scientific, ISBN: 978-981-4498-92-0.

DRYSTICK, 2015, DRYSTICK User Manual: Active Moisture Exchanger with Duty Controller, Revision 2015-12-16, http://www.durridge.com/.

DWS, 2015. Annual Report 2014/2015, Vote 42, Department of Water and Sanitation, Republic of South Africa, http://www.gov.za/sites/www.gov.za/files/DWA-annual-report-2014-15.pdf, online accessed on the 31-10-2016.

EISGE, 2014. The expert panel on harnessing science and technology to understand the environmental impacts of shale gas extraction, Council of Canadian Academies, Environmental Impacts of Shale Gas Extraction in Canada (EISGE), ISBN 978-1-926558-78-3 (pdf), pg. 93 – 94.

EIA, 2013. Technically Recoverable Shale Oil and Shale Gas Resources: An Assessment of 137 Shale Formations in 41 countries outside the United States, U.S. Energy Information Administration (EIA), Full Report.

EIA, 2011. World Shale Gas Resources: An initial Assessment of 14 Regions outside the United States, Accessed on: 15-05-2015, Online Source: http://www.adv-res.com/pdf/ARI%20EIA%20Intl%20Gas%20Shale%20APR%202011.pdf

EPA, 1993.United States Environmental Protection Agency, A Physician's Guide: Radon The health threat with a simple solution. Document 402- K-93-008.

EPA, 2011. Plan to study the potential impacts of hydraulic fracturing on drinking water resources: Office of Research and Development, U. S. Environmental Protection Agency, Washington, D.C., November 2011, EPA/600/R-11/122.

EU, 2001. European Union Commission Recommendation on the protection of the public against exposure to radon in drinking water supplies. Office Journal of the European Community, L 344, 28 December, 85–88.

Firestone, R.B., 1996. Table of Isotopes (CD ROM Edition, Ver 1.0), Eight Edition, Wiley-Interscience.

Gilkeson, R.H., Perry, E.C., Cowart, J.B., Holtzman, R.B., 1984. Isotopic studies of the natural sources of radium in groundwater in Illinois. Illinois Water Resources Center, Research Report, vol. 187.

Gingrich, J. E., 1984. Radon as geochemical exploration tool, Journal of Geochemical Exploration 21, 19-39, doi: 10.1016/0375-6742(84)90032-3.

Goldstein, S.D., Hopke, P.K., 1985, Environmental neutralisation of polonium-218. Environ Sci. Technol. 19:146–150, doi: 10.1021/es00132a006.

Grundl, T., Cape, M., 2006. Geochemical factors controlling radium activity in a sandstone aquifer, GroundWater 44, 518–527, doi:10.1111/j.1745-6584.2006.00162.x.

GWPC, 2009. Modern Shale Gas Development in the United States: A Primer (Report). DOE Office of Fossil Energy and National Energy Technology Laboratory. Ground Water Protection Council (GWPC), pp. 56–66. Retrieved 24 February 2012.

Haluszczak, L. O., Arthur, W.R., Kump, L.R., 2013, Geochemical evaluation of flowback brine from Marcellus gas wells in Pennsylvania, USA. Appl. Geochem, 28, 55-61, http://dx.doi.org/10.1016/j.apgeochem.2012.10.002.

Herczeg, A.L., Simpson, H.J., Anderson, R.F., Trier, R.M., Mathieu, G.G., Deck, B.L., 1988. Uranium and radium mobility in groundwaters and brines within the Delaware Basin, South eastern New Mexico, U.S.A. Chemical Geology, Isotope Geoscience Section 72, 181–196, doi: 10.1016/0168-9622(88)90066-8.

IAEA, 2009. World Distribution of Uranium Deposits (UDEPO) with Uranium Deposit Classification, 2009 Edition, IAEA-TECDOC-1629, pg. 11.

IARC, 2015. Agents Classified by the IARC monographs, Volumes 1-111. Retrieved (2015-02-02): http://monographs.iarc.fr/ENG/Classification/ClassificationsCASOrder.pdf.

IAEA, 2013, Underestimated threat - Radon in homes, http://www.iaea.org/newscenter/news/underestimated-threat-radon-homes, International Atomic Energy Agency (IAEA), Accessed: 2015-01-15.

IAEA, 2014. Radiation protection and safety of radiation sources: international basic safety standards.Vienna: IAEA; IAEA Safety Standards Series No. GSR Part 3.

ICRP Publication 126, 2014, Radiological Protection against Radon Exposure, Volume 43, No. 3, ISBN 9781473916586.

ICRP, 2010. Lung Cancer Risk from Radon and Progeny and Statement on Radon, ICRP Publication 115, Ann. ICRP 40(1).

Jackson, R. B., Vengosh, A., Darrah, T.H., Warner, N.R., Down, A., Poreda, R.J., Osborn, S.G., Zhao, K., Karr, J.D., 2013. Increased stray gas abundance in a subset of drinking water wells near Macellus shale gas extraction, Proceedings of the National Academy of Sciences of the United States of America (PNAS), doi: 10.1073/pnas.1221635110.

Jackson, R. B., Lowry E.R., Pickle, A., Kang, M., DiGiulio, D., Zhao, K., 2015. The Depths of Hydraulic Fracturing and Accompanying Water Use Across the United States, Environ Sci Technol. 2015 Aug 4;49(15):8969-76. doi: 10.1021/acs.est.5b0122.

Knoll, G.F., 2000. Radiation Detection and Measurement, Third Edition, ISBN 0-471-07338-5.

Kelley, S, 2016. Application of hydrochemistry and residence time constraints to distinguish groundwater systems in the Karoo Basin prior to shale-gas exploration, Master Thesis, University of Stellenbosch, http://hdl.handle.net/10019.1/98413.

King, P.T., Michel, J., Moore, W.S., 1982. Ground water geochemistry of ^{228}Ra, ^{226}Ra and ^{222}Rn. Geochimica et Cosmochimica Acta 46, 1173–1182, doi: 10.1016/0016-7037(82)90003-5.

Kojima, H, Nagano, K., 1999. The influence of meteorological and soil parameters on radon exhalation, In: Proc. Int. Conf. Radon in the Living Environment, 19e23 April 1999, Athens, Greece, p. 627e642.

Kraemer, T.F., Reid, D.F., 1984. The occurrence and behavior of radium in saline formation water of the U.S. Gulf Coast region. Isotope Geoscience 2, 153–174, doi: 10.1016/0009-2541(84)90186-4.

Landa, E.R., Phillips, E.J.P., Lovley, D.R., 1991. Release of 226Ra from uranium mill tailings by microbial Fe(III) reduction. Applied Geochemistry 6, 647–652.

Martin, A.J., Crusius, J., Jay McNee, J., Yanful, E.K., 2003. The mobility of radium-226 and trace metals in pre-oxidized subaqueous uranium mill tailings, Applied Geochemistry 18, 1095–1110, http://dx.doi.org/10.1016/S0883-2927(02)00243-3.

Mine water management in the Witwatersrand Gold Fields with special emphasis on acid mine drainage, 2010. Report to the inter-ministerial committee on acid mine drainage ORAU (Oak Ridge Associated Universities), 1999, www.arau.org/ptp/collection/brachytherapy/seeds.htm.

Osborn, G., S., Vengosh, A., Warner, N.R., Jackson, R.B., 2011. Methane contamination of drinking water accompanying gas-well drilling and hydraulic fracturing, PNAS, 8172–8176, vol. 108, no. 20, doi: 10.1073/pnas.1100682108.

Petitta, M., Primavera, P., Tuccimei, P., Aravena, R., 2011. Interaction between deep and shallow groundwater systems in areas affected by Quaternary tectonics (Central Italy): a geochemical and isotope approach, Journal of Environmental Earth Science, May 2011, Volume 63, Issue 1, pp 11–30, doi: 10.1007/s12665-010-0663-7.

Phillips, E.J.P., Landa, E.R., Kraemer, T., Zielinski, R., 2001. Sulfate-reducing bacteria release barium and radium from naturally occurring radioactive material in oil-field barite. Geomicrobiology Journal 18, 167–182, http://dx.doi.org/10.1080/01490450120549.

Porstendörfer, J., Zock, Ch, Wendt, J., Reineking, A., 1999. Radon parameters in outdoor air. Rio de Janeiro. In: Proc. Int. Symp., Technologically Enhanced Natural Radiation (TENR II), 12e17 September 1999, pp. 313e324.

RAD7, 2015, RAD7 Radon Detector User Manual, Revision 7.4.0, http://www.durridge.com/.

RAD H2O, 2016, RAD H2O User Manual: Radon in Water Accessory, Revision 2016-02-02, http://www.durridge.com/.

Rowan, E. L., Engle, M.A., Kirby, C.S., Kraemer, T.F., 2011, Radium Content of Oil- And Gas-Field Produced Waters in the Northern Appalachian Basin (USA) – Summary and Discussion of Data: U.S. Geological Survey Scientific Investigations Report 5135.

Rytz, A, 1973, Atomic Data and Nuclear Data Tables 12, page 479.

Santos, I. R., Bradley, B. D., 2011. Radon tracing of groundwater discharge an Australian estuary surrounded by coastal acid sulphate soils, Journal of Hydrology 396, 246 – 257, http://dx.doi.org/10.1016/j.jhydrol.2010.11.013.

Singh, M., Kumar, M., Jain, R.K., Chatrath, R.P., 1999. Radon in ground water related to seismic events, Journal of Radiation Measurements 30, 465 – 669, http://dx.doi.org/10.1016/S1350-4487(99)00049-9.

Slemr, F., Brunke, E.-G., Whittlestone, S. , Zahorowski, W., Ebinghaus, R. , Kock, H. H., Labuschagne, C., 2013. ^{222}Rn-calibrated mercury fluxes from terrestrial surface of southern Africa, Atmos. Chem. Phys., 13, 6421–6428, 2013, doi: 10.5194/acp-13-6421-2013.

Song, G., Wang, X., Chen, D., Chen, Y., 2011. Contribution of 222Rn-bearing water to indoor radon and indoor air quality assessment in hot spring hotels of Guangdong, China, J Environ Radioact. 2011 Apr;102(4):400-6. doi: 10.1016/j.jenvrad.2011.02.010.

Somlai, K., Tokonami, S., Ishikawa, T., Vancsura, P., Gaspar, M., Jobbagy, V., Somlai, J., Kovacs, T., 2007. ^{222}Rn concentrations of water in the Balaton Highland and in the southern part of Hungary, and the assessment of the resulting dose, Journal of Radiation Measurements, volume 42, 491-495, https://doi.org/10.1016/j.radmeas.2006.11.005.

StudyBlue, 2016. Movement of land masses, https://classconnection.s3.amazonaws.com

/359/flashcards/2453359/png/mass_wasting1355372890165.png, Retrieved: 10-02-2016.

Suchy, D. R., Newell, K. D., 2012. Hydraulic Fracturing of Oil and Gas Wells in Kansas, Kansas Geological Survey, Public Information Circular 32, Revised May 2012 Edition.

Szabo, Z., dePaul, V.T., Kraemer, T.F., Parsa, B., 2005. Occurrence of radium-224, radium-226, and radium-228 in water of the unconfined Kirkwood–Cohansey aquifer system, southern New Jersey. U.S. Geological Survey Scientific Investigations Report 2004–5224.

Szabo, Z., Zapecza, O.S., 1987. Relation between natural radionuclide activities and chemical constituents in ground water in the Newark Basin, New Jersey. In: Graves, B. (Ed.), Radon, Radium, and other Radioactivity in Ground Water. Lewis Publishers, Chelsea, MI, pp. 283–308.

Sturchio, N.C., Banner, J.L., Binz, C.M., Heraty, L.B., Musgrove, M., 2001. Radium geochemistry of groundwaters in Paleozoic carbonate aquifers, midcontinent, USA. Applied Geochemistry 16, 109–122, DOI: 10.1016/S0883-2927(00)00014-7.

Tan, Y., Xiao, Q., Tang, J., Shan, Q., Zhou, Q., Liu, X., 2014, Research on the lower detection efficiency of the RAD7 for ^{220}Rn than for ^{222}Rn, Journal of Instrumentation, Volume 9, http://dx.doi.org/10.1088/1748-0221/9/06/T06001.

UNSCEAR, 2008, Sources and effects of ionizing radiation, United Nations Scientific Committee on the effects of Atomic Radiation, Volume 1, Annex B, ISBN 978-92-1-142274-0, pp 236.

UNSCEAR, 2008, REPORT, Sources and Effects of Ionizing Radiation, United Nations Scientific Committee on the Effects of Atomic Radiation, Annex A: Exposures from Natural Sources of Radiation.

USNRC, 1999, Report of the Committee on Risk Assessment of Exposure to Radon in Drinking Water, Board on Radiation Effects Research, National Research Council (USNRC), Board on Radiation Effects Research, Commission on Life Sciences, Washington, DC: National Academy Press.

Vaupotic, J., 2008, Comparison of various methods of estimating radon dose at underground workplaces in wineries, 2008, Radiat Environ Biophys (2008) 47:527–534, doi: 10.1007/s00411-008-0174-z.

Vengosh, A., Jackson, R.B., Warner, N., Darrah, T.H., Kondash, A., 2014, A critical review of the risks to water resources from unconventional shale gas development and hydraulic fracturing in the United States, Environ. Sci. Technol., 2014, 48 (15), pp 8334–8348, doi**:** 10.1021/es405118y.

Vengosh, Warner, N, A., Jackson, R.B., Darrah, T.H., 2013 Surface water and stray gas shallow aquifer contamination, presentation: Technical workshop on case studies to assess potential impacts of hydraulic fracturing on drinking water resources July 20, 2013. Accessed: 2015-02-02 from:

Vinson, D. S., Vengosh, A., Hirschfeld, D., Dwyer, G. S., 2009, Relationships between radium and radon occurrence and hydrochemistry in fresh groundwater from fractured crystalline rocks, North Carolina (USA), Chemical Geology 260 (2009) 159–171, doi: 10.1016/j.chemgeo.2008.10.022.

Vogiannis, E., Nikolopoulos, D., Louizi, A., Halvadakis, C.P., 2004.Radon variations during treatment in thermal spas of Lesvos Island (Greece), J. Environ.Radioact., 75, 159-170, doi:10.1021/acs.est.5b01228

http://www2.epa.gov/sites/production/files/201308/documents/vengosh_surface_water_and_stray_gas_shallow_aquifer_contamination.pdf.

Warner, N., Jackson, R., Darrah, T., Dwyer, G.S., Vengosh, A., 2014, New Isotopic Tracers for Shale Gas and Hydraulic Fracturing Fluids, Nicholas School of Environment, Duke University.

Accessed on: 17-11-2016. www.epa.gov/sites/production/files/documents/vengosh.pdf

Wanty, R.B., Johnson, S.L., Briggs, P.H., 1991, Radon-222 and its parent radionuclides in groundwater from two study areas in New Jersey and Maryland, U.S.A. Applied Geochemistry 6, 305–318, doi:10.1016/0883-2927(91)90007-C.

Warner, N.R., Jackson, R.B., Darrah, T.H., Osborn, S.G., Down, A., Zhao, K., White, A., Vengosh, A.,2013, Geochemical evidence for possible natural migration of Marcellus Formation brine to shallow aquifers in Pennsylvania. Proc. Natl. Acad. Sci. U.S.A, 2012, 109 (30), doi: 10.1073/pnas.1121181109.

Warner, N. R., 2013, Impacts of Shale Gas Wastewater Disposal on Water Quality in Western Pennsylvania, Environ. Sci. Technol., 47, 11849−11857, doi: 10.1021/es402165b.

WHO, 2009, WHO handbook on indoor radon, a public health perspective. Geneva, World Health Organization (WHO).

WHO, 2011, Guidelines for Drinking-water Quality, Fourth Edition. Geneva, World Health Organization (WHO).

Wieser, M. E., 2006, Atomic weights of the elements 2005 (IUPAC Technical Report), Pure and Applied Chemistry 78 (11): 2051–2066. doi: 10.1351/pac200678112051.

Wood, W.W., Kraemer, T.F., Shapiro, A., 2004, Radon (222Rn) in groundwater of fractured rocks: a diffusion/ion exchange model. Ground Water 42, 552–567.

Won-Young, 2013, Induced seismicity associated with fluid injection into a deep well in Youngstown, Ohio, Journal of Geophysical Research-Solid Earth, 118, doi: 10.1002/jgrb.50247.

WRC, 2015, The use of chemistry, isotopes and gases as indicators of deeper circulating groundwater in the Main Karoo Basin, South African Water Research Commission (WRC), WRC Report No. 2254/1/15, ISBN 978-1-4312-0678-0.

Zdrojewicz, Z., 2006, Radon treatment controversy, Journal of Dose Response 4(2), 106-118, doi: 10.2203/dose-response.05-025.Zdrojewicz.

Yu, K.M, Leung, Y.Y., Nikezic, D., Leung, J.K.C, 2008. Equilibrium factor determination using SSNTDs, Radiation Measurements 43 (2008) S357–S363, http://dx.doi.org/10.1016/j.radmeas.2008.03.024.

Appendix

Table 1: Summary table of measurements results obtained during the first measurement series (F1) which were referred to in this thesis.

Site number, [S]	Sampling and measurement date	Radon-in-water activity concentration, [Bq/L]	Radon-in-water activity concentration uncertainty, [Bq/L]	Electrical conductivity, [µS/m]	Uranium in-water concentration, [µg/L]	Sample temperature, [°C]	Sample pH
1	04-03-2014	25.7	4.2	604	-		-
2	04-03-2014	2.5	1.5	557	1.323	22.6	7.78
3	04-03-2014	20.4	3.8	538	3.660	23	7.34
5	04-03-2014	16.4	3.4	556	0.534	24.2	7.21
6	04-03-2014	29.6	4.6	552	18.425	22.5	6.92
7	04-03-2014	27.7	4.4	558	18.392	22.1	7.45
8	04-03-2014	3.7	1.9	554	2.400	25.2	8.00
9	05-03-2014	3.3	1.7	893	0.432	29	9.55
10	05-03-2014	20	3.7	911	0.037	-	8.16
11	05-03-2014	31.3	4.7	894	0.017	21.9	9.6
12	05-03-2014	65.2	6.8	883	-	22.4	9.8
14	06-03-2014	35.4	4.9	729	0.003	21.1	7.66
15	06-03-2014	3.3	1.7	380	21.967	25.8	9.87
16	06-03-2014	4.9	2	419	0.006	24.3	7.34
17	07-03-2014	0.9	1	1393	1.248	33.6	9.16
18	07-03-2014	0.6	0.9	1383	-	33.4	9.1
19	07-03-2015	1.5	1	1393	0.001	-	-
20	07-03-2016	14.5	3.1	1393	-	33.6	9.1
21	07-03-2014	55.6	6.2	1350	-	21.6	8.32
22	08-03-2014	182.6	18.1	1283	0.001	21.7	7.46
23	08-03-2014	49.9	5.9	1119	6.757	20.5	7.56
24	08-03-2014	81.4	7.6	1308	6.985	19.8	7.36
25	08-03-2014	44.3	5.6	1317	10.134	18.4	7.2
26	08-03-2014	7.5	2.4	1314	35.497	28.1	7.87
28	09-03-2014	48.6	5.8	1269	0.019	19.9	8.05
29	09-03-2014	86.9	7.9	1318	0.026	20.1	7.1
30	09-03-2014	6.3	2.3	1326	2.678	20.5	7.2
31	09-03-2014	65.1	6.5	1305	4.127	20.8	7.3
32	10-03-2014	1.6	1.2	1361	2.601	30.8	9.04
33	10-03-2014	43	5.3	1368	0.000	19.6	7.5
34	10-03-2014	61.4	6.5	1347	2.596	20.7	7.5
35	10-03-2014	80.8	7.6	1354	3.031	19.6	7.11
37	11-03-2014	15.5	3.3	1288	10.066	28.7	9.48
38	11-03-2014	6.4	6.2	1288	0.002	-	-

39	11-03-2014	11.9	3	1288	0.002	28.7	9.48
40	11-03-2014	4.8	2	1320	0.002	24.5	9.51
41	13-03-2014	1.5	1.2	736	-	23.5	7.57
42	13-03-2014	46.8	5.7	771	2.283	22.3	7.24

Note: Electrical conductivity, uranium in-water concentration, sample temperature, and pH have been measured by a research team from the Department of Earth Science, Stellenbosch University (Kelley, 2016; WRC 2015).

Table 2: Summary table of measurement results obtained during the second measurement series (F2) referred to in this thesis.

Site number, [S]	Sampling and measurement date	Radon-in-water activity concentration, [Bq/L]	Radon-in-water activity concentration uncertainty, [Bq/L]	Electrical conductivity, [µS/m]	Uranium in-water concentration, [µg/L]	Sample temperature, [°C]	Sample pH
1	2014/07/07	1	1	-	-	-	-
4	2014/07/08	2	1	93	0.664	26.5	8.1
7	2014/07/07	14	2	53	4.118	20.3	7.9
8	2014/07/08	2	1	133	0.544	23.5	8.2
9	2014/07/06	2	1	21	0.048	29.4	9.8
14	2014/07/06	37	3	162	26.558	16.2	7.8
15	2014/07/04	4	1	82	0.001	23.5	10.0
16	2014/07/04	6	1	200	1.310	21.2	7.4
18	2014/06/30	1	1	201	0.004	30.0	9.1
21	2014/06/30	58	4	190	0.003	21.6	7.5
25	2014/07/01	39	4	85	40.851	18.1	7.4
26	2014/07/01	21	3	49	0.023	25.7	8.0
28	2014/07/02	54	4	54	0.040	18.2	8.4
30	2014/07/02	82	5	-	-	-	-
31	2014/07/02	46	4	58	3.141	17.3	7.5
32	2014/06/29	2	1	102	0.002	29.5	9.2
33	2014/06/29	49	4	50	3.594	18.2	7.7
35	2014/06/28	103	6	362	0.004	28.7	9.4
37	2014/06/28	9	2	-	-	-	-
38	2014/06/28	5	1	-	-	-	-
39	2014/06/28	8	2	-	-	-	-
42	2014/07/09	165	8	107	15.07	21.5	7.1
44	2014/06/26	89	6	-	-	-	-
43	2014/06/27	2	1	-	-	-	-
45	2014/06/27	80	5	-	-	-	-
46	2014/06/27	106	6	-	-	-	-
47	2014/06/27	114	7	-	-	-	-

48	2014/06/27	152	8	138	2.536	19.2	7.7
49	2014/07/04	39	4	-	11.784	-	-

Note: Electrical Conductivity, Uranium in-water concentration, sample temperature and pH has been measured research team of the Department of Earth Science, Stellenbosch (Kelley, 2016; WRC 2015).

Table 3: Summary table of measurements results obtained during the third measurement series (F3) which were referred to in this thesis.

Site Number, [S]	Sampling and Measurement Date	Radon-in-water activity concentration, [Bq/L]	Radon-in-water activity concentration uncertainty, [Bq/L]	Electric Conductivity, [µS/m]	Sample Temperature, [°C]	Sample pH
44	01/06/2016	53	4	111	14.4	5.2
45	01/06/2016	72	5	101	23	5.2
46	01/06/2016	100	6	101	23	5.8
48	01/06/2016	132	7	95	19.9	5.5
32	02/06/2016	2	1	226	25.6	11
33	02/06/2016	48	4	41	17.1	6.3
35	02/06/2016	78	5	109	17.6	5.2
50	03/06/2016	24	3	238	17.1	11.3
25	04/06/2016	48	4	144	16.1	4.7
31	05/06/2016	60	4	109	16.6	5.2
28	06/06/2016	61	5	126	17	4.9
14	07/06/2016	38	4	127	23.2	5.8
51	07/06/2016	121	6	115	22.4	5.1
52	07/06/2016	45	3	134	22.1	4.8
53	07/06/2016	30	8	-	-	-

Table 4: Summary table of unprocessed measurements results obtained during the third measurement series (F3) which were referred to in this thesis.

Date	Site Number	Detector	Four measurement cycles of radon-in-water activity concentration, [Bq/L]	Associated radon-in-water activity concentration uncertainty, [Bq/L]	Mean radon-in-water activity concentration, [Bq/L]	Representative mean radon-in-water activity concentration , [Bq/L]	Median radon-in-water activity concentration, [Bq/L]	Mean uncertainty radon-in-water activity concentration, [Bq/L]	Representative radon-in-water activity concentration Uncertainty, [Bq/L]
01/06/2016	44	C	49	4	51	53	51	4	4
			51	4					
			53	4					
			52	4					
01/06/2016		B	53	4	55		55	4	
			58	4					
			58	4					
			53	4					
01/06/2016	45	C	68	5	68	72	68	5	5
			73	5					
			63	5					
			68	5					
01/06/2016		B	76	5	76		76	5	
			78	5					
			75	5					
			77	5					
01/06/2016	46	C	92	6	97	99	98	6	6
			100	6					
			100	6					
			96	6					
01/06/2016		B	98	6	102		102	6	
			105	6					
			103	6					
			101	6					
01/06/2016	48	C	129	7	127	132	127	7	7
			127	7					
			126	6					
			127	6					
01/06/2016		B	132	7	137		138	7	
			140	7					
			139	7					
			136	7					
02/06/2016	32	C	3	1	2	2	2	1	1
			2	1					
			2	1					

			2	1					
02/06/2016		B	2	1	1		1	1	
			1	1					
			1	1					
			1	1					
02/06/2016	33	C	45	4	46	48	45	4	4
			45	4					
			47	4					
			45	4					
02/06/2016		B	50	4	50		50	4	
			50	4					
			49	4					
			50	4					
02/06/2016	35	C	76	5	75	78	75	5	5
			74	5					
			73	5					
			76	5					
02/06/2016		B	76	5	81		82	5	
			85	5					
			78	5					
			85	5					
03/06/2016	50	C	23	3	24	24	24	3	3
			25	3					
			23	3					
			25	3					
03/06/2016		B	21	3	23		24	3	
			23	3					
			24	3					
			24	3					
04/06/2016	25	C	47	4	47	48	47	4	4
			45	4					
			48	4					
			47	4					
04/06/2016		B	50	4	50		50	4	
			49	4					
			53	4					
			48	4					
05/06/2016	31	C	57	4	60	60	60	4	4
			60	4					
			59	4					
			64	4					
05/06/2016		B	58	4	60		59	5	

			62	5					
			59	5					
			59	4					
06/06/2016	28	C	54	4	57	61	57	4	5
			60	4					
			57	4					
			57	4					
06/06/2016		B	60	5	65		67	5	
			68	5					
			65	5					
			68	5					
07/06/2016	14	C	34	3	36	38	35	3	4
			35	3					
			39	3					
			35	3					
07/06/2016		B	38	4	40		40	4	
			40	4					
			40	4					
			40	4					
07/06/2016	51	C	111	6	113	121	113	6	6
			113	6					
			113	6					
			114	6					
07/06/2016		B	123	6	130		131	6	
			131	6					
			133	6					
			131	6					
07/06/2016	52	C	46	3	43	45	43	3	3
			43	3					
			41	3					
			42	3					
07/06/2016		B	43	3	46		46	3	
			50	3					
			48	3					
			44	3					
07/06/2016	51	C	96	6	101	104	102	6	6
			102	6					
			103	6					
			101	6					
07/06/2016		B	99	6	107		107	6	
			105	6					
			113	6					

			109	6					
07/06/2016	53	C	23	8	28	30	29	7	8
			30	7					
			30	7					
			28	7					
07/06/2016		B	28	7	32		33	8	
			31	8					
			35	8					
			35	8					

Code 1: Matlab script which was utilized to perform collective data analyses and plotting.

```
% Ryno Botha
% KRBM project (F1, F2, F3)
% Revised on 2016-08-01
% Version 1.006
% Activity measurements (RAD-7),KBRM (P1)
% DSA: Deep Shallow Analyses

clear all
close all
clc

%%%%%%%%%%%%%%%%%%%%%%%%%%%%%%%%%%%%%%%%%%%%%%%%%%%%%%%%%%%%%%%%%%%%%%%%%%%%%%%
% [A]Import Section
%%%%%%%%%%%%%%%%%%%%%%%%%%%%%%%%%%%%%%%%%%%%%%%%%%%%%%%%%%%%%%%%%%%%%%%%%%%%%%%

load('clean_F1.mat')
load('clean_F2.mat')
load('clean_F3.mat')
load('Inter.mat')
load('radium')

%%%%%%%%%%%%%%%%%%%%%%%%%%%%%%%%%%%%%%%%%%%%%%%%%%%%%%%%%%%%%%%%%%%%%%%%%%%%%%%
% [B]Calculation
%%%%%%%%%%%%%%%%%%%%%%%%%%%%%%%%%%%%%%%%%%%%%%%%%%%%%%%%%%%%%%%%%%%%%%%%%%%%%%%

% DSA Master

DSA_Rn_C =
[Rn_c_F1_shallow(1:20);Rn_c_F1_mixed(1:5);Rn_c_F1_deep(1:12);Rn_c_F2_shallo
w;Rn_c_F2_mixed;Rn_c_F2_deep;Rn_c_F3_shallow;Rn_c_F3_mixed;Rn_c_F3_deep];
DSA_mean = mean(DSA_Rn_C);

xxx = linspace(1,50,50);
DSA_mean_line = ones([1,50]).*DSA_mean;

% All data

Rn_C_MASTER = [Rn_c_F1_1(1:38);Rn_c_F1_2(2:35);Rn_c_F1_3];
```

```
master_mean = mean(Rn_C_MASTER);
master_min = min(Rn_C_MASTER);
master_max = max(Rn_C_MASTER);
master_stdev = std(Rn_C_MASTER);
master_median = median(Rn_C_MASTER);

% Inter check (F1 and F2), Radon

INT_diff_shallow = INT_Rn_C_F1_shallow - INT_Rn_C_F2_shallow;
INT_diff_mixed = INT_Rn_C_F1_mixed - INT_Rn_C_F2_mixed;
INT_diff_deep = INT_Rn_C_F1_deep - INT_Rn_C_F2_deep;

% Inter check (F3 and F2/F1), Radon

INT_Rn_C_F1_shallow;
INT_Rn_C_F2_shallow;
%INT_Rn_C_F3_shallow;

% Shallow Statistics, Radon

Rn_C_master_shallow =
[Rn_c_F1_shallow(1:20);Rn_c_F2_shallow;Rn_c_F3_shallow];
Rn_C_master_shallow_mean = mean(Rn_C_master_shallow);
Rn_C_master_shallow_min = min(Rn_C_master_shallow);
Rn_C_master_shallow_max = max(Rn_C_master_shallow);
Rn_C_master_shallow_stdev = std(Rn_C_master_shallow);
Rn_C_master_shallow_median = median(Rn_C_master_shallow);
Rn_C_master_shallow_data_points = size(Rn_C_master_shallow);

% Mixed Statistics, Radon

Rn_C_master_mixed = [Rn_c_F1_mixed(1:5);Rn_c_F2_mixed;Rn_c_F3_mixed];
Rn_C_master_mixed_mean = mean(Rn_C_master_mixed);
Rn_C_master_mixed_min = min(Rn_C_master_mixed);
Rn_C_master_mixed_max = max(Rn_C_master_mixed);
Rn_C_master_mixed_stdev = std(Rn_C_master_mixed);
Rn_C_master_mixed_median = median(Rn_C_master_mixed);
Rn_C_master_mixed_data_points = size(Rn_C_master_mixed);

% Deep Statistics, Radon

Rn_C_master_deep = [Rn_c_F1_deep(1:12);Rn_c_F2_deep;Rn_c_F3_deep];
Rn_C_master_deep_mean = mean(Rn_C_master_deep);
Rn_C_master_deep_min = min(Rn_C_master_deep);
Rn_C_master_deep_max = max(Rn_C_master_deep);
Rn_C_master_deep_stdev = std(Rn_C_master_deep);
Rn_C_master_deep_median = median(Rn_C_master_deep);
Rn_C_master_deep_data_points = size(Rn_C_master_deep);


%%%%%%%%%%%%%%%%%%%%%%  Uranium Statistics

% Master mean calculation

uranium_master = [U_F1_shallow; U_F1_mixed; U_F1_deep; U_F2_shallow;
U_F2_mixed; U_F2_deep];
uranium_master_mean = mean(uranium_master);
```

```
xx_uranium_master = linspace(0,45,100);
vector_uranium_mean = uranium_master_mean*ones(1,100);

% Inter check, Uranium  (Manual determination)

INT_U_shallow_Diff = [-1.718 -4.59 -0.54 -0.998 -4.3];
INT_U_shallow_Diff_sites = [7 14 31 33 42];

INT_U_mixed_Diff = [-0.114 -0.004 -0.014];
INT_U_mixed_Diff_sites = [8 26 28];

INT_U_deep_Diff = [0.004 0.002 -0.002];
INT_U_deep_Diff_sites = [15 21 37];

RATIO = [2.63 1.62 0.93 6.94 5.05 2.39]'; % Ra228/Ra-226 Ratio
SPRINGS = [3.3 14 7.5 1.6]';
RA226 = [0.002 0.008 0.007 0.002 0.002 0.006]';
RA228 = [0]';

%%%%%%%%%%%%%%%%%%%%%%%% Uncertainty in the mean analysis

Matrix = Rn_C_master_deep;
WWW1 = size(Matrix);
N = WWW1(1:1);
Range = max(Matrix)- min(Matrix);
MEAN_MASTER = mean(Matrix)
UNCERTAINTY = MEAN_MASTER/sqrt(N)

%%%%%%%%%%%%%%%%%%%%%%%%%%%%%%%%%%%%%%%%%%%%%%%%%%%%%%%%%%%%%%%%%%%%%%%%%%%%
% [C]Plot
%%%%%%%%%%%%%%%%%%%%%%%%%%%%%%%%%%%%%%%%%%%%%%%%%%%%%%%%%%%%%%%%%%%%%%%%%%%%
```



```
figure % DSA
errorbar(sites_F1_shallow, Rn_c_F1_shallow,
Rn_c_F1_U_shallow,'*b','LineWidth',2,'MarkerSize',8);
hold on
errorbar(sites_F1_mixed, Rn_c_F1_mixed,
Rn_c_F1_U_mixed,'*g','LineWidth',2,'MarkerSize',8);
hold on
errorbar(sites_F1_deep, Rn_c_F1_deep,
Rn_c_F1_U_deep,'*r','LineWidth',2,'MarkerSize',8);
hold on
errorbar(sites_F2_shallow, Rn_c_F2_shallow,
Rn_c_F2_U_shallow,'bs','LineWidth',2,'MarkerSize',8);
hold on
errorbar(sites_F2_mixed, Rn_c_F2_mixed,
Rn_c_F2_U_mixed,'gs','LineWidth',2,'MarkerSize',8);
hold on
errorbar(sites_F2_deep, Rn_c_F2_deep,
Rn_c_F2_U_deep,'rs','LineWidth',2,'MarkerSize',8);
hold on
errorbar(sites_F3_shallow, Rn_c_F3_shallow,
Rn_c_F3_U_shallow,'bd','LineWidth',2,'MarkerSize',8);
hold on
errorbar(sites_F3_mixed, Rn_c_F3_mixed,
Rn_c_F3_U_mixed,'gd','LineWidth',2,'MarkerSize',8);
hold on
```

```
errorbar(sites_F3_deep, Rn_c_F3_deep,
Rn_c_F3_U_deep,'rd','LineWidth',2,'MarkerSize',8);
hold on
plot(xxx, DSA_mean_line,'-m','LineWidth',2);

grid minor
title('^{222}Rn in-water activity concentration Karoo Basin baseline (F1 to
F3)','FontSize',18);
ylabel('Activity Concentration [Bq/L] ','FontSize',18);
xlabel('Site Number','FontSize',18);
ylim([0 210]);
xlim([0 51]);
legend('Shallow Source, F1', 'Mixed Source, F1', 'Deep Source, F1','Shallow
Source, F2', 'Mixed Source, F2', 'Deep Source, F2','Shallow Source, F3',
'Mixed Source, F3', 'Deep Source, F3','Mean');



figure %DSA - water temp, radon
errorbar(watertemp_shallow, Rn_c_F1_shallow,
Rn_c_F1_U_shallow,'*b','LineWidth',2,'MarkerSize',8);
hold on
errorbar(watertemp_mixed, Rn_c_F1_mixed,
Rn_c_F1_U_mixed,'*g','LineWidth',2,'MarkerSize',8);
hold on
errorbar(watertemp_deep, Rn_c_F1_deep,
Rn_c_F1_U_deep,'*r','LineWidth',2,'MarkerSize',8);
hold on
errorbar(watertemp_F2_shallow, Rn_c_F2_shallow,
Rn_c_F2_U_shallow,'bs','LineWidth',2,'MarkerSize',8);
hold on
errorbar(watertemp_F2_mixed, Rn_c_F2_mixed,
Rn_c_F2_U_mixed,'gs','LineWidth',2,'MarkerSize',8);
hold on
errorbar(watertemp_F2_deep, Rn_c_F2_deep,
Rn_c_F2_U_deep,'rs','LineWidth',2,'MarkerSize',8);
hold on
errorbar(watertemp_F3_shallow, Rn_c_F3_shallow,
Rn_c_F3_U_shallow,'bd','LineWidth',2,'MarkerSize',8);
hold on
errorbar(watertemp_F3_mixed, Rn_c_F3_mixed,
Rn_c_F3_U_mixed,'gd','LineWidth',2,'MarkerSize',8);
hold on
errorbar(watertemp_F3_deep, Rn_c_F3_deep,
Rn_c_F3_U_deep,'rd','LineWidth',2,'MarkerSize',8);
hold on

grid minor
title('^{222}Rn in-water activity concentration vs water temperature: Karoo
Basin baseline (F1 to F3)','FontSize',18);
ylabel('Activity Concentration [Bq/L] ','FontSize',18);
xlabel('Water temperature [^{o}C] ','FontSize',18);
ylim([0 210]);
xlim([15 36]);
legend('Shallow Source, F1', 'Mixed Source, F1', 'Deep Source, F1','Shallow
Source, F2', 'Mixed Source, F2', 'Deep Source, F2','Shallow Source, F3',
'Mixed Source, F3', 'Deep Source, F3');
```

```
figure
hist(Rn_C_MASTER,20)
title('^{222}Rn in-water activity concentration histogram: Karoo Basin
baseline (F1 to F3)','FontSize',18);
ylabel('Frequency','FontSize',18);
xlabel('Activity Concentration [Bq/L]','FontSize',18);
grid minor



% Intercomparison between different field trips check

figure
subplot(2,1,1);
errorbar(INT_sites__shallow, INT_Rn_C_F1_shallow,
INT_Rn_C_U_F1_shallow,'*b','LineWidth',2,'MarkerSize',8);
hold on
errorbar(INT_sites__mixed, INT_Rn_C_F1_mixed,
INT_Rn_C_U_F1_mixed,'*g','LineWidth',2,'MarkerSize',8);
hold on
errorbar(INT_sites__deep, INT_Rn_C_F1_deep,
INT_Rn_C_U_F1_deep,'*r','LineWidth',2,'MarkerSize',8);
hold on
errorbar(INT_sites__shallow, INT_Rn_C_F2_shallow,
INT_Rn_C_U_F2_shallow,'bv','LineWidth',2,'MarkerSize',8);
hold on
errorbar(INT_sites__mixed, INT_Rn_C_F2_mixed,
INT_Rn_C_U_F2_mixed,'gv','LineWidth',2,'MarkerSize',8);
hold on
errorbar(INT_sites__deep, INT_Rn_C_F2_deep,
INT_Rn_C_U_F2_deep,'rv','LineWidth',2,'MarkerSize',8);
hold on

grid minor
title('^{222}Rn in-water activity concentration comparison between F1 and
F2','FontSize',18);
ylabel('Activity Concentration [Bq/L] ','FontSize',18);
xlabel('Site Number','FontSize',18);
ylim([0 210]);
legend('Shallow Source, F1', 'Mixed Source, F1', 'Deep Source, F1','Shallow
Source, F2', 'Mixed Source, F2', 'Deep Source, F2','Shallow Source, F3');

subplot(2,1,2);
plot(INT_sites__shallow,
INT_diff_shallow,'ob','LineWidth',2,'MarkerSize',8);
hold on
plot(INT_sites__mixed, INT_diff_mixed,'og','LineWidth',2,'MarkerSize',8);
hold on
plot(INT_sites__deep, INT_diff_deep,'or','LineWidth',2,'MarkerSize',8);
ylabel('Activity Difference (F1-F2) [Bq/L] ','FontSize',18);
xlabel('Site Number','FontSize',18);
legend('Shallow Source difference, F1-F2', 'Mixed Source difference, F1-
F2', 'Deep Source difference, F1-F2');
ylim([-130 30]);
grid minor

 % Uranium DSA and Inter (F1-F2)
```

```
figure
subplot(2,1,1);
plot(sites_F1_shallow_U, U_F1_shallow,'*b','LineWidth',2,'MarkerSize',8);
hold on
plot(sites_F1_mixed_U, U_F1_mixed,'*g','LineWidth',2,'MarkerSize',8);
hold on
plot(sites_F1_deep_U, U_F1_deep,'*r','LineWidth',2,'MarkerSize',8);
hold on
plot(sites_F2_shallow_U, U_F2_shallow,'bv','LineWidth',2,'MarkerSize',8);
hold on
plot(sites_F2_mixed_U, U_F2_mixed,'gv','LineWidth',2,'MarkerSize',8);
hold on
plot(sites_F2_deep_U, U_F2_deep,'rv','LineWidth',2,'MarkerSize',8);
hold on
plot(xx_uranium_master,vector_uranium_mean,'-m','LineWidth',2);

grid minor
title(' Collective uranium in-water concentration in the Karoo
Basin','FontSize',18);
ylabel('Uranium [ug/L] ','FontSize',18);
xlabel('Site Number','FontSize',18);
ylim([-2 45]);
legend('Shallow Source, F1', 'Mixed Source, F1', 'Deep Source, F1','Shallow
Source, F2', 'Mixed Source, F2', 'Deep Source, F2','Mean');

subplot(2,1,2);
plot(INT_U_shallow_Diff_sites,
INT_U_shallow_Diff,'ob','LineWidth',2,'MarkerSize',8);
hold on
plot(INT_U_mixed_Diff_sites,
INT_U_mixed_Diff,'og','LineWidth',2,'MarkerSize',8);
hold on
plot(INT_U_deep_Diff_sites,
INT_U_deep_Diff,'or','LineWidth',2,'MarkerSize',8);
ylabel('Difference (F1-F2) [uq/L] ','FontSize',18);
xlabel('Site Number','FontSize',18);
legend('Shallow Source difference, F1-F2', 'Mixed Source difference, F1-
F2', 'Deep Source difference, F1-F2');
grid minor
xlim([0 45]);
ylim([-5 1]);

% Uranium and Radon correlation (F1, F2)

figure
plot(U, Rn_c_F1_3,'*r','LineWidth',2);
hold on
plot(U_F2, Rn_C_F2_U238,'*b','LineWidth',2);
grid on
title('^{222}Rn in-water activity concentration vs ^{238}U
concentration','FontSize',18);
ylabel('Radon activity Concentration [Bq/L] ','FontSize',18);
xlabel('Uranium concentration [µg/L]  ','FontSize',18);
legend('F1 Data', 'F2 Data ');
xlim([-1 45]);
ylim([-1 185]);
```

```
radium_sites = [15 18 28 7 33 42];   % Order is crucial to match vectors:
Deep then Mixed then Shallow

figure
subplot(2,1,2);
plot(INT_U_shallow_Diff_sites,
INT_U_shallow_Diff,'ob','LineWidth',2,'MarkerSize',8);
hold on
plot(INT_U_mixed_Diff_sites,
INT_U_mixed_Diff,'og','LineWidth',2,'MarkerSize',8);
hold on
plot(INT_U_deep_Diff_sites,
INT_U_deep_Diff,'or','LineWidth',2,'MarkerSize',8);
ylabel('Difference (F1-F2) [uq/L] ','FontSize',18);
xlabel('Site Number','FontSize',18);
legend('Shallow Source difference, F1-F2', 'Mixed Source difference, F1-
F2', 'Deep Source difference, F1-F2');
grid minor
xlim([0 45]);
ylim([-5 1]);
```

Code 2: The Matlab script which was utilized to perform data analyses and plotting for the third measurement series (F3). The coding structure utilized to perform data analyses and plotting for the first and second measurement series is generic to code 2.


```
% Ryno Botha
% KRBM project (P1, F3)
% Revised on 2016-08-01
% Version 1.0002
% Activity measurements (RAD7),KBRM
% Note: Data was extracted from Cleaned (Final), F3

clear all
close all
clc
whitebg('w');

%%%%%%%%%%%%%%%%%%%%%%%%%%%%%%%%%%%%%%%%%%%%%%%%%%%%%%%%%%%%%%%%%%%%%%%%%%%%
% [A]Import Section
%%%%%%%%%%%%%%%%%%%%%%%%%%%%%%%%%%%%%%%%%%%%%%%%%%%%%%%%%%%%%%%%%%%%%%%%%%%%

%%%%%%%%%%%%%%%%%%%%%%%%
% Import 1 Data Matrix
%%%%%%%%%%%%%%%%%%%%%%%%

load('clean_F3.mat');


%%%%%%%%%%%%%%%%%%%%%%%%%%%%%%%%%%%%%%%%%%%%%%%%%%%%%%%%%%%%%%%%%%%%%%%%%%%%
% [B]Calculations
%%%%%%%%%%%%%%%%%%%%%%%%%%%%%%%%%%%%%%%%%%%%%%%%%%%%%%%%%%%%%%%%%%%%%%%%%%%%

% DSA statistical analyses
```

```
mean_Rn_F3 = mean(Rn_c_F3_1);
mean_Rn_F3_shallow = mean(Rn_c_F3_shallow);
mean_Rn_F3_mixed = mean(Rn_c_F3_mixed);
mean_Rn_F3_deep = mean(Rn_c_F3_deep);

std_Rn_F3 = std(Rn_c_F3_1);
std_Rn_F3_shallow = std(Rn_c_F3_shallow);
std_Rn_F3_mixed = std(Rn_c_F3_mixed);
std_Rn_F3_deep = std(Rn_c_F3_deep);

xxx = linspace(1,50,50);
mean_line = ones([1,50]).*mean_Rn_F3;


%%%%%%%%%%%%%%%%%%%%%%%%%%%%%%%%%%%%%%%%%%%%%%%%%%%%%%%%%%%%%%%%%%%%%%%%%%%%
% [C] Plot
%%%%%%%%%%%%%%%%%%%%%%%%%%%%%%%%%%%%%%%%%%%%%%%%%%%%%%%%%%%%%%%%%%%%%%%%%%%%

errorbar(sites_F3_1, Rn_c_F3_1, Rn_c_F3_U_1,'*b','LineWidth',2);
grid on
title('^{222}Rn in-water activity concentration, F3','FontSize',18);
ylabel('Activity Concentration [Bq/L] ','FontSize',18);
xlabel('Site Number','FontSize',18);
ylim([0 210]);

figure
hist(Rn_c_F3_1,10)
title('^{222}Rn in-water activity concentration, F3','FontSize',18);
ylabel('Frequency','FontSize',18);
xlabel('Activity Concentration [Bq/L]','FontSize',18);
grid on


figure
errorbar(ec_F3, Rn_c_F3_2,Rn_c_F3_U_2,'*b','LineWidth',2);
grid on
title('^{222}Rn in-water activity concentration, F3','FontSize',18);
ylabel('Activity Concentration [Bq/L] ','FontSize',18);
xlabel('Water EC [µS/m] ','FontSize',18);

figure
errorbar(ph_F3, Rn_c_F3_2,Rn_c_F3_U_2,'*b','LineWidth',2);
grid on
title('^{222}Rn in-water activity concentration, F3','FontSize',18);
ylabel('Activity Concentration [Bq/L] ','FontSize',18);
xlabel('Water pH ','FontSize',18);
ylim([0 210]);


figure % DSA
errorbar(sites_F3_shallow, Rn_c_F3_shallow,
Rn_c_F3_U_shallow,'*b','LineWidth',2);
grid on
title('^{222}Rn in-water activity concentration, F3','FontSize',18);
ylabel('Activity Concentration [Bq/L] ','FontSize',18);
xlabel('Site Number','FontSize',18);
```

```
ylim([0 210]);
hold on
errorbar(sites_F3_mixed, Rn_c_F3_mixed,
Rn_c_F3_U_mixed,'*g','LineWidth',2);
grid on
title('^{222}Rn in-water activity concentration, F3','FontSize',18);
ylabel('Activity Concentration [Bq/L] ','FontSize',18);
xlabel('Site Number','FontSize',18);
ylim([0 210]);
hold on
errorbar(sites_F3_deep, Rn_c_F3_deep, Rn_c_F3_U_deep,'*r','LineWidth',2);
grid on
title('^{222}Rn in-water activity concentration, F3','FontSize',18);
ylabel('Activity Concentration [Bq/L] ','FontSize',18);
xlabel('Site Number','FontSize',18);
ylim([0 100]);
xlim([20 51]);
hold on
plot(xxx, mean_line,'-*r','LineWidth',2);
legend('Shallow Source', 'Mixed Source', 'Deep Source','Mean');

figure %DSA - water temp
errorbar(watertemp_F3_shallow, Rn_c_F3_shallow,
Rn_c_F3_U_shallow,'*b','LineWidth',2);
grid on
title('^{222}Rn in-water activity concentration, F3','FontSize',18);
ylabel('Activity Concentration [Bq/L] ','FontSize',18);
xlabel('Water temperature [^{o}C] ','FontSize',18);
ylim([0 210]);
hold on
errorbar(watertemp_F3_mixed, Rn_c_F3_mixed,
Rn_c_F3_U_mixed,'*g','LineWidth',2);
grid on
title('^{222}Rn in-water activity concentration, F3','FontSize',18);
ylabel('Activity Concentration [Bq/L] ','FontSize',18);
xlabel('Water temperature [^{o}C] ','FontSize',18);
ylim([0 100]);
hold on
errorbar(watertemp_F3_deep, Rn_c_F3_deep,
Rn_c_F3_U_deep,'*r','LineWidth',2);
grid on
title('^{222}Rn in-water activity concentration, F3','FontSize',18);
ylabel('Activity Concentration [Bq/L] ','FontSize',18);
xlabel('Water temperature [^{o}C] ','FontSize',18);
ylim([0 100]);
legend('Shallow Source', 'Mixed Source', 'Deep Source');
```